Aus dem Institut für Radiologie
der Medizinischen Fakultät Charité - Universitätsmedizin Berlin

# DISSERTATION

# Eisen(III)-*t*CDTA-Derivate als MRI-Kontrastmittel
# Iron(III)-*t*CDTA Derivatives as MRI Contrast Agents

Zur Erlangung des akademischen Grades
Doktor rerum medicinalium (Dr. rer. medic.)

vorgelegt der Medizinischen Fakultät
Charité - Universitätsmedizin Berlin

von

Jing Xie
aus Jiangsu (China Mainland)

Datum der Promotion: 30.11.2023

# Preface

## Parts of the results from this thesis has been published:

- **Xie J**, Haeckel A, Hauptmann R, Ray IP, Limberg C, Kulak N, Hamm B, Schellenberger E. **Iron(III)-*t*CDTA derivatives as MRI contrast agents: Increased T1 relaxivities at higher magnetic field strength and pH sensing.** Magn Reson Med. 2021 Jun;85(6):3370-3382. doi: 10.1002/mrm.28664. Epub 2021 Feb 4. PMID: 33538352.
- **Patent 1:** Method for preparing an Fe-*t*CDTA contrast agent and product obtainable by the method. Patentnummer (PCT): WO2020/001950 A1
- **Patent 2:** Iron(III) complexes having new contrast agent properties, for magnetic resonance imaging. Patentnummer (PCT): WO2021074369A1

# TABLE OF CONTENTS

# List of Abbreviations

| | |
|---|---|
| GBCAs | Gadolinium-based contrast agents |
| IBCAs | Iron(III) complex-based contrast agents |
| MRI | Magnetic resonance imaging |
| *t*CDTA | *trans*-1,2-diaminocyclohexane-N,N,N',N'-tetra-acetic acid |
| tCDTA-MA | *trans*-1,2-diaminocyclohexane-N,N,N',N'-tetra-acetic acid monoanhydride |
| HPLC | High Performance Liquid Chromatography |
| NMR | Nuclear Magnetic Resonance |
| DCE-MRI | Dynamic Contrast-enhanced MRI |
| MRA | Magnetic Resonance Angiography |
| *en* | Ethylenediamine |
| *en-t*CDTA | *ethylenediamine-t*CDTA |
| *en-Di-t*CDTA | *ethylenediamine-t*CDTA *dimer* |
| *trans* | *trans*-1,4-*diaminocyclohexane-t*CDTA |
| *trans-Di-t*CDTA | *trans*-1,4-*diaminocyclohexane-t*CDTA *dimer* |
| *ethoxyaniline-t*CDTA | 4-Ethoxyaniline-*t*CDTA |
| DMSO | Dimethyl sulfoxide |
| Gd-DTPA | Gadolinium diethylenetriaminepentaacetic acid |
| IR | Infrared Spectroscopy |
| FCS | Fetal Calf Serum |
| TR | Repetition Times |
| TE | Echo Time |
| ROI | Regions of Interest |
| IS | Inner Sphere |
| SS | Second Sphere |
| OS | Outer Sphere |
| NMRD | Nuclear Magnetic Resonance Dispersion |
| Gd-EOB-DTPA | Gadoxetic acid |

| | |
|---|---|
| Gd-BOPTA | Gadobenate dimeglumine |
| MW | Molecular Weight |
| MIP | Maximum Intensity Projection |
| MALDI-TOF | Matrix Assisted Laser Desorption Ionization - Time of Flight |
| NSF | Nephrogenic Systemic Fibrosis |
| EMA | European Medicine Agency |
| GDD | Gadolinium Deposition Disease |
| HPLC | High Performance Liquid Chromatography |
| FOV | Field of View |

# List of Figures

# List of Tables

# Abstrakt

Die Magnetresonanztomographie (MRT) ist eine der am häufigsten verwendeten klinischen nicht-invasiven und nicht-ionisierenden diagnostischen Bildgebungsmodalitäten, die hervorragende anatomische Details liefert. Die kontinuierlichen technologischen Fortschritte und die Einführung von exogenen Kontrastmitteln (CA) ermöglichen diagnostische und therapeutische Anwendungen mit exzellenter räumlicher Auflösung sowie zusätzlichen funktionellen und metabolischen Informationen. Kontrastmittel für die $T_1$-gewichtete MRT enthalten paramagnetische Metallionen mit ungepaarten Elektronen und verkürzen die longitudinale und transversale Relaxationszeit von Protonen in benachbarten Wassermolekülen, wodurch hyperintense Signale in der $T_1$-gewichteten MRT entstehen. Die meisten $T_1$-Kontrastmittel im klinischen Einsatz basieren auf dem Gadolinium-Ion, Gd(III). Trotz des Erfolgs dieser gadoliniumbasierten Kontrastmittel (GBCA) regten Bedenken über Ablagerungen von Gadolinium, insbesondere bei Patienten mit eingeschränkter Nierenfunktion, die Forschung über die Langzeitsicherheit von GBCA und das Interesse an neuen CA mit weiter verbesserter Sicherheit an.

Als biologisch essentielles Element mit hoher Bedeutung in zahllosen physiologischen Prozessen ist Eisen(III) ein vielversprechender Kandidat für Gd-freie MRT-Kontrastmittel, da es mit 5 ungepaarten Elektronen starken Paramagnetismus bietet und möglicherweise langfristig sicherer für klinische Anwendungen ist. Bisher konnten wir zeigen, dass Eisen(III)-Komplex-basierte Kontrastmittel (IBCA), insbesondere $[Fe(tCDTA)]^-$, vielversprechende Alternativen zu GBCAs für die kontrastverstärkte, $T_1$-gewichtete MR-Bildgebung sind.

Das Ziel dieser Arbeit war es, neue IBCA auf Basis von $[Fe(tCDTA)]^-$ mit weiter verbesserten Eigenschaften für die MRT zu entwickeln. Zu diesem Zweck konnten Chelatoren für fünf neue Eisen(III)-Komplexe in zwei Schritten synthetisiert werden: zunächst wurde das Monoanhydrid von *t*CDTA erzeugt, das im zweiten Schritt an Amine gekoppelt wurde. Die neuen IBCA zeigen höhere Relaxivitätswerte und eine auf den pH-Wert ansprechende Eigenschaft sowie eine auf die Leber gerichtete Funktion.

Die neuen $[Fe(tCDTA)]^-$ Derivate hatten ähnliche Stabilitäten im Vergleich zu $[Fe(tCDTA)]^-$ Die Relaxivitäten der *trans*-1,4-*Diaminocyclohexan*-Derivat-Chelate nahmen mit zunehmender Magnetfeldstärke zu, wobei die Spitze bei 3,4 $L \cdot mmol^{-1} \cdot s^{-1}$ pro Eisen und 6,8 $L \cdot mmol^{-1} \cdot s^{-1}$ pro Molekül für das *trans*-1,4-*Diaminocyclohexan-t*CDTA-Dimer im gleichen Bereich wie GBCAs bei 3 T lag. Der $[Fe(en\text{-}tCDTA)]^+$ Komplex zeigt eine pH-abhängige Relaxivität im biologisch relevanten pH-Bereich, insbesondere bei schwach sauren pH-Werten, wie sie für verschiedene Krebsarten typisch sind. Das [Fe(4-e*thoxyanilin-t*CDTA)] wurde schnell vom hepatobiliären System aufgenommen und über die Nieren und das biliäre System ausgeschieden. Somit kann [Fe(4-Ethoxyanilin-*t*CDTA)] als MRT-Kontrastmittel für die Leber verwendet werden.

# Abstract

Magnetic resonance imaging (MRI) is one of the most commonly used clinical noninvasive and non-ionising diagnostic imaging modalities, providing exquisite anatomical details. The continuous technological advances and the introduction of exogenous contrast agents (CAs) enable diagnostic and therapeutic applications with excellent spatial resolution as well as additionally functional and metabolical information. Contrast agents for $T_1$-weighted MRI contain paramagnetic metal ions with unpaired electrons and shorten the longitudinal and transversal relaxation time of protons in adjacent water molecules, producing hyperintense signals in $T_1$-weighted MRI. Most $T_1$ contrast agents in clinical use are based on the gadolinium ion, Gd (III). Despite the success of these gadolinium-based contrast agents (GBCAs), concerns about depositions of gadolinium, especially in patients with impaired renal function, stimulated research about the long-term safety of GBCAs and the interest in new CAs with further improved safety.

As a biologically essential element with high importance in countless physiological processes, iron(III) is a promising candidate for Gd-free MRI contrast agents, since it provides with 5 unpaired electrons strong paramagnetism and is possibly safer for clinical applications in the long term. Previously we could demonstrate that iron (III) complex-based contrast agents (IBCAs), especially [Fe(*t*CDTA)], are promising alternatives for GBCAs for contrast enhanced, $T_1$-weighted MR imaging.

The goal of this project was to develop new IBCAs based on $[Fe(tCDTA)]^-$ with further improved properties for MRI. To this end, chelators for five new iron(III) complexes could be synthesised in two steps: first, the mono-anhydride of *t*CDTA was generated, which was coupled to amines in the second step. New IBCAs displaying higher relaxivity values and pH sensing responsive property as well as liver-targeting functional images.

The new [Fe(*t*CDTA)] derivatives had similar stabilities in comparison to [Fe(*t*CDTA)]. The relaxivities of *trans*-1,4-diaminocyclohexane derivatives chelates were increased with increasing magnetic field strengths topping at 3.4 $L \cdot mmol^{-1} \cdot s^{-1}$ per iron and 6.8 $L \cdot mmol^{-1} \cdot s^{-1}$ per molecule for the *trans*-1,4-Diaminocyclohexane-*t*CDTA-Dimer and thus in the same range as GBCAs at 3 T. The $[Fe(en\text{-}tCDTA)]^+$ complex exhibits pH-responsive relaxivity in the biology relevant pH range, particularly at weakly acidic pH values, which are typical for various cancers. The [Fe(4-*ethoxyaniline*-*t*CDTA)] was rapidly taken up by hepatobiliary system and excreted by the kidneys and the biliary system. Thus, [Fe(4-*ethoxyaniline*-*t*CDTA)] may be used as a liver-targeting MRI contrast agent.

# 1. Introduction

## 1.1. Magnetic Resonance Imaging

Magnetic resonance imaging (MRI) is a powerful diagnostic imaging modality on the basis of its flexibility and sensitivity to a broad range of tissue properties, such as with avoidance of invasion and ionizing radiation characters, high spatial and temporal resolution. With recent advances in technology, MRI is considered as one of the essential techniques of modern medicine owing to its high spatial resolution, tomographic 3-dimensional presentation and monitoring of dynamic physiological changes.

MR imaging is based on the analysis of water protons. The principle of clinical MRI scanning is a combination of a two-step process. At the first phase, $^{1}H$ spin orientation in water atomic nuclei is manipulated through the assortment of applied magnetic fields. At the second phase, realignments would be measured by the interaction of protons magnetic field with conductive coils. This $^{1}H$ nuclear magnetic resonance (NMR) signals of inherent water are reconstructed into MR imaging via computer programs.[2]

## 1.2. Relaxation Mechanism

Relaxation is the process in which spins release the energy absorbed from a radio frequency (RF) pulse. MRI signal is influenced, among other factors, by two types of relaxation according to the time constant, $T_1$ (spin-lattice, longitudinal relaxation), $T_2$ (spin-spin or transverse relaxation) and $T_2$* (reflecting both $T_2$ relaxation and magnetic field inhomogeneities).[3] The differences in relaxation of variable water mobility molecules in different tissues and fluids form the basis of image contrast in MRI. Thereby, $T_1$- or $T_2$-weighted images are acquired and entitle medical diagnosis.

To enhance image contrast effect, exogenous contrast agents with the ability to shorten the relaxation times of surrounding water protons are often implied prior to imaging. To date, clinical contrast agents' usage is dominated by non-specific gadolinium based chelates with $T_1$ relaxation properties. In a single year, exceed 10 million MRI procedures are performed with gadolinium in total.[4] Gd-based chelates accumulate in certain tissues, reducing $T_1$ relaxation times relative to adjacent tissues without targeted contrast agents. Given the signal intensity increase by $T_1$ agents lowering effect, these compounds are referred as positive contrast agents.

Paramagnetic relaxation enhancement relies on the dipole-dipole interactions between magnetic moment of proton nucleus (water in living tissues) and electron spins at the metallic centre. The efficiency of $T_1$ MR contrast probes is termed as relaxivity ($r_1$ for $T_1$ relaxation). It defined as the modification in the relaxation rate of water protons per molar concentration of paramagnetic contrast agents. The conventional unit for relaxivity is $mM^{-1}s^{-1}$ (per millimolar per second, and sometimes $L \cdot mmol^{-1}s^{-1}$). Primarily, the relaxivity is contributed by directly bounded water molecules (inner sphere, IS), by water bound to metal complex and possibly counter ions (second sphere, SS) and by water diffusing in the vicinity of paramagnetic centre (outer sphere, OS)[5-7] (equ 1).

$$r1 = r1^{IS} + r1^{SS} + r1^{OS} \quad (1)$$

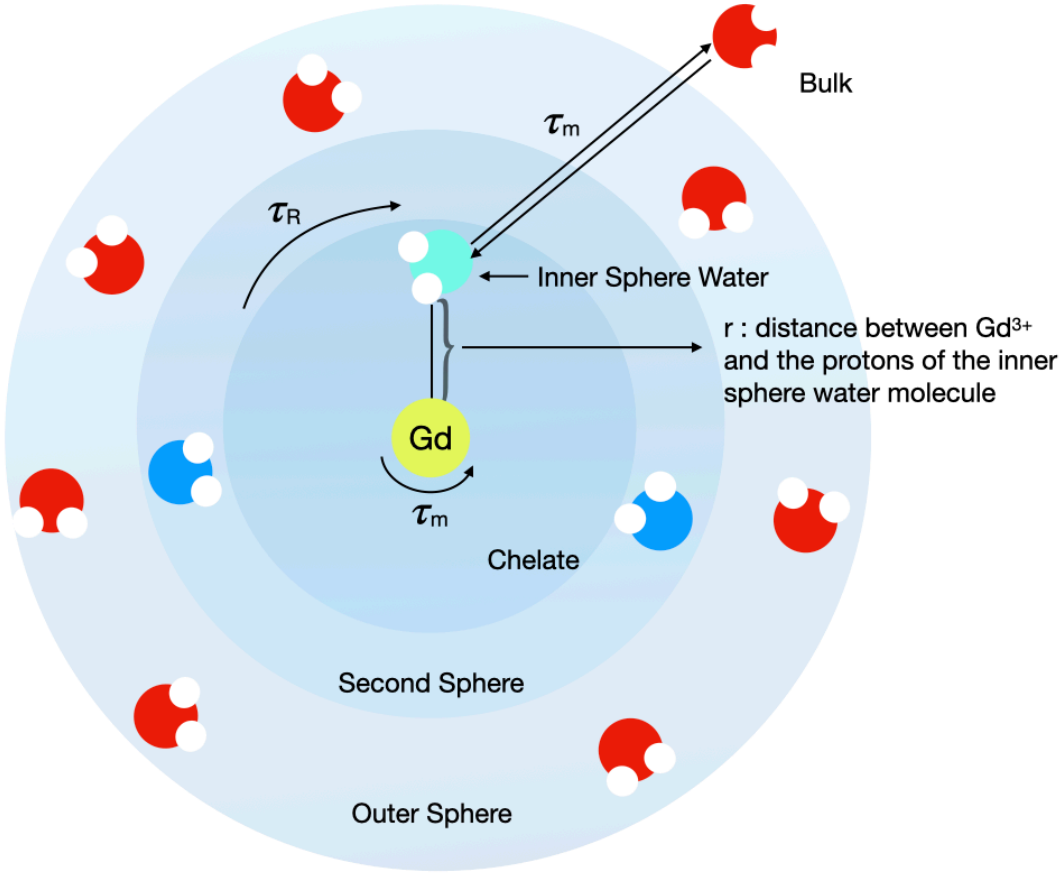


**Figure 1. Schematic representation of factors influencing solvent water relaxation.** The Gd-based complex has an inner sphere of a coordinated water molecule (inner sphere water, its oxygen is coloured light cyan) in solvent water (bulk water, oxygen is red). Second sphere water molecules (water oxygens are blue) are close to the carboxylate groups with their hydrogens. Abbreviations: see main text. (Based on (Kuźnik, Wyskocka et al, 2005)

The inner sphere, which represents the most valuable contribution to $r_1$ and the efforts towards to contrast agents of improved efficacy have been directed mainly for optimisation. This could be owing to the free coordination site and is easily identified by the geometry analysis and the number of bound

water molecules could be confirmed with luminescence spectroscopy.[8] A detailed interpretation was presented in Caravan *et. al.* review.[9]

$$r_1 = Cq\mu_{eff}^2\tau_c r^{-6} \qquad (2)$$

C: constant, $q$: number of inner sphere water molecules, $\mu_{eff}$: effective magnetic moment, $\tau_c$: molecular correlation time, $r$: metal-H distance.

$$\frac{1}{\tau_c} = \frac{1}{\tau_s} + \frac{1}{\tau_m} + \frac{1}{\tau_R} \qquad (3)$$

$\tau_s$: electronic correlation time, $\tau_m$: bound water protons residency time, $\tau_R$: metal ion electronic relaxation time.

## 1.3. Gadolinium - based MRI Contrast Agents

The rapid development of magnetic resonance imaging (MRI) technique and the application of paramagnetic metal complexes as contrast agents (CAs) have provided substantial enhancement of image quality and contrast between normal and pathologic tissues and organ function.[10] During the last three decades, due to the high magnetic moment caused by seven unpaired electrons, Gadolinium-based contrast agents (GBCAs) with a strong influence on $T_1$ relaxation of water protons, are routinely used in the clinics for positive enhancement in $T_1$-weighted MRI and were considered as very safe drugs.[11] In comparison with other pharmaceuticals, GBCAs are in favor of an excellent safety profile with a very low rate of severe adverse events (only 1 in 40,000 injections).[12] Consequently, approximately 40 % of all clinical MRI exams employ GBCAs for diagnostic and prognostic information. To date, nearly 50 tons of doses of gadolinium have been administered worldwide every year.[13]

Free gadolinium ions are highly toxic to biological systems; therefore, chelating agents or ligands must be incorporated to reduce toxicity and the risk of complex dissociation *in vivo*. The application of GBCAs was widely believed to be safely administered intravenously and excreted in the early 2000s.[14] However, recently nephrogenic systemic fibrosis (NSF) was identified as a severe late adverse reaction associated with exposure to gadolinium originated from linear GBCAs in patients with impaired renal function. Additionally, emerging studies demonstrated traces of gadolinium have been found in several organs including skin, bone and certain brain regions, which seem to occur dose-dependently while no dependence on age, weight, sex, renal function status and blood-brain barrier integrity.[15-22.] These findings resulted in restrictions and suspensions for some intravenous linear GBCAs, which have higher rates of Gd dechelation than macrocyclic GBCAs according to the European Medicine Agency's (EMA), Pharmacovigilance Risk Assessment Committee in 2017.[23] In Japan, the usage of GBCAs as a percentage of both types (linear and macrocyclic) has reduced strikingly

from 64.7% in 2014 to 24.7% in 2016.[24] Similarly, Health Canada announces that the use of macrocyclic GBCAs may be preferable in certain patients, in particular, those for whom repetitive MRI exams with CAs could be necessary, and vulnerable patients including pregnant women.[25] Furthermore, there is an ongoing discussion about the chronic tissue-related chronic symptoms from GBCAs exposure, termed as gadolinium deposition disease (GDD).[26-29] Thus, taking long term into consideration, other cells and organs, and immune system in particular, should be investigated concerning the potential gadolinium adverse effects which are not described or recognized currently. These critical complications as well as the low but accumulated contamination of rivers and drinking water by gadolinium [30-33] have motivated us to investigate low molecular weight iron(III) complexes, iron-based contrast agents (IBCAs) as alternatives for MRI, even though macrocyclic GBCAs are advocated for imaging and are continued to be considered as safe administrations.

Also worthy of note is that for Gd-based CAs, commercial ones applied compounds in clinical MRI practice, $r_1$ relaxivities typically decrease with increasing magnetic field strength (above 3 T) while $r_2$ effects become more predominate. In a consequence of fast rotational correlation rates at ultra-high fields.[34,35] In the study of Pietsch *et. al,* three macrocyclic GBCAs relaxivities decreased with increasing applied field strength by approximately -15% to -20% from 1.5 T to 7 T in human plasma and blood.[36] However, with the rapid development of techniques, ultra-high field strength MRI systems beyond 3 T have becoming clinically relevant. Higher fields result in greater signal to noise ratio and higher spatial resolution. In the Neurospin centre at CEA Saclay of France, a whole body 11.7 T MRI magnet was installed for neurological disease imaging.[37] Nevertheless, currently approved CAs are less effectively to meet the need at ultra-high field strengths.

Thus, despite the diagnostic benefit accomplished by GBCA-enhanced MR imaging, for rising safety concerns, there is a pressing urgency for clinical necessities to develop alternative MR imaging contrast agents, which are gadolinium-free and provide similar $T_1$-shortening effects for a substantial diagnostic need. In addition, contrast agents that could provide competent contrast enhancement to fulfil a broad spectrum of field strengths and particular in ultra-high magnetic field strengths will have to be developed.

## 1.4. Iron-based MRI Contrast Agents

Since early years, Gd(III) ion has been the primary focus for MR imaging contrast agents development, followed by Mn(II) and to a less extent by iron(III).[38]

Iron is a vital component for numerous fundamental biologic processes.[39] It is the most abundant transition metal in human body, involves oxidation-reduction reactions and metabolism related proteins, lipids carbohydrates and nucleic acids, which are essential for cellular and organ functions. Humans have mechanisms to keep free iron ions within limits. It is estimated that almost 4.0-5.0 g iron are present in a 70 kg healthy individual.[40,41] Accordingly, iron could be an outstanding option as non-gadolinium probe for MRI.

Besides having only five unpaired electrons instead of seven in gadolinium, conceivable advantages of iron(III) complexes for their application as $T_1$ contrast agents are the short distance between the ion metal centre and water protons, as well as the highly polarising nature of trivalent iron ion. The short metal-to-water proton distance will favour high $T_1$ relaxation with a $1/r^6$ according to equation (2). Moreover, according to NMRD profiles, the dispersion of iron(III) could shift to higher magnetic fields because of it the faster electron spin relaxation, while the relaxivity of classic Gd-based contrast agents show a modest to sharp decrease with increasing field strength.[34,42] It is noteworthy that for clinical imaging, 3 T imagers instead of 1.5 T show improved signal-to-noise ratio by 30-50% and contrast-to-noise up to 96%.[43,44] Therefore, new iron(III)-based $T_1$ contrast agents could work efficiently at high field scanners and provide high relaxivity over a range of field strengths given the increasing magnetic fields used in modern MRI scanners.

Iron (III) complexes with several coordinated organic molecules have been preclinically investigated since the availability of initial NMR imaging in 1980s.[45] Marotti *et. al* demonstrated iron (III)-based contrast agents (IBCAs) including Fe(EDTA), Fe(DTPA), Fe(CDTA) for urinary system MR imaging in rats in 1987.[46] After very limited attention during the past three decades, IBCAs have sparked considerable attention again in MRI contrast agents research due to their ubiquity in organisms and endogenous character with a well understood biochemistry and physiology.

Davies et al. generated iron(III)-catecholate derivative complexes and administered them to rats for $T_1$-weighted MR imaging and the IBCA showed substantially accumulation in the kidney.[47] Similarly, Miao *et. al.* reported IBCAs completed with polyDOPA-*b*-polysarcosine (PDOPA-*b*-PSar) copolymers with a longitudinal relaxivity comparable to GBCAs. A drawback in this study is peak enhancement after injection was 25 minutes in comparison with 5 mins for the standard GBCAs.[48] Recently, innovative iron (III) macrocyclic chelators coordinated with yeast-derived β-glucan particles (GPs) were recently reported as effective MRI contrast agents by the Morrow group. GPs could serve as an immune cells-targeted delivery vehicle and can be delivered to macrophages. These incorporated iron(III)-GPs produced enhanced T1 relaxivity at mildly acidic conditions. But the uptake and release of iron(III)-based particles in macrophages needed to be determined.[49] Wang and co-

workers presented that biochemically responsive MRI can be achieved by introducing redox-activatable $Fe^{3+/2+}$-PyC3A complexes. However, the oxidation efficacy between $Fe^{3+}$-PyC3A and $Fe^{2+}$-PyC3A in complex biological systems required further investigation.[50] Research from Morrow group focused on iron(III)-based triazacyclononane (TACN) macrocyclic complexes and tested coordinating sultanate or hydroxyl groups. These analysed as [Fe(L)X]X chelates showed stable solubility in acid solutions (pH<1) or in the blood. Noticeably, even with the increasing magnetic field strengths from 4.7 T to 9.4 T, Fe(L1)$(OH)_2$ $r_1$ relaxivity value remained nearly the same at 2.0 $mM^{-1}\cdot s^{-1}$. In comparison, the increase in field strengths significantly induced a decrease in the $r_1$ relaxivity value of Gd(DTPA) to 2.5 $mM^{-1}\cdot s^{-1}$ from 3.1 $mM^{-1}\cdot s^{-1}$. [51,52]

## 1.5. pH-responsive MRI Contrast Agents

Nowadays, thrust of preclinical research for MR imaging has shifted towards functional detection areas, including activatable and targeted contrast agents. Activatable GBCAs elicits relaxivity change in response to physiological events, triggered by an acidic pH, enzyme activities, temperature change, metal ion binding or redox environment, for instance. A common strategy is to alter the MR parameters: rotational correlation time in particular (such as $q$ and $\tau_R$), thereby switching the activatable contrast agents from the "off state" to the "on state".[53] Compared with the clinical utility of GBCAs that are referred as extracellular fluid (ECF) agents since they freely distribute through extravascular, all tissue extracellular space and have little specificity, the responsive CAs present advantages of visualizing dynamic biological processes and obtain pathology information as biomarkers for the early diagnosis and therapy evaluation.

A decreased extracellular pH value is a common characteristic of the microenvironment of various cancers as well as of chronic inflammatory diseases.[54] Accordingly, driving force from detecting cancer at early stage to reduce morbidity and mortality is propelling researchers to pursue the design of pH-responsive CAs to determine acidic tissue pH, particular in the approximate range between 5.5 and 6.8, since it is considered as a cancer biomarker. The strategy is focused on magnetization transfer by either endogenous or exogenous hydrogen donors. An early and effective pH-responsive MRI contrast agent, Gd-DOTA-4AmP$^{5-}$ was proposed by Sherry and colleagues with following extensive investigations.[55-58] The derivative of DOTA (1,4,7,10-tetraazacyclo-dodecane-N,N′,N″,N‴-tetraacetate ) with a non-coordinating amido-phosphonate moiety exhibited a 1.5 fold $r_1$ increase over the pH between 6 and 9.5. As a result of protonation of phosphonate groups provide catalytic exchange of Gd(III) bound water protons with those of bulk water.

## 1.6. Hepatobiliary MRI Contrast Agents

MRI is the most versatile non-invasive imaging modality for comprehensive assessment of focal liver lesions and diffuse liver diseases in clinical practice. Liver-specific GBCAs play a pivotal role in non-invasive imaging techniques to detect, characterize and stage hepatocellular lesions by improving the lesion-to-liver contrast. Studies of hepatocyte specific GBCAs showed satisfying performances in predicting postoperative early recurrence in hepatocellular carcinoma as well as in the evaluation of paediatric liver lesions.[59-63] To date, the only approved and worldwide vastly used $T_1$-enhancing contrast agents are gadobenate dimeglumine (Gd-BOPTA, MultihanceTM) and gadoxetic acid (Gd-EOB-DTPA, Primovist, Eovist). However, these two CAs are linear GBCAs and thus less stable than macrocyclic GBCAs, potentially causing a higher risk of toxic adverse reactions.

Brady and co-workers developed a series iron(III)-N,N′-ethylenebis[(2-hydroxyphenyl)glycine][Fe(EHPG)]$^-$ derivatives as paramagnetic hepatobiliary contrast probes for MRI.[38] The complexes displayed lipophilicity and high binging affinities to human serum albumin (HSA). Biodistribution and tissue relaxation time studies showed enhanced liver-to-blood ratio and excreted via biliary pathway in rats.[38,64] N,N′-bis(2-hydroxybenzyl)ethylenediamine-N,N′-diacetic acid (HBED) could form highly stable iron(III) chelates with a high binding coefficient (logK) of 39. Based on this character, HBED was under investigations as an iron chelator for the treatment of alcoholic liver disease.[65,66] Iron(III)-HBED is taken up and cleared primarily via liver which raised the interest of its evaluation as a liver-specific MRI CAs in preclinical studies.[67,68] Iron(III)-HBED complexes with a hydrogen bond in the outer coordination sphere as well as phenyl substituted ligand to increase nucleophilicity were designed and synthesized by Domagala group, which are expected as MRI contrast agents.[69] To further improve Iron(III)-HBED complexes relaxivity performance, Roberts and coworkers modified and proposed Iron(III)-HBED analogs. Improved MRI signal was achieved by increasing second sphere hydration with phosphoric acid moiety integration and incorporated hydrophilic substituents to reduce protein association. The biodistribution was evaluated in mice imaging studies of the kidney and liver. However, the $r_1$ of Fe-HBEDP-(CH2OH)3 is 1.5 $mM^{-1}\cdot s^{-1}$ at 1.5 T, which is the highest relaxivity among Fe-HEBD analogs, presumably because of the intermediate level of protein binding.[70] These studies spur extensive research to develop iron(III)-based hepatobiliary-specific contrast agents which are taken up by functional hepatocytes and then excreted through the biliary system for liver evaluation.

# 2. Motivation, Hypotheses and Objectives

## 2.1. Motivation

Despite the overwhelming success of Gd-based contrast agents, concerns of potential toxicity and long-term retention make the development of alternatives to Gd(III) desirable. Iron(III) is an outstanding metal for the generation of Gd-free MRI contrast agents based on its paramagnetic properties and biologic characters. Unlike in Gd(III), where the unpaired spins originate from inner electrons, the magnetic properties of iron(III) stem are from outer unpaired electrons.[42] Under this circumstance, the magnetic property of iron(III) is substantially determined by its coordination sphere with ligands. Our group has reported, IBCAs at slightly higher concentrations in comparison with GBCAs perform similar contrast effects in typical applications as dynamic contrast-enhanced MRI (DCE-MRI) and magnetic resonance angiography (MRA) with the same pulse sequence parameters for $T_1$-weighted imaging.[71] Notably, in the iron(III) complex of *trans*-cyclohexane diamine tetraacetic acid [Fe(*t*CDTA)]$^-$ manifested comparable enhancement by only doubling the typically administrated dose of Magnevist® (Bayer Healthcare, gadolinium diethylenetriaminepentaacetic acid (Gd-DTPA)) and showed similar pharmacokinetics and eliminations. Furthermore, in contrast to Fe(DTPA), where all coordination sides are fully saturated, in terms of [Fe(*t*CDTA)]$^-$ complex, one coordination side of *t*CDTA remains available for exchangeable coordination of water molecules, contributing to its relatively high $T_1$ effect.[71,72]

## 2.2. Hypotheses

Based on the encouraging results previously achieved with the [Fe(*t*CDTA)]$^-$ complex, the hypotheses for this thesis were:

- *t*CDTA can be chemically modified by coupling amine compounds to generate [Fe(*t*CDTA)]$^-$ complex derivatives.
- The new [Fe(*t*CDTA)]$^-$ derivatives will have improved or modified contrast properties, especially higher relaxivities.
- The [Fe(*t*CDTA)]$^-$ derivatives will retain the high iron(III) complex stabilities.
- Due to the structural similarity to Gd-EOB-DTPA (Primovist, Bayer Pharma AG), coupling of 4-*Ethoxyaniline* to *t*CDTA will result in a liver-specific [Fe(*t*CDTA)]$^-$ derivative.

## 2.3. Objectives

- *t*CDTA derivatives will be synthesised in two steps:
  - Mono-anhydride of *t*CDTA will be prepared by acetic anhydride with the presence of pyridine as proton acceptor.
  - *t*CDTA mono-anhydride will be coupled in different ratios with the amine-containing compounds ethylenediamine, *trans*-1,4-Diaminoclyclohexane and 4-Ethoxyaniline.
- After purification, the *t*CDTA derivatives will be validated and characterized by HPLC, IR and externally by MS and NMR.
- Iron(III) complexes will be prepared by reaction with iron(III) chloride.
- Stability of the new iron(III) complexes will be compared with $[Fe(tCDTA)]^-$ by absorption spectrometry under acid challenge.
- The $r_1$ and $r_2$ relaxivity of 5 iron(III) complexes in water and serum will be assessed on relaxometer and MRI scanners at currently relevant magnetic field strengths (1.5, 3 and 7 T).
- Effectiveness of [Fe(4-Ethoxyaniline-*t*CDTA)] as a hepatobiliary-specific contrast agent will be evaluated *in vivo*.

# 3. Methods

Unless stated otherwise, all regents and chemicals were obtained from Merck KGaA (Darmstadt, Germany).

## 3.1. Synthesis of trans-1,2-diaminocyclohexane-N,N,N',N'-tetraacetic acid mono anhydride (*t*CDTA-MA)

To a solution of acetic anhydride (12.87 mL, 136.2 mmol) and pyridine (2.75 mL, 34.0 mmol) was added trans-1,2-diaminocyclohexane-N,N,N',N'-tetraacetic acid (6.53 g, 17.9 mmol) (*t*CDTA; Carl Roth GmbH, Karlsruhe, Germany). The reaction mixture was stirred for 24 hours under an argon insert atmosphere at room temperature, then was filtered and washed by acetic anhydride followed by excess ethyl acetate. The residue was collected and dried in vacuo to give 5.30 g (81.2%) of the white solid *t*CDTA-MA.[73]

## 3.2. Synthesis and Characterization of Ligands

### 3.2.1. Synthesis of ethylenediamine-*t*CDTA monomer (*en*-*t*CDTA)

Small portions of solid *t*CDTA-MA (14.4 mmol, 5 g) were slowly added to a mixture solution of ethylenediamine (19.31 mL , 289 mmol) and DMSO (23.75 mL) over a period of six hours under argon atmosphere and then the mixture was stirred overnight at room temperature. After that, the reaction was evaporated to dryness under reduced pressure (8 mbar) to a thick orange oil which solidified upon standing. Purified 3.98 g (80%) of white powers were obtained by recrystallization in methanol at ambient temperature. A significant signal of 388.42/389.18 $[M+H]^+$ in MALDI mass spectrometry (MALDI-TOF/TOF 4700 Proteomics Analyzer, Applied Biosystems, Canada) confirms molecular anion of *en*-*t*CDTA (Figure 4). $^1$H-NMR (400 MHz, $D_2O$): 3.57 (s, 3H), 3.53 (s, 3H), 3.48 (s, 1H), 3.44 (s, 1H), 3.03 (t, 2H), 2.92 (m, 4H), 2.16 (m, 2H), 1.82 (m, 2H), 1.26 (m, 4H). $^{13}$C-NMR ($D_2O$): 170.88, 60.26, 50.86, 39.58, 24.17, 23.29. Elemental C,H,N-analysis [%]: C 43.94, H 8.12, N 15.07; calculated for $C_{16}H_{27}N_4O_7(NH_4)$ x 2 $H_2O$: C 43.98, H 7.84, N 15.23; max. deviation: 0.28.

### 3.2.2. Synthesis of ethylenediamine-*t*CDTA dimer (*en*-D*i*-*t*CDTA)

Small portions of solid *t*CDTA-MA (13.5 mmol, 4.66 g) were slowly added to a mixture solution of ethylenediamine (0.45 mL, 6.7 mmol), DMSO(22.15 mL) and pyridine (4.36 mL, 53.9 mmol) over a period of six hours under argon atmosphere and then the mixture was stirred overnight at room temperature. Extraction with excess ethanol, washing, drying and purified by semi-preparative HPLC (5 mM ammonium bicarbonate buffer with pH 7.78, 2-66% acetonitrile gradient over 20 min). The fractions containing *en*-D*i*-*t*CDTA were identified by HPLC and lyophilized. MALDI mass spectrometry measurements (MALDI-TOF/TOF 4700 Proteomics Analyzer, Applied Biosystems, Canada) confirmed the expected/measured signal of 716.74/699.11 $[M+H]^+$ -18 (dehydration, see results and Figure 4). $^1$H-NMR (400 MHz, D2O): 3.65-3.85 (16H), 3.35 (m, 4H), 3.08 (m, 4H), 2.17 (m, 4H), 1.84 (m, 4H), 1.29 (m, 8H).). Elemental C,H,N-analysis [%]: C 46.72, H 7.02, N 10.96; calculated for $C_{30}H_{47}N_6O_{14}Na$ x 2.15 $H_2O$: C 46.35, H 6.65, N 10.81; max.

### 3.2.3. Synthesis of *trans*-1,4-diaminocyclohexane-*t*CDTA monomer (*trans*-*t*CDTA)

Small portions of solid *t*CDTA-MA (6.93 mmol, 2.4 g) were slowly added to a solution of DMSO (18.24 mL) in the presence of *trans*-1,4-Diaminoclyclohexane (3.17 g, 27.7 mmol) under argon at approx. 90 °C in 6 hours and stirred for another 4 hours. The mixture was stirred continuedly overnight. After evaporation under reduced pressure (8 mbar) to give an ashen solid. Completely dissolved in methanol, then a precipitate formed after approx. 48 hours at ambient temperature. The precipitate was further washed by methanol several times to yield a white solid 1.89 g (79%). MALDI mass spectrometry measurements (MALDI-TOF/TOF 4700 Proteomics Analyzer, Applied Biosystems, Canada) confirmed the expected/measured signal of 442.51/443.26 $[M+H]^+$ (Figure 4). $^1$H-NMR (400 MHz, D2O): 3.55 (m, 8H), 2.93 (m, 2H), 2.16 (m, 2H), 2.07 (m, 2H), 1.83 (m, 2H), 1.50 (m, 8H), 1.25 (m, 4H). $^{13}$C-NMR ($D_2O$): 172.94, 170.24, 63.16, 60.10, 54.75, 49.08, 48.41, 29.11, 27.98, 24.12, 24.04. Elemental C,H,N-analysis [%]: C 51.09, H 8.3, N 13.19; calculated for $C_{20}H_{34}N_4O_7$ x 0.5 $NH_3$ x 1.15 $H_2O$: C 50.92, H 8.08, N 13.36; max. deviation: 0.22.

### 3.2.4. Synthesis of *trans*-1,4-diaminocyclohexane-*t*CDTA dimer (*trans*-D*i*-*t*CDTA)

Small portions of solid *t*CDTA-MA (17.9 mmol, 5.16 g) were slowly added to a solution of *trans*-1,4-diaminocyclohexane (7.4 mmol, 0.85 g) in pyridine (4.82 mL, 59.6 mmol and DMSO(58.80 mL) within 6 hours. The reaction mixture was stirred overnight under argon at ambient temperature. After solvent evaporation, a whitish solid was obtained. Then the residue was filtrated with ethanol, the filtrate was collected and lyophilized to give the pure white powder. The MALDI mass spectrometry

measurements (Mikroflex MALDI mass spectrometer, Bruker, Germany) confirmed the expected/measured signal of 770.83/771.18 $[M+H]^+$ (Figure 4). $^1$H-NMR (400 MHz, D2O): 3.36 (m, 4H), 3.13 (m, 12H), 2.95 (m, 4H), 2.32 (m, 4H), 1.94 (m, 4H), 1.87 (m, 2H), 1.68 (m, 8H), 1.30 (m, 8H). $^{13}$C-NMR ($D_2O$): 172.68, 60.34, 52.57, 47.73, 38.77, 25.12, 23.47. Elemental C,H,N-analysis [%]: C 47.62, H 7.15, N 9.01; calculated for $C_{34}H_{55}N_6O_{14}(HCO_3)$ x 3.2 $H_2O$: C 47.21, H 7.06, N 9.44; max.

### 3.2.5. Synthesis of 4-Ethoxyaniline-*t*CDTA monomer (4-ethoxyaniline-*t*CDTA)

Small portions of solid *t*CDTA-MA (9.12 mmol, 3.16g) were slowly added to 4-ethoxyaniline (23.49 mL, 182 mmol) under argon atmosphere within 6 hours, and the stirring was continued at ambient temperature. After reaction, the mixture was completely dissolving in absolute diethyl ether. Afterwards, precipitation was formed at the ambient temperature, washing with diethyl ether to yield a white solid of 4-ethoxyaniline-*t*CDTA , which was purified by Dionex™ OnGuard™ II H Cartridges, 2.5 mL (Thermo Scientific™, Germany) to remove the excess of 4-ethoxyaniline starting component. The effluent was then collected and lyophilized to give a white powder. The MALDI mass spectrometry measurements (Mikroflex MALDI mass spectrometer, Bruker, Germany) confirmed the expected/measured signal of 466.2/466.108 $[M+H]^+$ (Figure 4).

## 3.3. Preparation of Iron(III) Complexes

Trivalent metal complexes were generated by addition of the *t*CDTA chelating agents (see above) to a stoichiometric equivalent of $FeCl_3$ solution to bound with the metal centers (1:1 ratio as monomers versus 2:1 ratio as dimers). The pH of the solution was adjusted to 7.4 slowly with the saturated meglumine. After 24 hours, the excess insoluble iron(III) hydroxide was removed by centrifuging resulting iron complexes solutions over 20 mins at 13,800 g, and after which they were passed through 0.45 µm syringe filters.

## 3.4. HPLC Analysis

After purification, the chelators were analyzed by reverse-phase high-performance liquid chromatography (HPLC) via a DIONEX UltiMate 3000 system. The performed conditions and results are given in the following results chapter. Samples were accessed by absorption detection at 210 nm through a diode array detector (DIONEX UltiMate 3000).

## 3.5. Mass Spectrometry Analysis of Ligands

In addition to HPLC evaluation, these *t*CDTA derivatives were determined by MALDI-TOF mass spectrometry on the reflector mode at 4700 Proteomics Analyzer (Applied Biosystems) and Microflex LRF (Bruker Daltonics) instruments. Analyses were performed by the Shared Facility of Mass Spectrometry of the Institute of Biochemistry, Charité - Universitätsmedizin Berlin. The measurement results are reported in the following results chapter.

## 3.6. Infrared Spectroscopy

IR spectra of lyophilized substances were obtained by a Bruker Compact FT-IR spectrometer ALPHA-P with the OPUS software (OPUS 6.5, Bruker Optik GmbH, Germany).

## 3.7. NMR

NMR spectra were acquired using a Bruker AV 400 NMR spectrometer (1H and 13C 400 MHz) with $D_2O$ as solvent at room temperature. Chemical shifts are presented in ppm referenced to residual proton signals of $D_2O$ (4.8 ppm). For *trans*-D*i*-*t*CDTA performance, the sodium salt was added, by the cause of low solubility of the free acid.

## 3.8. Stability Determination

In order to determine the stability of the iron compounds, the changes of absorption spectra in the range of 220 and 500 nm over time with challenge of 100 mM HCl according to Snyder et al. {Snyder et al., 2019, #33283} were compared. In addition, the absorption spectra of $FeCl_3$ in 100 mM HCl, *t*CDTA in 100 mM HCl, and Fe-*t*CDTA in 1 M HCl were paralleled as well.

## 3.9. Cyclic Voltammogram Analysis

Electrochemical experiment was recorded by a PalmSens EmStat Blue potentiostat in a practical one-compartment three electrodes cell: a glassy carbon electrode (ID 1.6 mm) for the working electrode, a platinum bead (5 x 5 mm) for the counter electrode, and a silver wire in aqueous AgCl solution for the pseudo-reference electrode. All procedures were implemented in demonized and degassed

$H_2O$ solutions with the presence of 0.1 M KCl at pH 5.9 under argon condition at room temperature. The voltammograms scan rate was 0.1 V/s.

## 3.10. Relaxivity Measurement by Relaxometer

For relaxivity measurement, all iron complexes were diluted in water or fetal calf serum (FCS, Gibco, Thermo Fisher Scientific, Rockford, IL) at concentrations of 0.125, 0.25, 0.5, and 1.0 mmol/L, at pH 7.4, and loaded into glass NMR tubes (5 mm outside diameter; Wilmad-Lab Glass company). Measurements at 0.94 T measurements were performed using an NMR relaxometer (Bruker Minispec mq 40, Karlsruhe, Germany) according to the manufacturer's instructions. For measurements of the pH dependence, samples of $Fe^{3+}$-*en*-*t*CDTA in the concentrations above were dissolved in water or FCS and adjusted to the different pH values.

## 3.11. Relaxivity Measurement by MR imaging Scanners

The relaxivities of newly generated complexes were determined at 1.5 T, 3 T, and 7 T MR imaging scanners. Up to 7 samples were prepared and placed in a circular phantom holder at ambient temperature. For relaxivity measurements at 37 ℃, the phantom holder and prepared samples were kept at 37 ℃± 1℃ during the MR measurements by water heating supply, temperature was monitored using a fiber optic temperature probe. At 1.5 T (MAGNETOM Sonata, SIEMENS, Erlangen, Germany) and 3 T (MAGNETOM Lumina SIEMENS, Erlangen, Germany) scanners, T1-weighted images were acquired by a standard 2D spin echo sequence. Different repetition times (TRs) of 100, 150, 300, 600, and 1000 milliseconds were applied to obtain $T_1$ times and to calculate $r_1$ relaxivities. Echo time (TE) was 11 milliseconds for 1.5 T and 13 milliseconds for 3 T, respectively. Left imaging parameters were: an imaging matrix of 256 × 256 was employed with a field of view of 75 × 75 $mm^2$, slice thickness was 5 mm. The $T_1$-weighted maps were analyzed by the acquired image datasets using ImageJ software (National Institutes of Health NIH, USA) with the MRI Analysis Calculator plug-in from Karl Schmidt (kfschmidt@bwh.harvard.edu, 2002/06/19).

For 7 T MR imaging experiment, a BioSpec small animal MRI scanner (Bruker, Ettlingen, Germany) with a built-in dedicated multi-TR spin echo sequence (TRs : 25, 72, 125, 186, 258, 346, 459, 617, 882, and 2000 milliseconds; TE 9.0 milliseconds; matrix 256 × 256; FOV 50 mm; slice thickness 1 mm) was introduced to generate $T_1$ map. The $T_1$ times of the investigated compounds were acquired by circular regions of interest (ROI) of constant size placed in the center of the cross sections of each phantom in the $T_1$-weighted images.

The values of $T_1$ and $T_2$ were acquired based on linear regression calculation from 1/T vs. metal ion concentration of the iron complexes using Prism software in GraphPad (Version 5.0a).

## 3.12. Molecular Modeling

Perspective molecular structures of the new generated complexes was illustrated on the basis of reported $Fe^{3+}$-*t*CDTA[72] X-ray crystal structure using Marvin software (version 19.17, 2019, ChemAxon (www.chemaxon.com)) and PyMOL Molecular Graphics System (version 1.8.2.1. Open Source, on Apple Quartz 2.7.11 X Window System).

# 4. Results

## 4.1. Generation of *t*CDTA derivatives

In this work, I deploy a two-steps synthetic route, developed by Gestin *et.al* [73] to obtain *t*CDTA derivatives (Figure 2). Commencing from commercially available *t*CDTA, acetic anhydride and involving pyridine as proton acceptor, followed by filtration by acetic anhydride and excess of ethyl acetate to remove dianhydrides, was the first step to prepare a mono anhydride of *t*CDTA (*t*CDTA-MA). Reaction of the carboxylic acid anhydride moiety on *t*CDTA-MA either with an excess of or with less than half-molar amount of the diamine compounds resulted in amide bond formation, generating monomers (named as the 1:1 addition target obtains) or dimers (named as the 2:1 addition target obtain). By this means, the reaction with ethylenediamine brought out the monomer ethylenediamine-*t*CDTA (*en*-*t*CDTA, Figure 2B, MW 388.42) and the dimer ethylenediamine-D*i*-*t*CDTA (en-D*i*-*t*CDTA, Figure 2C, MW 716.74). In the same manner, reacting *t*CDTA-MA with exceeding *trans*-1,4-diaminocyclohexane generated the monomer *trans*-1,4-diaminocyclohexane-*t*CDTA (*trans*-*t*CDTA, Figure 2D, MW 442.51) whereas reaction with a half-molar amount of *trans*-1,4-diaminocyclohexane ended in the dimer *trans*-1,4-diaminocyclohexane-Di-*t*CDTA (*trans*-D*i*-*t*CDTA, Figure 2E, MW 770.83). Reaction with of 4-ethoxyaniline in excess generated the monomer ethoxyaniline-*t*CDTA (Figure 2F, MW 465.21).

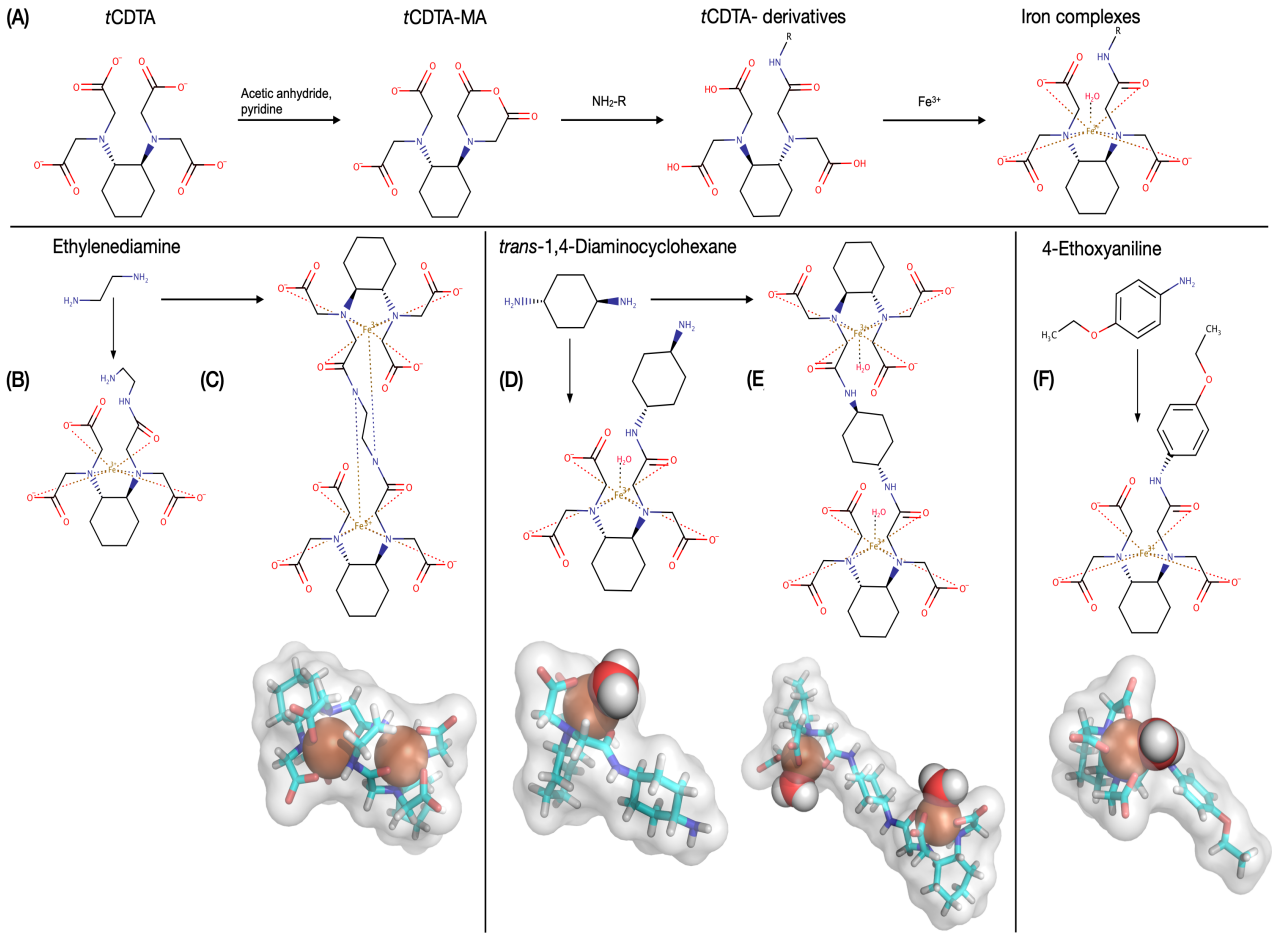


**Figure 2.** (A) Two-step synthesis of *t*CDTA chelator derivatives. (B-F) Chemical structures and conceivable molecular models of 5 different carboxamide derivatives of *t*CDTA.[1]

## 4.2. Validation and Performance Analysis

### 4.2.1. Purity and Validation Analysis

The purities of the resulting amides were determined from reverse phase HPLC measurements (Figure 3) with the following peak area percentages: en-*t*CDTA: 98.1%, en-D*i*-*t*CDTA: 96.6%, *trans*-*t*CDTA: 99.0%, *trans*-D*i*-*t*CDTA: 98.4% and ethoxyaniline-*t*CDTA 98.0%.

The absence of relevant residuals of the *t*CDTA precursor in the products, was an important precondition for further characterisation, in particular for relaxivity measurements to leave out contributions from the corresponding iron compound. The successful synthesis and isolation of the products was confirmed by MALDI mass spectrometry (Figure 4), along with $^{1}H$ and $^{13}C$ NMR (Figure 5) and elemental analysis. The prime mass peaks of en-D*i*-*t*CDTA (and to a very small extent also those of *en*-*t*CDTA) were reduced by 18 Da, which can be attributed to dehydration in the MALDI mass

spectrometry analyzasion.[74] For verification, infrared spectrometry (Figure 6) was conducted to validate the IR spectra of *t*CDTA, *t*CDTA-MA, *en*-*t*CDTA, *en*-D*i*-*t*CDTA, and ethoxyaniline-*t*CDTA in comparison. As expected, the distinctive bands for anhydrides was exclusively for the *t*CDTA-MA probe.

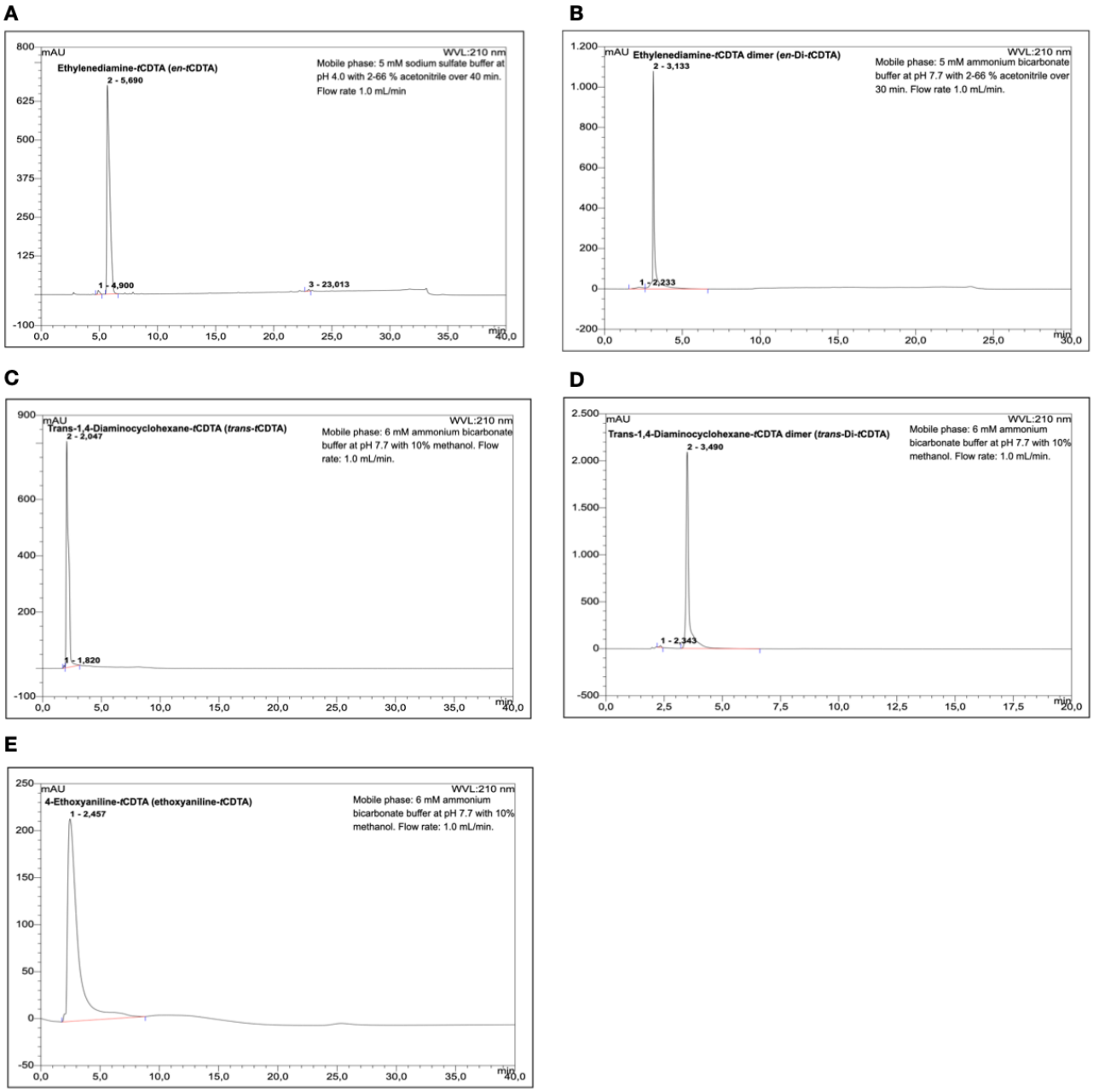


**Figure 3. HPLC analysis of purified compounds.** (A) Ethylenediamine-*t*CDTA (*en*-*t*CDTA), (B) Ethylenediamine-*t*CDTA dimer (*en*-Di-*t*CDTA), (C) Trans-1,4-Diaminocyclohexane-*t*CDTA (*trans*-*t*CDTA), (D) Trans-1,4-Diaminocyclohexane-*t*CDTA dimer (*trans*-Di-*t*CDTA), (E) 4-Ethoxyaniline-*t*CDTA (ethoxyaniline-*t*CDTA). All HPLC analyses were performed using a reverse phase Nucleosil® 120-5C18 column (5 µm particle, 25 cm length, 4.6 mm diameter). Samples were detected by absorption measurement using a diode array detector at 210 nm.

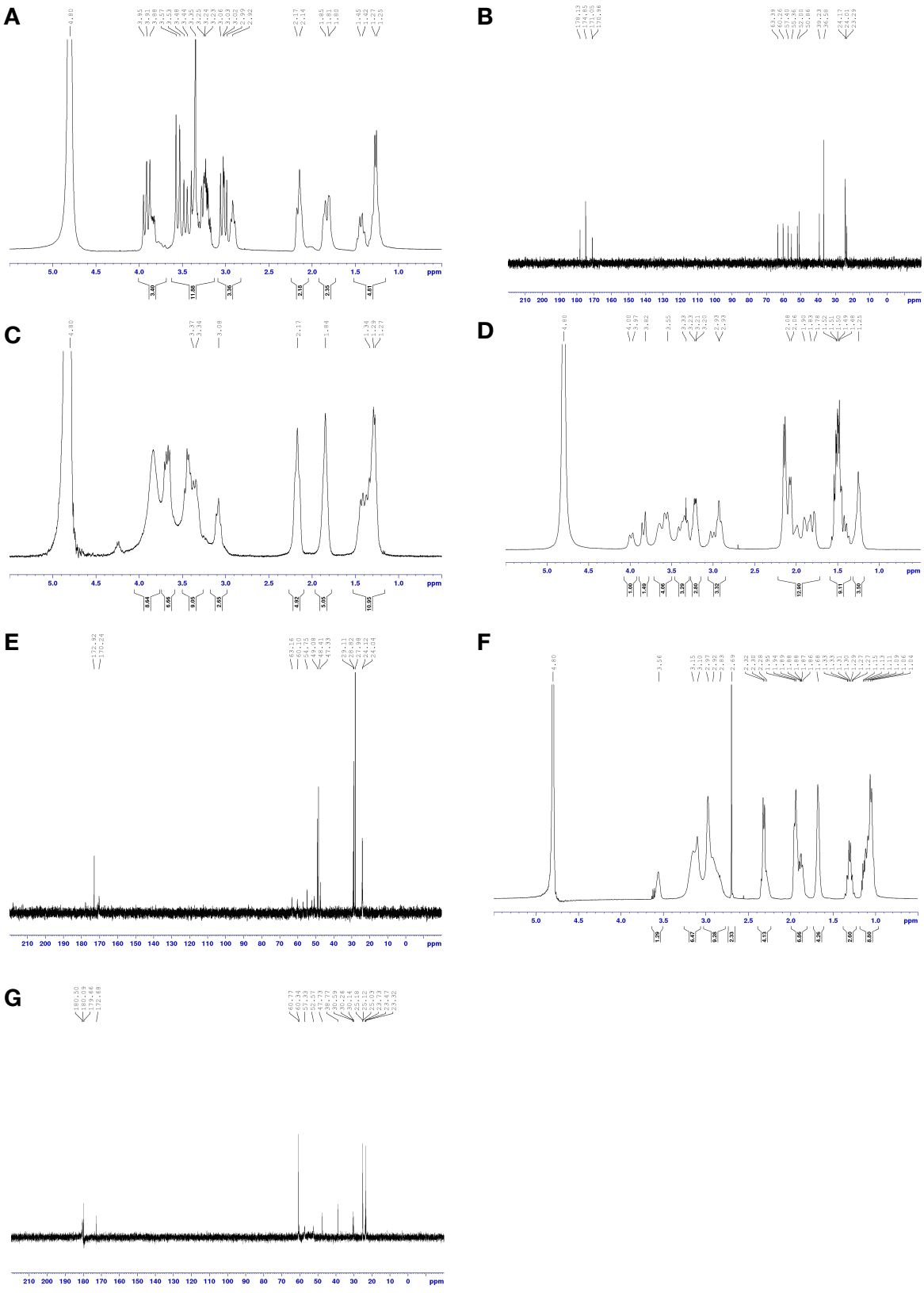


**Figure 4. Nuclear magnetic resonance analysis.** (A) $^{1}H$ NMR of *en-t*CDTA in $D_2O$. (B) $^{13}C$ NMR of *en-t*CDTA in $D_2O$. (C) $^{1}H$ NMR of *en*-Di-*t*CDTA in $D_2O$. (D) $^{1}H$ NMR of *trans-t*CDTA in $D_2O$. (E) $^{13}C$ NMR of *trans-t*CDTA in $D_2O$. (F) $^{1}H$ NMR of *trans*-Di-*t*CDTA neutralized with NaOH in $D_2O$. (G) $^{13}C$ NMR of *trans*-Di-*t*CDTA neutralized with NaOH in $D_2O$. (Provided by Prof. Dr. Christian Limberg, Department of Chemistry, Humboldt - Universität zu Berlin)

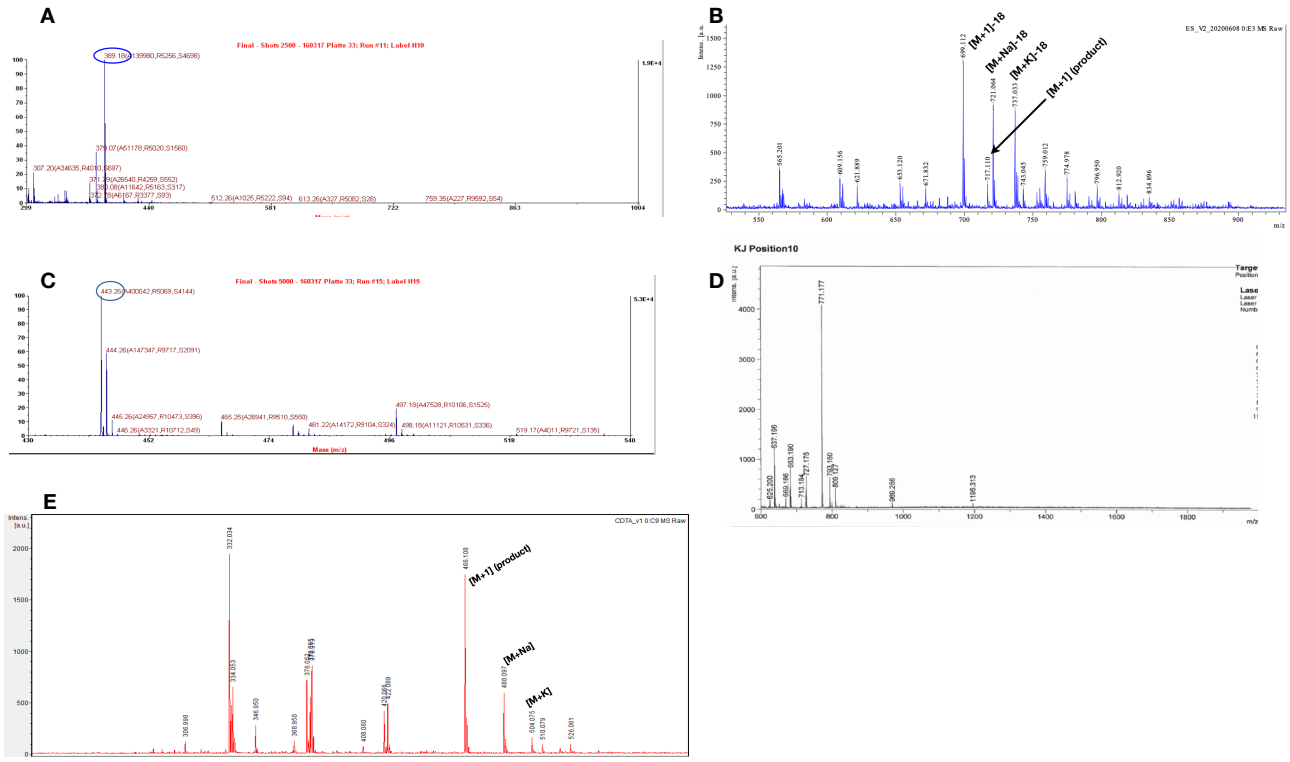


**Figure 5. Mass spectrometry.** (A) *en*-*t*CDTA, MW 388.42. (B) *en*-Di-*t*CDTA, MW 716.74. (C) *trans*-*t*CDTA, MW 422.51. (D) *trans*-Di-*t*CDTA, MW 770.83. (E) ethoxyaniline-*t*CDTA, MW 465.21. MALDI matrix: α-cyano-4-hydroxycinnamic acid. (Provided by Dr. Katharina Janek, Institut für Biochemie, Charité - Universitätsmedizin Berlin)

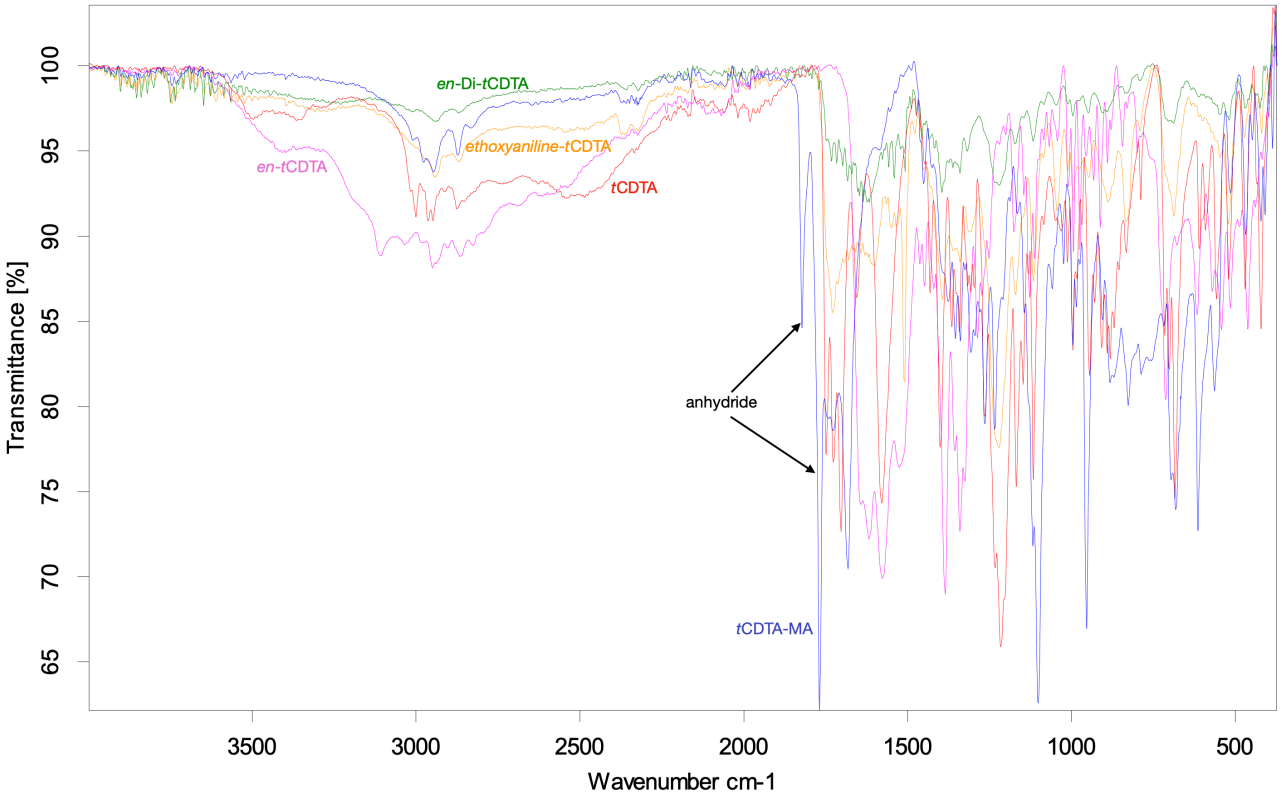


**Figure 6. Infrared spectroscopy analysis of iron(III) complexes of *t*CDTA and new derivatives.** The black arrows illustrate that for *t*CDTA-MA contains anhydrides groups exclusively.

### 4.2.2. Complex Stability Measurements

To prepare the iron(III) complexes, the chelators was stirred with iron(III) chloride and neutralized with meglumine. The new iron complexes stabilities were compared with that of [Fe(*t*CDTA)]$^-$, taking published high complex stability constant Log K of [Fe(*t*CDTA)]$^-$ , 27.5[75] or 29.3[76] as references. Figure 7 shows the dissociation of [Fe(*t*CDTA)]$^-$ (A), [Fe(*en*-*t*CDTA)]$^+$ (B), [Fe(*trans*-*t*CDTA)]$^+$ (C),

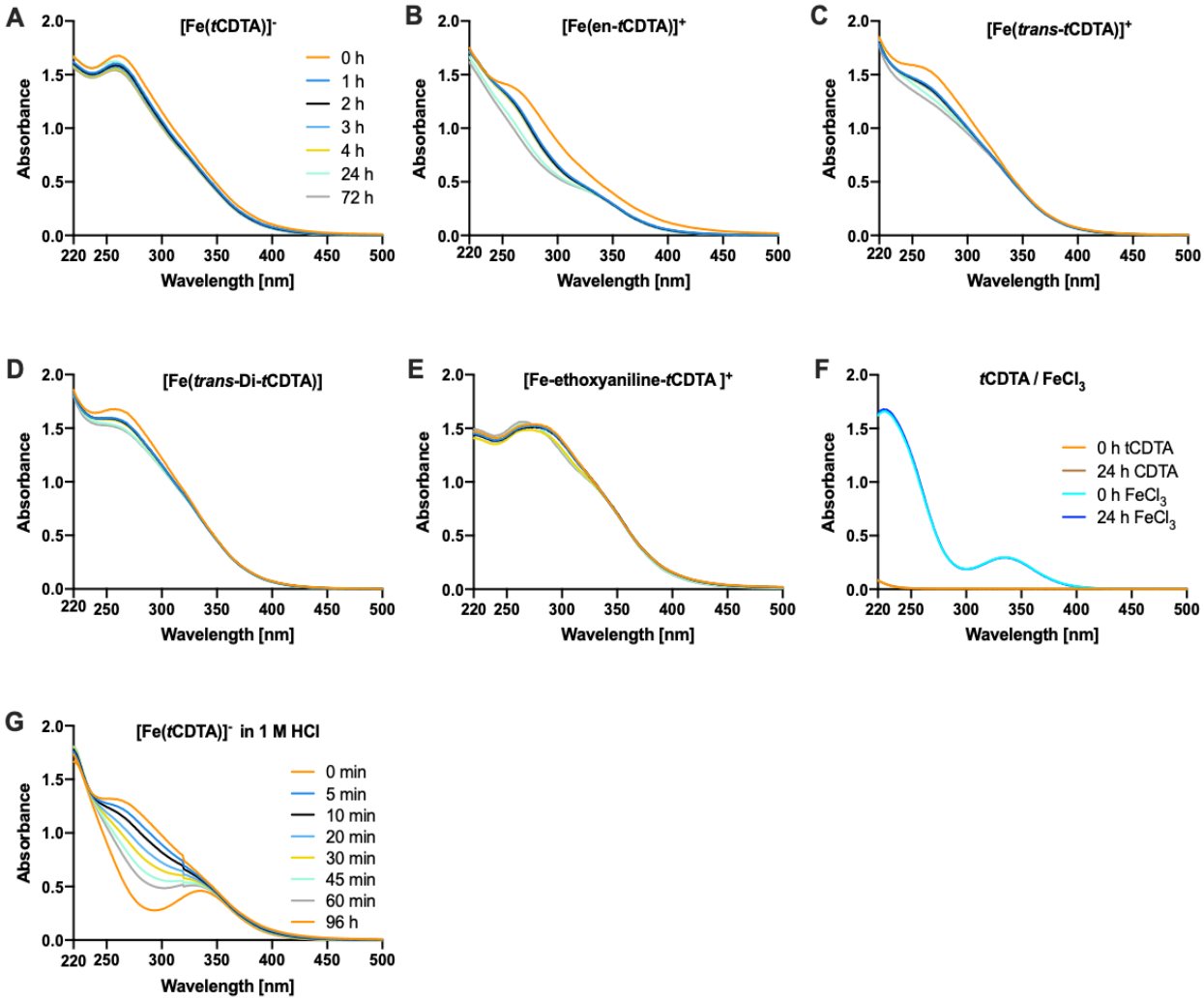


**Figure 7.** Comparison of kinetic stabilities of the iron(III) complexes of ***t*CDTA and new derivatives over time under acid challenge.** (A-E) Solutions contained iron complexes (1.0 mM Fe) dissolved in 100 mM HCl. Observing the reduction of absorbance at 300 nm according to Snyder *st at.*[24] (E) Minimum absorption of free $FeCl_3$ is at 300 nm and below 250 nm is for *t*CDTA (both in 100mM HCl). (F) [Fe(*t*CDTA)]$^-$shows a time-depending dissociation in stark treatment with 1 M HCl. All Fe(*t*CDTA)]$^-$ derivatives were stable at 100 mM HCl. [Fe(*t*CDTA)]$^-$, iron(III) complex of trans-cyclohexane diamine tetraacetic acid; [Fe(en-*t*CDTA)]$^+$, iron(III) complex of ethylenediamine-*t*CDTA; [Fe(trans-*t*CDTA)]$^+$, iron(III) complex of *trans*-1,4-diaminocyclohexane-*t*CDTA; [Fe(*trans*-Di-*t*CDTA)], iron(III) complex of *trans*-1,4-diaminocyclohexane-Di-*t*CDTA. [Fe(ethoxyaniline-*t*CDTA)], iron(III) complex of 4-Ethoxyaniline.

[Fe(*trans*-D*i*-*t*CDTA)] (D) and [Fe(4-ethoxyaniline-*t*CDTA)] (E), which was monitored by absorption spectra measurement (0.1 mM Fe) over time during a challenge with 100 mM HCl and observing the absorbance decrease at 300 nm on the report of Snyder *et al.*[52] (F) as reference, free $FeCl_3$ and *t*CDTA has an absorption minimum at 300 nm, and below 250 nm, separately (both in 100 mM HCl). Since the complexes remained stable in 100 mM HCl, a time-dependent dissociation of $[Fe(tCDTA)]^-$ with stark treatment in 1M HCl was further studied to demonstrate dissociation (F), all tested iron(III) complexes showed merely slight initial absorbance changes in 100 mM HCl and thus differed from iron(III) chloride in 100 mM HCl and to $[Fe(tCDTA)]^-$ in 1 M HCl, indicating the notable stabilities for all $[Fe(tCDTA)]^-$ derivatives in 100 mM HCl.

### 4.2.3. Cyclic Voltammograms

The redox properties of new $[Fe(tCDTA)]^-$ derivatives were analysed by cyclic voltammetry with a glassy carbon-based electrode and KCl as a supporting electrolyte as shown in Figure 8. All three complexes produced one reversible redox wave in the anodic scan (Ea ≈ +0.06 V for $[Fe(tCDTA)]^-$ and around + 0.1 V for the other complexes). In comparison of reversible cathodic waves of $[Fe(tCDTA)]^-$ and $[Fe(trans\text{-}tCDTA)]^+$, the other two compounds displayed two small cathodic peak potentials, implying two distinctive species presence. The peak potentials detected for the oxidation/reduction reactions were yielded (referenced to an Ag/AgCl electrode) and Half-wave potentials E1/2 between - 0.05 and 0.06 V were shown in Table 1.

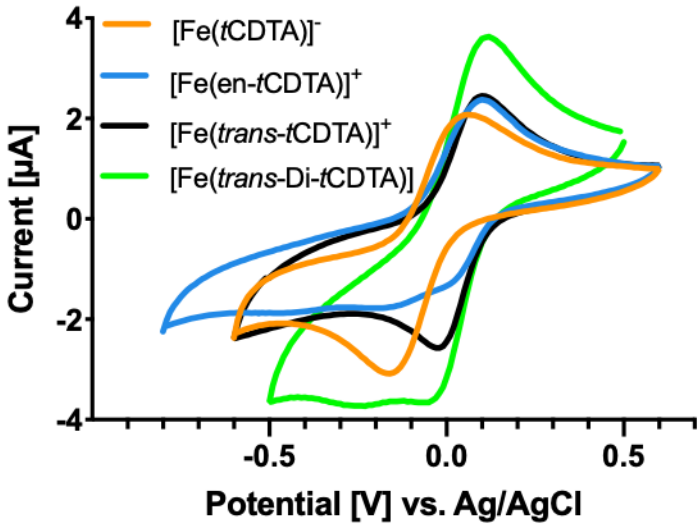


**Figure 8. Cyclic voltammograms of** $[Fe(tCDTA)]^-$ and its derivatives **at neutral pH.** Solutions contained 1.0 mM of the compounds and 100 mM KCl as the supporting electrolyte. Scan rate is 100 mV/s.[1] (Provided by Prof. Dr. Christian Limberg, Department of Chemistry, Humboldt - Universität zu Berlin)

| Complex | $E_a$ | $E_c$ | $E_{1/2}$ |
|---|---|---|---|
| Fe-tCDTA | 0.058 | -0.16 | -0.051 |
| Fe-en-*t*CDTA | 0.100 | 0.03 | 0.065 |
| Fe-*trans*-*t*CDTA | 0.100 | -0.018 | 0.040 |
| Fe-*trans*-Di-*t*CDTA | 0.109 | -0.037 | 0.036 |

**Table 1. Cyclic voltammograms. Cathodic, anodic and half-wave potentials of iron-complexes.** Half-wave potential (E1/2) was determined according to the following equation: $E_{1/2} = (E_c+E_a)/2$. $E_c$: cathodic peal potential, $E_a$: anodic peak potential. All peak potentials are reported vs. Ag/AgCl reference electrode.[1] (Provided by Prof. Dr. Christian Limberg, Department of Chemistry, Humboldt - Universität zu Berlin)

## 4.3. Evaluation of Contrast Properties by Relaxometer and MRI Measurements

### 4.3.1. IBCAs with Enhanced Properties : Increased $T_1$ Relaxivities at Higher Magnetic Field Strength and pH Sensing

To characterise the magnetic properties in comparison to we performed relaxometry and MRI measurements of the complexes in the range of clinically available magnetic field strengths from 1.5 to 7 T (Table 2). The iron(III)-based compounds of the chelators *en*-*t*CDTA (Figure 2B) and *en*-D*i*-*t*CDTA (Figure 2C), that were produced with ethylenediamine, showed relatively low relaxivities at 0.94 T and neutral pH versus [Fe(*trans*-*t*CDTA)]$^+$ (Figure 2D) and [Fe(*trans*-D*i*-*t*CDTA)] (Figure 2E) had similar relaxivities as [Fe(*t*CDTA)]$^-$ at the same field strength. But which worth the whistle is that the $r_1$ values increased substantially within the increasing field strengths and were highest at 7 T for the [Fe(*trans*-D*i*-*t*CDTA)] (Figure 2E) gave 4.71 ±0.37 L·mmol$^{-1}$·s$^{-1}$ per iron and 9.42 ±0.74 L·mmol$^{-1}$·s$^{-1}$ per dimeric molecule in serum and 3.80 ±0.04 L·mmol$^{-1}$·s$^{-1}$ / 7.60 ±0.08 L·mmol$^{-1}$·s$^{-1}$ in water (Table 2). MRI phantoms images of [Fe(*trans*-*t*CDTA)]$^+$ (Figure 9A, B), [Fe(*trans*-D*i*-*t*CDTA)] (Figure 9C, D) and [Fe(4-ethoxyaniline-*t*CDTA)] (Figure 9E, F) illustrate the contrast effects at different concentrations at neutral pH in water and in serum, separately.

| Field strength (temperature) | Solvent | *t*CDTA | Ethylenediamine-*t*CDTA | Ethylenediamine-Di-*t*CDTA | *Trans*1,4-Diaminocyclohexane-*t*CDTA | *Trans*1,4-Diaminocyclohexane-*t*CDTA-Dimer | 4-Ethoxyaniline-*t*CDTA |
|---|---|---|---|---|---|---|---|
| 0.94 T 37°C | r1 in water | 1.56 ± 0.28 | 0.82 ± 0.26 | 1.24 ± 0.05<br>(2.48 ± 0.10) | 1.92 ± 0.10 | 1.99 ± 0.10<br>(3.98 ± 0.20) | 1.43 ± 0.05 |
| | r1 in serum | 1.99 ± 0.13 | 0.72 ± 0.02 | 1.44 ± 0.03<br>(2.88 ± 0.06) | 2.01 ± 0.04 | 2.18 ± 0.04<br>(4.36 ± 0.08) | 1.95 ± 0.07 |
| | r2 in water | 1.72 ± 0.06 | 0.85 ± 0.57 | 1.50 ± 0.08<br>(3.00 ± 0.16) | 2.16 ± 0.09 | 2.25 ± 0.29<br>(4.50 ± 0.58) | 1.56 ± 0.01 |
| | r2 in serum | 2.79 ± 0.36 | 0.75 ± 0.03 | 1.68 ± 0.01<br>(3.36 ± 0.02) | 2.49 ± 0.09 | 2.73 ± 0.03<br>(5.46 ± 0.06) | 2.09 ± 0.17 |
| 1.5 T 23°C | r1 in water | – | – | – | 2.27 ± 0.01 | 2.75 ± 0.21<br>(5.50 ± 0.42) | 1.83 ± 0.10 |
| | r1 in serum | – | – | – | 2.74 ± 0.03 | 3.26 ± 0.41<br>(6.52 ± 0.82) | 2.10 ± 0.12 |
| 3 T 37°C / 23°C | r1 in water | 2.07 ± 0.08 / 2.06 ± 0.13 | – | – | 2.64 ± 0.04 / 2.64 ± 0.37 | 2.99 ± 0.32 / 2.80 ± 0.03<br>(5.98 ± 0.64 / 5.60 ± 0.06) | 1.85 ± 0.26 / 1.86 ± 0.17 |
| | r1 in serum | 2.35 ± 0.03 / 2.46 ± 0.17 | – | – | 3.06 ± 0.07 / 3.08 ± 0.06 | 3.39 ± 0.16 / 3.53 ± 0.02<br>(6.76 ± 0.32 / 7.06 ± 0.04) | 2.10 ± 0.23 / 2.17 ± 0.10 |
| 7 T 37°C / 23°C | r1 in water | 1.87 ± 0.04 / 1.88 ± 0.07 | – | – | 2.38 ± 0.07 / 3.40 ± 0.00 | 2.65 ± 0.15 / 3.80 ± 0.04<br>(5.30 ± 0.30 / 7.60 ± 0.08) | 1.77 ± 0.07 / 2.70 ± 0.28 |
| | r1 in serum | 2.71± 0.07 / 2.79 ± 0.04 | – | – | 2.641± 0.26 / 3.88 ± 0.07 | 3.23 ± 0.35 / 4.71 ± 0.37<br>(6.46 ± 0.70 / 9.42 ± 0.74) | 2.13 ± 0.26 / 3.66 ± 0.14 |

**Table 2. Relaxivitity values of** [Fe(*t*CDTA)]$^{-}$ **derivatives [mM$^{-1}$S$^{-1}$] per metal ion determined at 0.94, 1.5, 3.0 and 7.0 T** (for dimers per molecule in brackets).All measurements were performed in FCS or buffer-free water at pH 7.4,

$r_1$, $T_1$ relaxivity; $r_2$, $T_2$ relaxivity; T, Tesla; *t*CDTA, trans-cyclohexane diamine teraacetic acid.

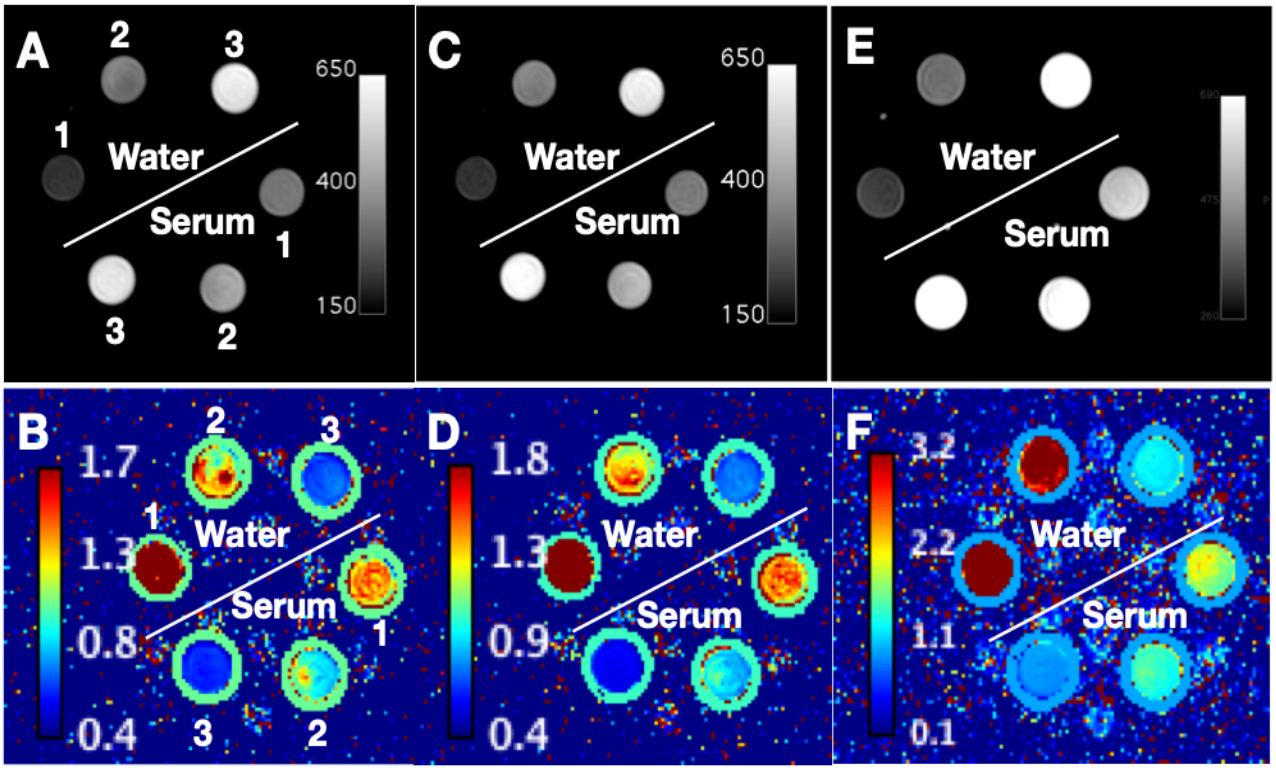


**Figure 9. $T_1$-weighted MR phantom imaging.** [Fe(*trans*-*t*CDTA)]$^+$ (A, B) , [Fe(*trans*-Di-*t*CDTA)] (C, D) and Fe(4-*ethoxyaniline*-*t*CDTA)]$^+$ (E, F) in 3 Fe concentrations (1: 125 µM, 2: 250 µM, and 3: 500 µM) at 3 T in water or 100% FBS at neutral pH, 37°C. [1]

Surprisingly, in water (Figure 10A), the $T_1$ relaxivity of [Fe(*en*-*t*CDTA)]$^+$ was 0.82 L·mmol$^{-1}$·s$^{-1}$ at pH 7.4, and of which was 1.77 L·mmol$^{-1}$·s$^{-1}$ at pH 5.1, indicating pH-dependent property. Additionally, in serum (Figure 10B), there was a three-fold increasement in $T_1$ between the lowest 0.72 L·mmol$^{-1}$·s$^{-1}$ at pH 7.4 and highest 2.24 L·mmol$^{-1}$·s$^{-1}$ at pH 5.0. The sigmoidal dose response plots demonstrated a 50% pH of 6.79 ± 0.07 in water and a 50% pH of 6.17 ± 0.11 ($T_1$) in serum. Accordingly, Figure 11 presented MR profiles of [Fe(*en*-*t*CDTA)]$^+$ pH-responsive relaxivities at 1.5 T and 7 T in serum, which were verified by MR imaging with TR variation at a clinical 1.5 T SIEMENS Sonata and a experimental 7 T Bruker small animal scanner.

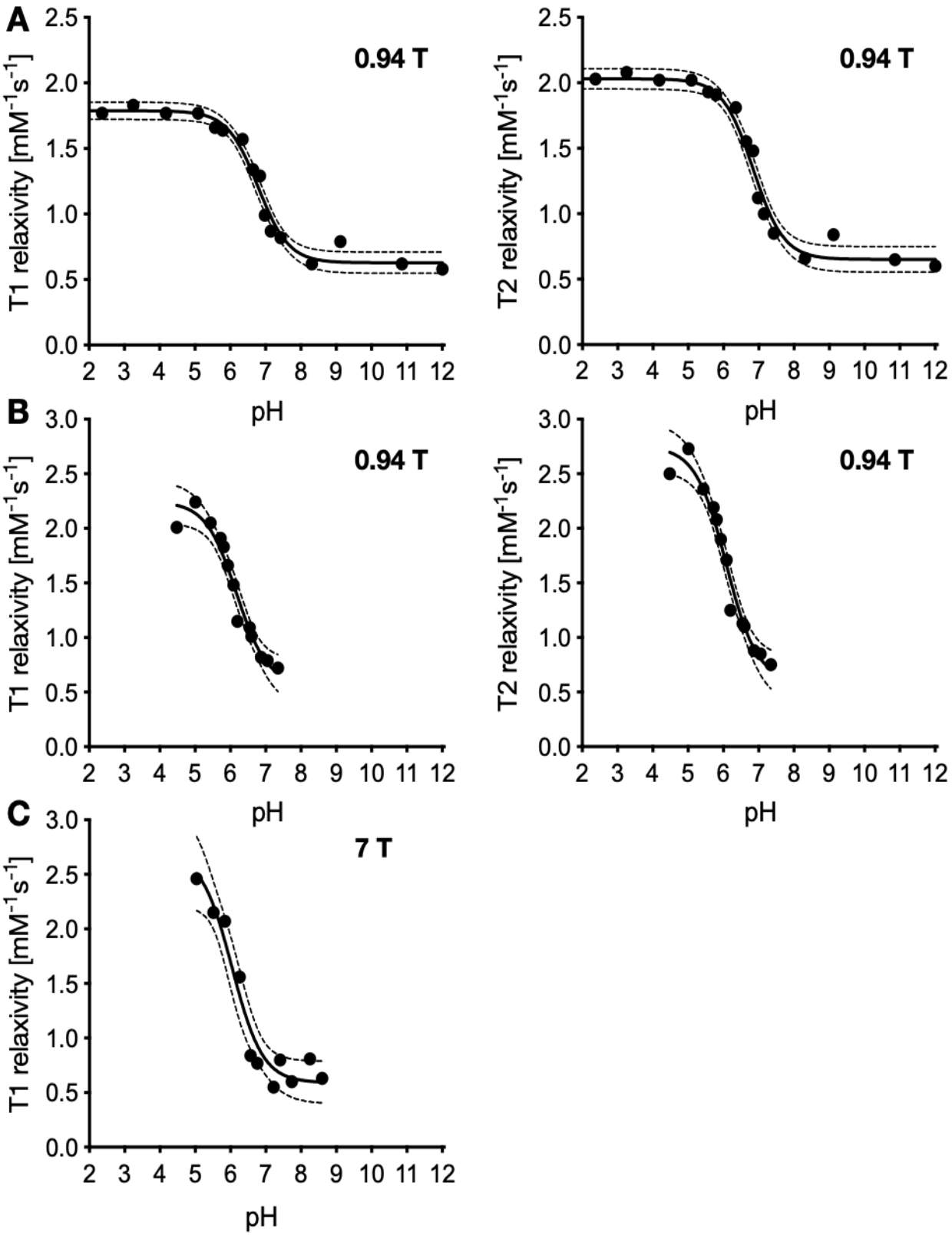


**Figure 10. pH related relativity changes of [Fe(*en*-*t*CDTA)]$^+$.** pH-responsive relaxivities of [Fe(*en*-*t*CDTA)]$^+$ in water (A) and in serum (B) at 0.94 T. (C) pH-responsive relaxivities of [Fe(*en*-*t*CDTA)]$^+$ in serum at 7 T. Curves illustrated the sigmoidal dose-response fited with 95% confidence bands (dotted lines). [1]

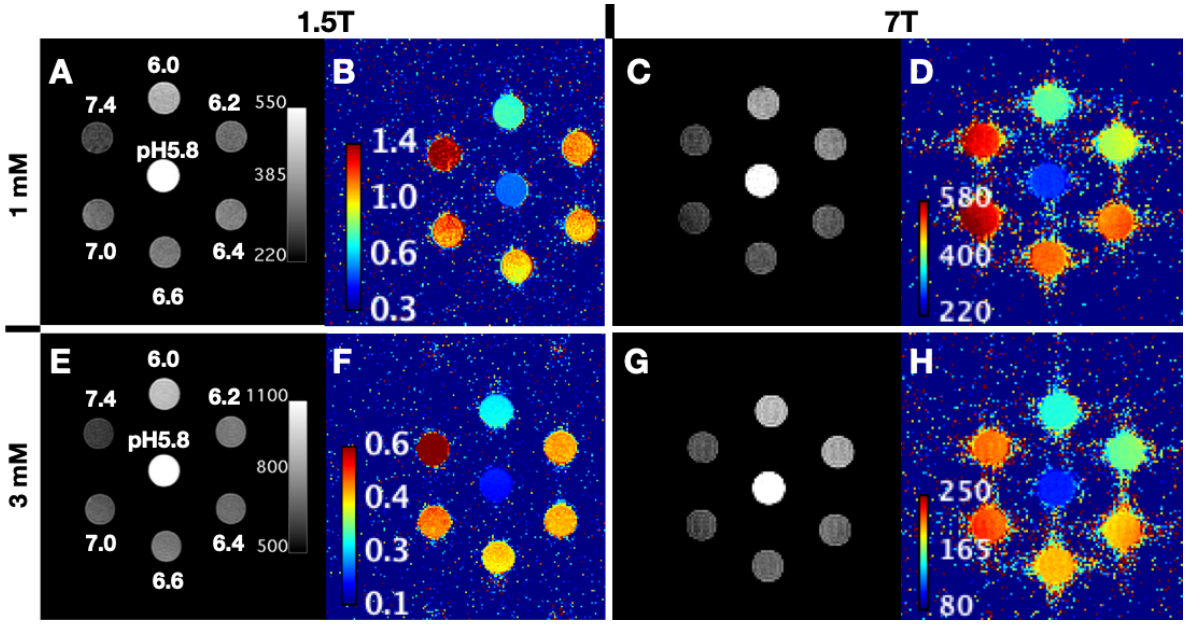


**Figure 11. $T_1$-weighted MR images of pH-responsive property of [Fe(*en*-*t*CDTA)]$^+$ at 1.5 T and 7 T.** Seven phantoms of [Fe(*en*-*t*CDTA)]$^+$ at 1 mM (A-D) or 3 mM (E-F) in serum with prepared pHs between 5.8 and 7.4 were imaged at 1.5 and 7 T. (A, E) Signal intensity images (spin echo sequence, TR 150 ms, TE 11 ms) and (B, F) corresponding $T_1$ maps obtained at 1.5 T MRI. (C, G) Signal intensity images (spin echo sequence, TR 71.8 ms, TE 9 ms) and corresponding $T_1$ maps (D, H) procured at a 7 T small animal MRI scanner. [1]

Given the distant amine groups to the iron(III) ion coordination, or alternatively, hydroxide iron coordination may be responsible for the unexpected low relaxivities of iron complexes of chelators *en*-*t*CDTA and *en*-D*i*-*t*CDTA in comparison to *trans*-*t*CDTA and *trans*-D*i*-*t*CDTA at neutral pH (Figure 14).

It is curious that at higher pH conditions, the relaxivity of the *trans*-1,4-diaminocyclohexane containing complexes [Fe(*trans*-*t*CDTA)]$^+$ and [Fe(*trans*-Di-*t*CDTA)] with rigid diamine decreased as well (Figure 12). This relativity drop at high pH could be attributed to increased presence hydroxide and the formation of hydroxide-iron complexes that block fast exchange of coordinated water.

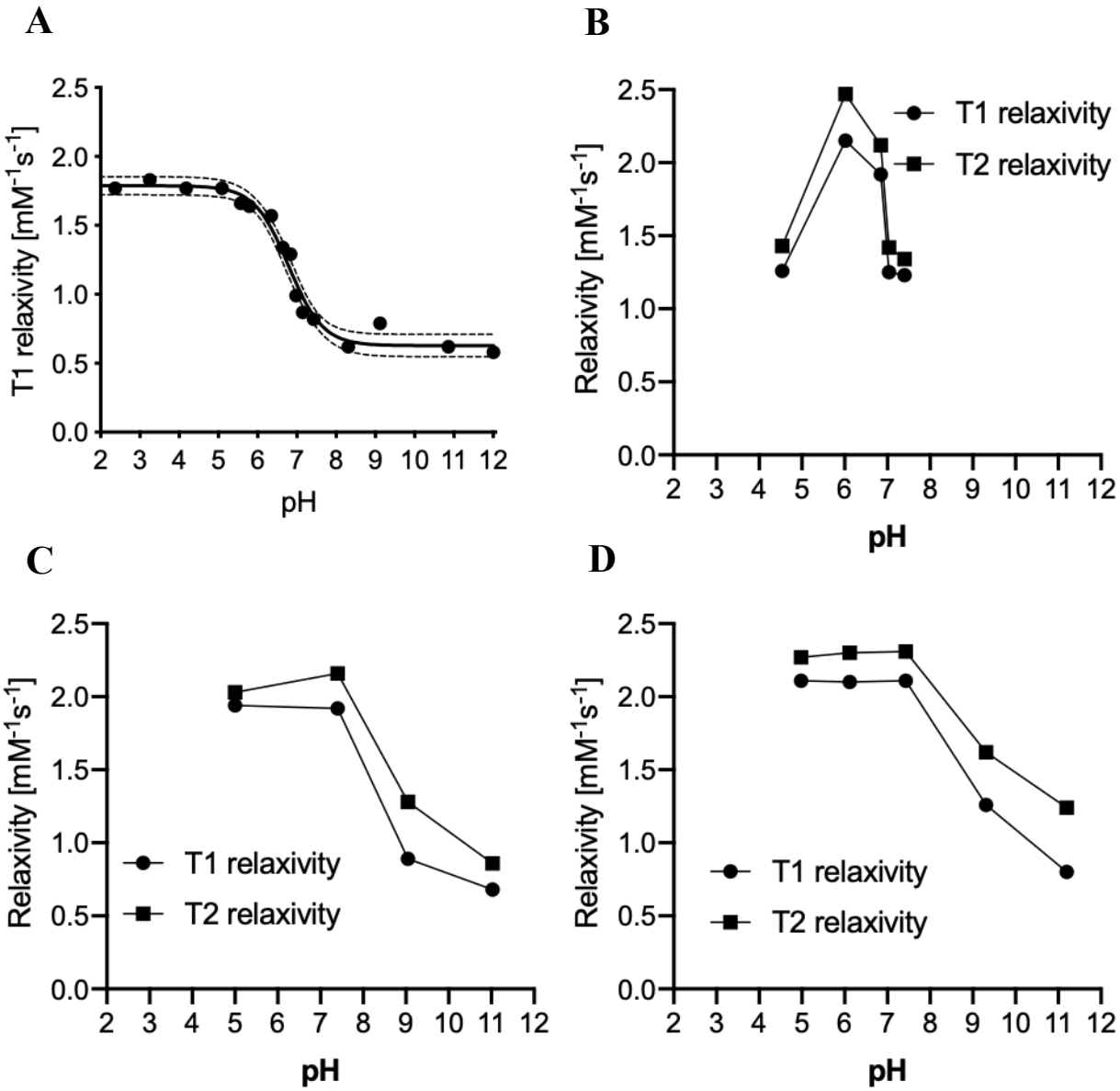


**Figure 12**: **Comparison of the pH-responsive relaxivities of the [Fe(*en*-*t*CDTA)]$^+$ derivates chelated with flexible ethylenediamine (*en*) versus rigid trans-1,4-diaminoclyclohexane (*trans*).** (A) [Fe(*en*-*t*CDTA)]$^+$, (B) [Fe(*en*-Di-*t*CDTA)], (C) [Fe(*trans*-*t*CDTA)]$^+$, and (D) [Fe(*trans*-Di-*t*CDTA)]. The relaxivity decrease occurred for the *en* derivates below pH 7.4 and for the *trans* derivatives above pH 7.4. Relaxivities were acquired on a relaxometer in water at 0.94, 37°C. [1]

### 4.3.2. Novel IBCA for MR imaging of Hepatobiliary

In Europe, linear GBCAs are restrained due to gadolinium disposition and delayed toxicity concerns, but intravenous linear GBCAs remain available for liver diagnostics, since there is an important diagnostic need and no macrocyclic replacement available at this time. Nonetheless, appreciably less research to date has focused on developing Gd-free liver-targeting contrast agents. This study reports

the development of a iron(III)-based contrast agent with the aim to provide safer alternatives for hepatobiliary MR imaging.

The synthesis and validation are described in chapter 3.2.5 and 4.2.1. To study the contrast effect of [Fe(4-ethoxyaniline-*t*CDTA)], we performed relaxometry and MRI measurements at different filed strengths. The relaxivity values of [Fe(4-ethoxyaniline-*t*CDTA)] are summarised in Table 2. We also measured relaxivity in FCS. Despite slightly lower relaxivities than *trans*-*t*CDTA and *trans*-D*i*-*t*CDTA, the $T_1$ values of [Fe(4-ethoxyaniline-*t*CDTA)] increased with the higher field strengths. Conversely, gadoxetic acid disodium (Gd-EOB-DTPA, Primovist/Eovist) and gadobenate dimeglumine (Gd-BOPTA, MultiHance), the two typical clinical hepatobiliary specific MRI contrast agents used for evaluation of liver function, decreases their $T_1$ relaxivities with increasing field strength by approximately -32% to -25% from 1.5 to 7 T. Measured $r_1$ values at 1.5 T (3 T/7 T) were 7.2 ± 0.2 (5.5 ± 0.3/4.9 ± 0.1) for Gd-EOB-DTPA, and 6.2 ± 0.5 (5.4 ± 0.3/4.7 ± 0.1) for Gd-BOPTA respectively, indicating the relaxivities of GBCAs are higher, but decrease with increasing field strengths.[77]

## 4.4. Exemplary in vivo MRI with [Fe(4-ethoxyaniline-*t*CDTA)]

To demonstrate liver targeting property of [Fe(4-ethoxyaniline-*t*CDTA)], $T_1$-weighted MR imaging was performed with 12-week-old female Balb/c mice after tail vein bolus injection (dose: 0.2 mmol/kg body weight). The most characteristic MR feature of [Fe(4-ethoxyaniline-*t*CDTA)] is the contrast enhancement of the liver that remains high even after 22 mins post injection. Subsequently, the contrast of gallbladder, intestines and urinary bladder is clearly visible, strongly indicating the excretion of [Fe(4-ethoxyaniline-*t*CDTA)] via hepatobiliary and renal pathways (Figure 13). The dual elimination property of [Fe(4-ethoxyaniline-*t*CDTA)] is similar to the clinically approved liver-targeted contrast agents Gd-EOB-DTPA and Gd-BOPTA.


**Figure 13. MIP image shows [Fe(4-ethoxyaniline-*t*CDTA)] dual elimination in vivo $T_1$ contrast effects. Recorded 22 min post injection reveals a strong enhancement of the gall bladder, the urinary bladder and the small intestines, proving the excretion of [Fe(4-ethoxyaniline-*t*CDTA)] via the hepatobiliary and renal pathways. MIP : maximum intensity projection.** (provided by Fei Ni, Institute of Radiology, Charité – Universitätsmedizin Berlin).

# 5. Discussion

IBCAs, especially [Fe(*t*CDTA)]$^-$ showed promising potential as replacements of GBCAs in contrast-enhanced $T_1$-weighted MRI.[78] Hence, we modified *t*CDTA for the purpose to generate iron chelates with further improved relaxivities and modified contrast agent properties for various clinical applications. By employing the straightforward two steps synthesis strategy as shown in Figure 2 and three amine-containing compounds ethylenediamine, *trans*-1,4-Diaminoclyclohexane and 4-Etoxyaniline, we could generate 5 new *t*CDTA derivatives. After confirming purity of the derivatives and the absence of the initiating component, *t*CDTA, MALDI mass spectrometry, elemental analyses and NMR were performed to obtain proofs of identity and to avoid the contribution from [Fe(*t*CDTA)]$^-$ for the following relaxivities evaluations.

6-coordinated [Fe(*t*CDTA)]$^-$ complex leaves one coordination site open for water or for other ligands, allowing inner sphere relaxation, which contributes to relatively high relaxivity.[71,72] In contrast, the relatively low relaxivities of [Fe(*en*-*t*CDTA)]$^+$ and [Fe(*en*-D*i*-*t*CDTA)] at neutral pH could resulted from the occupancy of all seven coordination sites of iron(III) by coordination with the terminal amine (Fig. 2). Figure 14 gives a hypothetic mechanism for the pH-dependent of Fe(*en*-*t*CDTA)]$^+$: at low pH, the terminal amine could be protonated, which would forbid the coordination of the iron and thus remains one accessible iron(III) coordination site for water coordination (Figure 14A). As the same analogize, the relatively low relaxivity and pH dependency of the [Fe(*en*-D*i*-*t*CDTA)] can be explained by that the two added amides of the ethylenediamine bridge possibly coordinate with the two trivalent metal ion centers, and thus restrain the coordination of inner-sphere water and relaxation. Alternatively, the low relaxivities at neutral and higher pHs could be the consequences of central iron(III) obstruction by coordinatively hydroxide ions at higher concentrations, which could inhibit inner sphere relaxation simultaneously (Figure 14C, E). This mechanism seems to become relevant only at higher pHs as shown for the rigid iron complexes as shown in Figure 12C and D, which in contrast extends over a wide pH range.

The pH-responsive $T_1$ relaxivity property of [Fe(*en*-*t*CDTA)]$^+$ could be exploited in the future for the detection or characterisation of cancer by MRI and the designation of salvable tissues in stroke that typically have lower pH than normal tissues.[79-82] In comparison to pH nano-sensors, the low molecular weight iron (III)-based complexes should be superior as regards quicker and more extensive bio-distribution, as well as a more efficient excretion.[83,84]

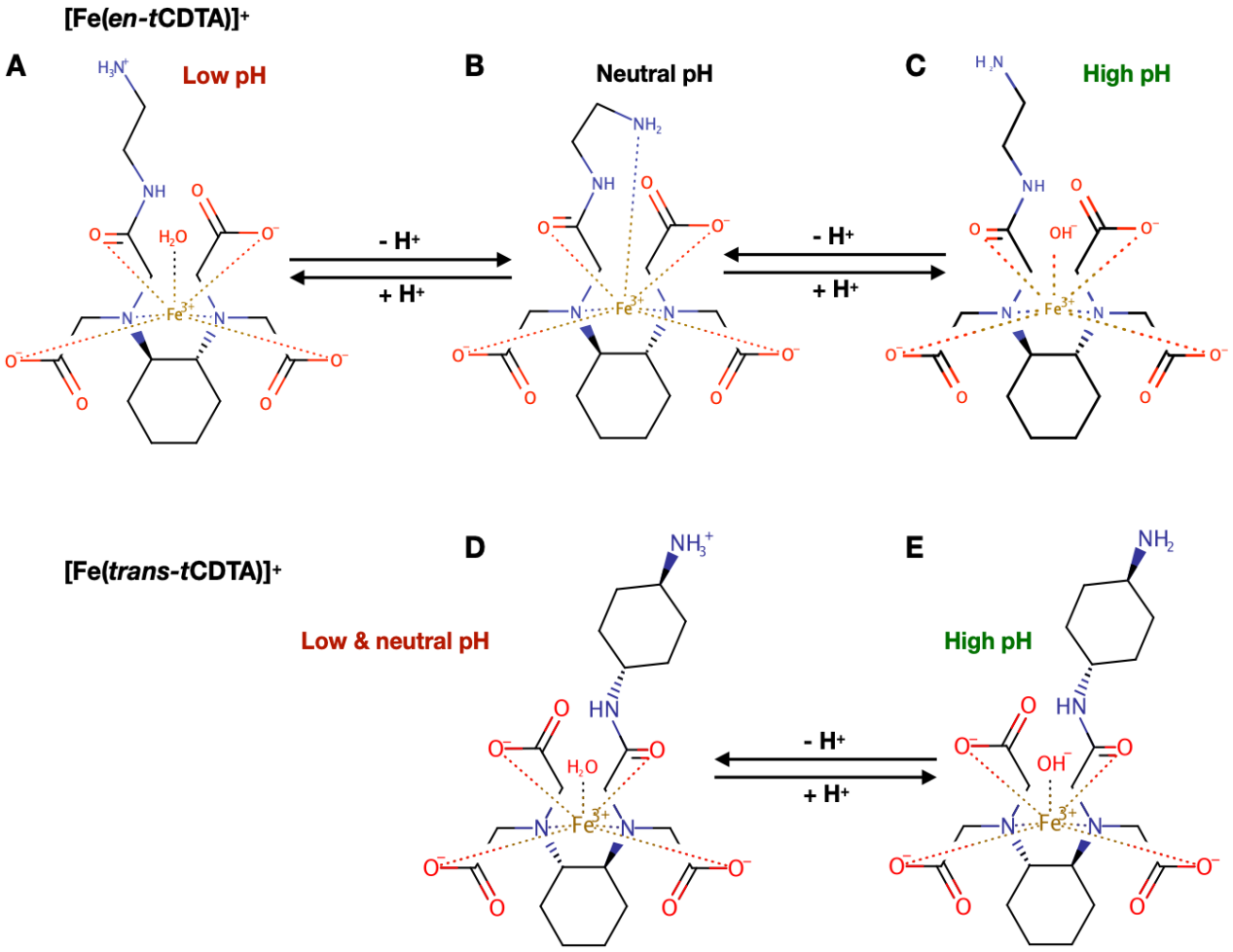


**Figure 14**. **Hypothetical mechanisms of the observed pH-dependent relaxivity changes of [Fe(en-*t*CDTA)]$^+$ and [Fe(*trans*-*t*CDTA)]$^+$.** (A) At slightly acidic pH, the terminal free amine group could be protonated, which in turn would prevent the iron coordination. Consequently, one coordination site would be available for water coordination allowing efficient inner sphere relaxation. (B) At neutral and high pH, the terminal amine group becomes deprotonated and thus could coordinate to central iron, block water coordination, and prevent efficient inner sphere relaxation. (C) At neutral and higher pH, higher concentrations of hydroxide ions can coordinate the central iron and thus block water coordination and inner sphere relaxation. (B) and (C) could coexist, but (C) seems more likely to occur at higher pHs. (D) The terminal free amine group of the rigid *trans*-1,4-diaminocyclohexane cannot coordinate the iron, which would explain the relatively high relaxivity at neutral and low pH (Figure 12). (E) At higher pH, high concentrations of hydroxide ions can coordinate to iron and thus block water access and reduce relaxivity. The pH dependent relaxivities of the dimers [Fe(en-Di-*t*CDTA)] and [Fe(*trans*-Di-*t*CDTA)] could be explained accordingly to the correspondent monomers. [1]

As shown through relaxivity measurements, at neutral pH, the iron (III)-based complexes of *trans*-1,4-diaminocyclohexane derivatives showed considerably higher relaxivities than their ethylenediamine analogues. Notably, $T_1$ relaxivities of the iron complexes demonstrated an increasement with

increasing magnetic field strengths. [Fe(*trans*-*t*CDTA)]$^+$ and [Fe(*trans*-D*i*-*t*CDTA)] showed particularly high relaxivities at clinically available field strengths of 1.5 T and 3 T and continued to be higher relaxivities at 7 T. In contrast, two of the three macrocyclic GBCAs products, the most frequently applied compounds in clinical MRI in Europe, $T_1$ relaxivities decrease with increasing field strengths.[36] At 3 T, [Fe(*trans*-D*i*-*t*CDTA)] dimer in serum even had slightly higher $T_1$ relaxivity per metal ion than that of gadoteridol (ProHance®, Bracco Diagnostic Inc) and gadoterate (Dotarem®, Guerbet LLC) and vaguely lower $T_1$ relaxivity in comparison to gadobutrol (Gadovist®, Bayer AG) in blood plasma, while its $T_1$ relaxivity per molecule is higher than that of all above three contrast agents. In the presence of serum, the $T_1$ relaxivity increasement versus in water were slightly lower than the mentioned macrocyclic GBCAs in plasma. These data suggesting their similar low plasma protein adsorption.[34] As a consequence, [Fe(*trans*-*t*CDTA)]$^+$ and [Fe(*trans*-D*i*-*t*CDTA)] could be as promising alternatives to GBCAs for MR imaging. In addition, through the terminal amino group as linker, [Fe(*trans*-*t*CDTA)]$^+$ might serve as an MRI-detectable label by applying the terminal amino group as linker, e.g., coupled to targeted and/or functional imaging probes.

It is noteworthy that, *t*CDTA and new generated *t*CDTA derivatives remained remarkably intact in 100 mM HCl over a period of 72 h, which was not the character for the iron(III)-based macrocyclic complexes reported by Snyder and co-workers[51]. Their stability could be explained by the four left over coordinated oxygens. The two exhibited cathodic peak potentials for [Fe(*trans*-D*i*-*t*CDTA)] complex and for [Fe(*en*-*t*CDTA)]$^+$ complex might originate from two different explanations: the existence of different metal-bound species in solution, such as Fe-$OH_2$ and Fe-OH (the aqua form is reduced more promptly than the hydroxide form[72] and/or, in the event of the [Fe(*trans*-D*i*-*t*CDTA)], slightly different potentials for the two trivalent metal ion centers. For now, the extent of redox cycling will occur in blood and other fluids comprising the extracellular spaces is remaining unclear. Studies in the future will be necessary to better understand biological redox activity.

[Fe(4-ethoxyaniline-*t*CDTA)] shares a very similar relaxivity profile with [Fe(*t*CDTA)]$^-$ at increasing field strength (Table 2). Results of our in vitro phantom experiment and in vivo imaging study in a mouse model reveal similar liver-specificity of [Fe(4-ethoxyaniline-*t*CDTA)] as Gadobenate and gadoxetate, the two exceptions of suspended linear GBCAs by the Commission of the European Community for liver imaging.[23] When conducted with a clinical 3 T MRI system, [Fe(4-ethoxyaniline-*t*CDTA)] generated sufficient $T_1$ contrast after injection. The effective accumulation in the liver, gall, and urinary bladder demonstrates the hepatobiliary and renal elimination of [Fe(4-ethoxyaniline-*t*CDTA)], showing a promising potential as a diagnostic agent for liver imaging as well as for other organs that are reached by the blood vessels and for the urinary system due to the partial kidney excretion. Although [Fe(4-ethoxyaniline-*t*CDTA)] was used at a dose of 0.2 mmol/kg of body

weight, which is roughly four times the clinically recommended dose of Gd-EOB-DTPA (0.025 mmol/kg of body weight), it is worth noting that the signal of the IBCAs could be further increased by higher dosing, owing to the potentially lower long-term risk caused by depositions in comparison to GBCAs. In future research, the hepatocyte targeting mechanism and tumor imaging properties of [Fe(4-ethoxyaniline-*t*CDTA)] enhancement remains to be investigated.

# 6. Conclusions

In conclusion, the presented convenient approach to modify *t*CDTA by an efficient two steps synthesis prompted the development of two[Fe(*t*CDTA)]$^-$ derivatives, [Fe(*trans*-*t*CDTA)]$^+$ monomer and [Fe(*trans*-D*i*-*t*CDTA)] dimer with preferable $T_1$ relaxivities, while retaining highly steady inertness to dissociation compared with [Fe(*t*CDTA)]$^-$ in acid. The five new iron (III)-based complexes show favorable $T_1$ relaxivities throughout the range of clinically available MR imaging scanners at 1.5, 3, and 7 T. A third iron complex [Fe(*en*-*t*CDTA)]$^+$, provides a pH-responsive relaxivity increase at weakly acidic pH and could facilitate visualisation of biologic changes of pH and fined MRI-based characterisation of cancer diagnosis and/or salvageable tissues in stroke. The study *in vivo* confirmed [Fe(4-ethoxyaniline-*t*CDTA)] as a potential non-Gd-based liver-specific MRI contrast agent that may serve for comprehensive assessment of liver function and liver diseases.

# Bibliography


1. Xie J, Haeckel A, Hauptmann R, Ray IP, Limberg C, Kulak N, Hamm B, Schellenberger E. Iron(III)-tCDTA derivatives as MRI contrast agents: Increased T(1) relaxivities at higher magnetic field strength and pH sensing. Magn Reson Med 2021;85(6):3370-3382. (In eng). DOI: 10.1002/mrm.28664.
2. Young IR. Methods in Biomedical Magnetic Resonance Imaging and Spectroscopy, 2 Volume Set: Wiley, 2000.
3. Relaxation. MRI Basic Principles and Applications2015:17-25.
4. Aime S, Caravan P. Biodistribution of gadolinium-based contrast agents, including gadolinium deposition. J Magn Reson Imaging 2009;30(6):1259-67. (In eng). DOI: 10.1002/jmri.21969.
5. Solomon I. Relaxation Processes in a System of Two Spins. Physical Review 1955;99(2):559-565. DOI: 10.1103/PhysRev.99.559.
6. Morgan LO, Nolle AW. Proton Spin Relaxation in Aqueous Solutions of Paramagnetic Ions. II. Cr+++, Mn++, Ni++, Cu++, and Gd+++. The Journal of Chemical Physics 1959;31(2):365-368. DOI: 10.1063/1.1730360.
7. Caravan P. Strategies for increasing the sensitivity of gadolinium based MRI contrast agents. Chemical Society Reviews 2006;35(6):512-523. (10.1039/B510982P). DOI: 10.1039/B510982P.
8. Viswanathan S, Kovacs Z, Green KN, Ratnakar SJ, Sherry AD. Alternatives to gadolinium-based metal chelates for magnetic resonance imaging. Chem Rev 2010;110(5):2960-3018. (In eng). DOI: 10.1021/cr900284a.
9. Caravan P, Ellison JJ, McMurry TJ, Lauffer RB. Gadolinium(III) Chelates as MRI Contrast Agents: Structure, Dynamics, and Applications. Chem Rev 1999;99(9):2293-352. (In eng). DOI: 10.1021/cr980440x.
10. Granato L, Laurent S, Vander Elst L, Djanashvili K, Peters JA, Muller RN. The Gd3+ complex of 1,4,7,10-tetraazacyclododecane-1,4,7,10-tetraacetic acid mono(p-isothiocyanatoanilide) conjugated to inulin: a potential stable macromolecular contrast agent for MRI. Contrast Media Mol Imaging 2011;6(6):482-91. (In eng). DOI: 10.1002/cmmi.448.
11. Lin SP, Brown JJ. MR contrast agents: physical and pharmacologic basics. J Magn Reson Imaging 2007;25(5):884-99. (In eng). DOI: 10.1002/jmri.20955.
12. Prince MR, Zhang H, Zou Z, Staron RB, Brill PW. Incidence of immediate gadolinium contrast media reactions. AJR Am J Roentgenol 2011;196(2):W138-43. (In eng). DOI: 10.2214/ajr.10.4885.
13. Wahsner J, Gale EM, Rodríguez-Rodríguez A, Caravan P. Chemistry of MRI Contrast Agents: Current Challenges and New Frontiers. Chemical Reviews 2019;119(2):957-1057. DOI: 10.1021/acs.chemrev.8b00363.
14. Thomsen HS. Nephrogenic systemic fibrosis: a serious adverse reaction to gadolinium - 1997-2006-2016. Part 1. Acta Radiol 2016;57(5):515-20. (In eng). DOI: 10.1177/0284185115626480.
15. Thomsen HS. Nephrogenic systemic fibrosis: A serious late adverse reaction to gadodiamide. Eur Radiol 2006;16(12):2619-21. (In eng). DOI: 10.1007/s00330-006-0495-8.
16. McDonald RJ, McDonald JS, Kallmes DF, Jentoft ME, Murray DL, Thielen KR, Williamson EE, Eckel LJ. Intracranial Gadolinium Deposition after Contrast-enhanced MR Imaging. Radiology 2015;275(3):772-782. DOI: 10.1148/radiol.15150025.
17. Murata N, Gonzalez-Cuyar LF, Murata K, Fligner C, Dills R, Hippe D, Maravilla KR. Macrocyclic and Other Non-Group 1 Gadolinium Contrast Agents Deposit Low Levels of Gadolinium in Brain and Bone Tissue: Preliminary Results From 9 Patients With Normal Renal Function. Invest Radiol 2016;51(7):447-53. (In eng). DOI: 10.1097/rli.0000000000000252.

18. Bjørnerud A, Vatnehol SAS, Larsson C, Due-Tønnessen P, Hol PK, Groote IR. Signal Enhancement of the Dentate Nucleus at Unenhanced MR Imaging after Very High Cumulative Doses of the Macrocyclic Gadolinium-based Contrast Agent Gadobutrol: An Observational Study. Radiology 2017;285(2):434-444. (In eng). DOI: 10.1148/radiol.2017170391.
19. Gulani V, Calamante F, Shellock FG, Kanal E, Reeder SB. Gadolinium deposition in the brain: summary of evidence and recommendations. Lancet Neurol 2017;16(7):564-570. (In eng). DOI: 10.1016/s1474-4422(17)30158-8.
20. McDonald RJ, McDonald JS, Dai D, Schroeder D, Jentoft ME, Murray DL, Kadirvel R, Eckel LJ, Kallmes DF. Comparison of Gadolinium Concentrations within Multiple Rat Organs after Intravenous Administration of Linear versus Macrocyclic Gadolinium Chelates. Radiology 2017;285(2):536-545. (In eng). DOI: 10.1148/radiol.2017161594.
21. Fingerhut S, Sperling M, Holling M, Niederstadt T, Allkemper T, Radbruch A, Heindel W, Paulus W, Jeibmann A, Karst U. Gadolinium-based contrast agents induce gadolinium deposits in cerebral vessel walls, while the neuropil is not affected: an autopsy study. Acta Neuropathol 2018;136(1):127-138. (In eng). DOI: 10.1007/s00401-018-1857-4.
22. El-Khatib AH, Radbruch H, Trog S, Neumann B, Paul F, Koch A, Linscheid MW, Jakubowski N, Schellenberger E. Gadolinium in human brain sections and colocalization with other elements. Neurol Neuroimmunol Neuroinflamm 2019;6(1):e515. (In eng). DOI: 10.1212/nxi.0000000000000515.
23. <prac-concludes-assessment-gadolinium-agents-used-body-scans-recommends-regulatory-actions-including_en.pdf>.
24. Mugikura S, Takase K. Fear of linear gadolinium-based contrast agents and the Japanese radiologist's choice. Jpn J Radiol 2017;35(11):695-696. (In eng). DOI: 10.1007/s11604-017-0682-3.
25. Health Product InfoWatch - May 2018 Ottawa (ON): Health Canada; 2018:. (https://www.canada.ca/en/health-canada/services/drugs-health-products/medeffect-canada/health-product-infowatch/health-product-infowatch-may-2018/page-2.html#a33).
26. Sharon Williams HG. Gadolinium Toxicity A Survey of the Chronic Effects of Retained Gadolinium from Contrast MRIs. (https://gdtoxicity.files.wordpress.com/2017/08/lighthouse-symptom-survey-copy-for-docket-fda-2017-n-1957.pdf).
27. Burke LM, Ramalho M, AlObaidy M, Chang E, Jay M, Semelka RC. Self-reported gadolinium toxicity: A survey of patients with chronic symptoms. Magn Reson Imaging 2016;34(8):1078-80. (In eng). DOI: 10.1016/j.mri.2016.05.005.
28. Semelka RC, Ramalho J, Vakharia A, AlObaidy M, Burke LM, Jay M, Ramalho M. Gadolinium deposition disease: Initial description of a disease that has been around for a while. Magn Reson Imaging 2016;34(10):1383-1390. (In eng). DOI: 10.1016/j.mri.2016.07.016.
29. Layne KA, Wood DM, Dargan PI. Gadolinium-based contrast agents - what is the evidence for 'gadolinium deposition disease' and the use of chelation therapy? Clin Toxicol (Phila) 2020;58(3):151-160. (In eng). DOI: 10.1080/15563650.2019.1681442.
30. Lindner U, Lingott J, Richter S, Jakubowski N, Panne U. Speciation of gadolinium in surface water samples and plants by hydrophilic interaction chromatography hyphenated with inductively coupled plasma mass spectrometry. Anal Bioanal Chem 2013;405(6):1865-73. (In eng). DOI: 10.1007/s00216-012-6643-x.
31. González V, Vignati DA, Pons MN, Montarges-Pelletier E, Bojic C, Giamberini L. Lanthanide ecotoxicity: first attempt to measure environmental risk for aquatic organisms. Environ Pollut 2015;199:139-47. (In eng). DOI: 10.1016/j.envpol.2015.01.020.
32. Birka M, Wehe CA, Hachmöller O, Sperling M, Karst U. Tracing gadolinium-based contrast agents from surface water to drinking water by means of speciation analysis. J Chromatogr A 2016;1440:105-111. (In eng). DOI: 10.1016/j.chroma.2016.02.050.

33. Parant M, Perrat E, Wagner P, Rosin C, Py JS, Cossu-Leguille C. Variations of anthropogenic gadolinium in rivers close to waste water treatment plant discharges. Environ Sci Pollut Res Int 2018;25(36):36207-36222. (In eng). DOI: 10.1007/s11356-018-3489-6.
34. Rohrer M, Bauer H, Mintorovitch J, Requardt M, Weinmann HJ. Comparison of magnetic properties of MRI contrast media solutions at different magnetic field strengths. Invest Radiol 2005;40(11):715-24. (In eng). DOI: 10.1097/01.rli.0000184756.66360.d3.
35. Fries P, Morelli JN, Lux F, Tillement O, Schneider G, Buecker A. The issues and tentative solutions for contrast-enhanced magnetic resonance imaging at ultra-high field strength. Wiley Interdiscip Rev Nanomed Nanobiotechnol 2014;6(6):559-73. (In eng). DOI: 10.1002/wnan.1291.
36. Szomolanyi P, Rohrer M, Frenzel T, Noebauer-Huhmann IM, Jost G, Endrikat J, Trattnig S, Pietsch H. Comparison of the Relaxivities of Macrocyclic Gadolinium-Based Contrast Agents in Human Plasma at 1.5, 3, and 7 T, and Blood at 3 T. Invest Radiol 2019;54(9):559-564. (In eng). DOI: 10.1097/rli.0000000000000577.
37. Quettier L, Aubert G, Belorgey J, Berriaud C, Bourquard A, Bredy P, Dubois O, Gilgrass G, Juster FP, Lannou H, Molinié F, Nusbaum M, Nunio F, Payn A, Schild T, Schweitzer M, Scola L, Sinanna A, Stepanov V, Vedrine P. Iseult/INUMAC Whole Body 11.7 T MRI Magnet. IEEE Transactions on Applied Superconductivity 2017;27(4):1-4. DOI: 10.1109/TASC.2016.2627501.
38. Lauffer RB, Greif WL, Stark DD, Vincent AC, Saini S, Wedeen VJ, Brady TJ. Iron-EHPG as an hepatobiliary MR contrast agent: initial imaging and biodistribution studies. J Comput Assist Tomogr 1985;9(3):431-8. (In eng). DOI: 10.1097/00004728-198505000-00001.
39. Dev S, Babitt JL. Overview of iron metabolism in health and disease. Hemodial Int 2017;21 Suppl 1(Suppl 1):S6-s20. (In eng). DOI: 10.1111/hdi.12542.
40. Nriagu JO SE. Metal Homeostasis during Development, Maturation, and Aging. (https://www.ncbi.nlm.nih.gov/books/NBK569694/).
41. Gozzelino R, Arosio P. Iron Homeostasis in Health and Disease. Int J Mol Sci 2016;17(1) (In eng). DOI: 10.3390/ijms17010130.
42. Pierre VC, Allen M. Contrast Agents for MRI: Experimental Methods. 2017.
43. Kuhl CK, Textor J, Gieseke J, von Falkenhausen M, Gernert S, Urbach H, Schild HH. Acute and subacute ischemic stroke at high-field-strength (3.0-T) diffusion-weighted MR imaging: intraindividual comparative study. Radiology 2005;234(2):509-16. (In eng). DOI: 10.1148/radiol.2342031323.
44. Alexander AL, Lee JE, Wu YC, Field AS. Comparison of diffusion tensor imaging measurements at 3.0 T versus 1.5 T with and without parallel imaging. Neuroimaging Clin N Am 2006;16(2):299-309, xi. (In eng). DOI: 10.1016/j.nic.2006.02.006.
45. Lauffer RB. Paramagnetic metal complexes as water proton relaxation agents for NMR imaging: theory and design. Chemical Reviews 1987;87(5):901-927. DOI: 10.1021/cr00081a003.
46. Marotti M, Schmiedl U, White D, Ramos E, Johnson T, Engelstad B. Metal chelates as urographic contrast agents for magnetic resonance imaging. A comparative study. Rofo 1987;146(1):89-93. (In eng). DOI: 10.1055/s-2008-1048448.
47. Schwert DD, Richardson N, Ji G, Radüchel B, Ebert W, Heffner PE, Keck R, Davies JA. Synthesis of two 3,5-disubstituted sulfonamide catechol ligands and evaluation of their iron(III) complexes for use as MRI contrast agents. J Med Chem 2005;48(23):7482-5. (In eng). DOI: 10.1021/jm0501984.
48. Miao Y, Xie F, Cen J, Zhou F, Tao X, Luo J, Han G, Kong X, Yang X, Sun J, Ling J. Fe3+@polyDOPA-b-polysarcosine, a T1-Weighted MRI Contrast Agent via Controlled NTA Polymerization. ACS Macro Letters 2018;7(6):693-698. DOI: 10.1021/acsmacrolett.8b00287.

49. Patel A, Asik D, Snyder EM, Dilillo AE, Cullen PJ, Morrow JR. Binding and Release of FeIII Complexes from Glucan Particles for the Delivery of T(1) MRI Contrast Agents. ChemMedChem 2020;15(12):1050-1057. (In eng). DOI: 10.1002/cmdc.202000003.
50. Wang H, Jordan VC, Ramsay IA, Sojoodi M, Fuchs BC, Tanabe KK, Caravan P, Gale EM. Molecular Magnetic Resonance Imaging Using a Redox-Active Iron Complex. J Am Chem Soc 2019;141(14):5916-5925. (In eng). DOI: 10.1021/jacs.9b00603.
51. Asik D, Smolinski R, Abozeid SM, Mitchell TB, Turowski SG, Spernyak JA, Morrow JR. Modulating the Properties of Fe(III) Macrocyclic MRI Contrast Agents by Appending Sulfonate or Hydroxyl Groups. Molecules 2020;25(10) (In eng). DOI: 10.3390/molecules25102291.
52. Snyder EM, Asik D, Abozeid SM, Burgio A, Bateman G, Turowski SG, Spernyak JA, Morrow JR. A Class of Fe(III) Macrocyclic Complexes with Alcohol Donor Groups as Effective T(1) MRI Contrast Agents. Angew Chem Int Ed Engl 2020;59(6):2414-2419. (In eng). DOI: 10.1002/anie.201912273.
53. Carril M. Activatable probes for diagnosis and biomarker detection by MRI. Journal of Materials Chemistry B 2017;5(23):4332-4347. (10.1039/C7TB00093F). DOI: 10.1039/C7TB00093F.
54. White KA, Grillo-Hill BK, Barber DL. Cancer cell behaviors mediated by dysregulated pH dynamics at a glance. Journal of Cell Science 2017;130(4):663-669. DOI: 10.1242/jcs.195297.
55. Zhang S, Wu K, Sherry AD. A Novel pH-Sensitive MRI Contrast Agent. Angew Chem Int Ed Engl 1999;38(21):3192-3194. (In eng).
56. Raghunand N, Howison C, Sherry AD, Zhang S, Gillies RJ. Renal and systemic pH imaging by contrast-enhanced MRI. Magn Reson Med 2003;49(2):249-57. (In eng). DOI: 10.1002/mrm.10347.
57. Garcia-Martin ML, Martinez GV, Raghunand N, Sherry AD, Zhang S, Gillies RJ. High resolution pHe imaging of rat glioma using pH-dependent relaxivity. Magnetic Resonance in Medicine 2006;55(2):309-315. DOI: https://doi.org/10.1002/mrm.20773.
58. Frullano L, Catana C, Benner T, Sherry AD, Caravan P. Bimodal MR-PET agent for quantitative pH imaging. Angew Chem Int Ed Engl 2010;49(13):2382-4. (In eng). DOI: 10.1002/anie.201000075.
59. Lee S, Kim SH, Lee JE, Sinn DH, Park CK. Preoperative gadoxetic acid-enhanced MRI for predicting microvascular invasion in patients with single hepatocellular carcinoma. J Hepatol 2017;67(3):526-534. (In eng). DOI: 10.1016/j.jhep.2017.04.024.
60. Jiang HY, Chen J, Xia CC, Cao LK, Duan T, Song B. Noninvasive imaging of hepatocellular carcinoma: From diagnosis to prognosis. World J Gastroenterol 2018;24(22):2348-2362. (In eng). DOI: 10.3748/wjg.v24.i22.2348.
61. Ahn SJ, Kim JH, Park SJ, Kim ST, Han JK. Hepatocellular carcinoma: preoperative gadoxetic acid-enhanced MR imaging can predict early recurrence after curative resection using image features and texture analysis. Abdom Radiol (NY) 2019;44(2):539-548. (In eng). DOI: 10.1007/s00261-018-1768-9.
62. Ayyala RS, Anupindi SA, Gee MS, Trout AT, Callahan MJ. Intravenous gadolinium-based hepatocyte-specific contrast agents (HSCAs) for contrast-enhanced liver magnetic resonance imaging in pediatric patients: what the radiologist should know. Pediatr Radiol 2019;49(10):1256-1268. (In eng). DOI: 10.1007/s00247-019-04476-4.
63. Lee S, Kim KW, Jeong WK, Kim MJ, Choi GH, Choi JS, Song GW, Lee SG. Gadoxetic acid-enhanced MRI as a predictor of recurrence of HCC after liver transplantation. Eur Radiol 2020;30(2):987-995. (In eng). DOI: 10.1007/s00330-019-06424-0.
64. Lauffer RB, Vincent AC, Padmanabhan S, Villringer A, Saini S, Elmaleh DR, Brady TJ. Hepatobiliary MR contrast agents: 5-substituted iron-EHPG derivatives. Magn Reson Med 1987;4(6):582-90. (In eng). DOI: 10.1002/mrm.1910040609.

65. Krokhin OV, Kuzina OV, Hoshino H, Shpigun OA, Yotsuyanagi T. Potential of ethylenediaminedi(o-hydroxyphenylacetic acid) and N,N′-bis(hydroxybenzyl)ethylenediamine-N,N′-diacetic acid for the determination of metal ions by capillary electrophoresis. Journal of Chromatography A 2000;890(2):363-369. DOI: https://doi.org/10.1016/S0021-9673(00)00554-9.
66. Samuni AM, Afeworki M, Stein W, Yordanov AT, DeGraff W, Krishna MC, Mitchell JB, Brechbiel MW. Multifunctional antioxidant activity of HBED iron chelator. Free Radical Biology and Medicine 2001;30(2):170-177. DOI: https://doi.org/10.1016/S0891-5849(00)00459-7.
67. Larsen SK, Jenkins BG, Memon NG, Lauffer RB. Structure-affinity relationships in the binding of unsubstituted iron phenolate complexes to human serum albumin. Molecular structure of iron(III) N, N'-bis(2-hydroxybenzyl)ethylenediamine-N,N'-diacetate. Inorganic Chemistry 1990;29(6):1147-1152. DOI: 10.1021/ic00331a008.
68. Stark DD, Elizondo G, Fretz CJ. Liver-specific contrast agents for MRI. Invest Radiol 1990;25 Suppl 1:S58. (In eng). DOI: 10.1097/00004424-199009001-00027.
69. Kuźnik N, Szafraniec-Gorol G, Oczek L, Grucela A, Jewuła P, Kuźnik A, Zassowski P, Domagala W. A study on the synthesis and properties of substituted EHBG-Fe(III) complexes as potential MRI contrast agents. Journal of Organometallic Chemistry 2014;769:100-105. DOI: https://doi.org/10.1016/j.jorganchem.2014.07.011.
70. Bales BC, Grimmond B, Johnson BF, Luttrell MT, Meyer DE, Polyanskaya T, Rishel MJ, Roberts J. Fe-HBED Analogs: A Promising Class of Iron-Chelate Contrast Agents for Magnetic Resonance Imaging. Contrast Media Mol Imaging 2019;2019:8356931. (In eng). DOI: 10.1155/2019/8356931.
71. Boehm-Sturm P, Haeckel A, Hauptmann R, Mueller S, Kuhl CK, Schellenberger EA. Low-Molecular-Weight Iron Chelates May Be an Alternative to Gadolinium-based Contrast Agents for T1-weighted Contrast-enhanced MR Imaging. Radiology 2018;286(2):537-546. (In eng). DOI: 10.1148/radiol.2017170116.
72. Sabine Seibig RvE. <Structural information on trans-1,2-diaminocyclohexane-N,N′-tetraacetateferrate(III) in the solid and aqueous phase.pdf>. 1998.
73. Gestin JF, Faivre-Chauvet A, Mease RC, Sai-Maurel C, Thédrez P, Slinkin M, Meinken GE, Srivastava SC, Chatal JF. Introduction of five potentially metabolizable linking groups between 111In-cyclohexyl EDTA derivatives and F(ab')2 fragments of anti-carcinoembryonic antigen antibody--I. A new reproducible synthetic method. Nucl Med Biol 1993;20(6):755-62. (In eng). DOI: 10.1016/0969-8051(93)90162-n.
74. Giordanengo R, Viel S, Allard-Breton B, Thevand A, Charles L. Tandem mass spectrometry of poly(methacrylic Acid) oligomers produced by negative mode electrospray ionization. J Am Soc Mass Spectrom 2009;20(1):25-33. DOI: 10.1016/j.jasms.2008.09.019.
75. Fornasiero D, Bellen JC, Baker RJ, Chatterton BE. Paramagnetic complexes of manganese(II), iron(III), and gadolinium(III) as contrast agents for magnetic resonance imaging. The influence of stability constants on the biodistribution of radioactive aminopolycarboxylate complexes. Invest Radiol 1987;22(4):322-7. (In eng). DOI: 10.1097/00004424-198704000-00008.
76. Bond J, Jones TI. Iron chelates of polyaminocarboxylic acids. Transactions of the Faraday Society 1959;55(0):1310-1318. (10.1039/TF9595501310). DOI: 10.1039/TF9595501310.
77. Shen Y, Goerner FL, Snyder C, Morelli JN, Hao D, Hu D, Li X, Runge VM. T1 relaxivities of gadolinium-based magnetic resonance contrast agents in human whole blood at 1.5, 3, and 7 T. Invest Radiol 2015;50(5):330-8. DOI: 10.1097/RLI.0000000000000132.
78. Laurent S, Elst LV, Muller RN. Comparative study of the physicochemical properties of six clinical low molecular weight gadolinium contrast agents. Contrast Media Mol Imaging 2006;1(3):128-37. (In eng). DOI: 10.1002/cmmi.100.
79. Webb BA, Chimenti M, Jacobson MP, Barber DL. Dysregulated pH: a perfect storm for cancer progression. Nat Rev Cancer 2011;11(9):671-7. (In eng). DOI: 10.1038/nrc3110.

80. Harston GW, Tee YK, Blockley N, Okell TW, Thandeswaran S, Shaya G, Sheerin F, Cellerini M, Payne S, Jezzard P, Chappell M, Kennedy J. Identifying the ischaemic penumbra using pH-weighted magnetic resonance imaging. Brain 2015;138(Pt 1):36-42. (In eng). DOI: 10.1093/brain/awu374.
81. Thews O, Riemann A. Tumor pH and metastasis: a malignant process beyond hypoxia. Cancer Metastasis Rev 2019;38(1-2):113-129. (In eng). DOI: 10.1007/s10555-018-09777-y.
82. Wu L, Jiang L, Sun PZ. Investigating the origin of pH-sensitive magnetization transfer ratio asymmetry MRI contrast during the acute stroke: Correction of T(1) change reveals the dominant amide proton transfer MRI signal. Magn Reson Med 2020;84(5):2702-2712. (In eng). DOI: 10.1002/mrm.28313.
83. Li B, Gu Z, Kurniawan N, Chen W, Xu ZP. Manganese-Based Layered Double Hydroxide Nanoparticles as a T(1) -MRI Contrast Agent with Ultrasensitive pH Response and High Relaxivity. Adv Mater 2017;29(29) (In eng). DOI: 10.1002/adma.201700373.
84. Lu J, Sun J, Li F, Wang J, Liu J, Kim D, Fan C, Hyeon T, Ling D. Highly Sensitive Diagnosis of Small Hepatocellular Carcinoma Using pH-Responsive Iron Oxide Nanocluster Assemblies. J Am Chem Soc 2018;140(32):10071-10074. (In eng). DOI: 10.1021/jacs.8b04169.

# Statutory Declaration

"I, **Jing Xie**, by personally signing this document in lieu of an oath, hereby affirm that I prepared the submitted dissertation on the topic: **Iron(III)-*t*CDTA Derivatives as MRI Contrast Agents / Eisen(III)-*t*CDTA-Derivate als MRI-Kontrastmittel**", independently and without the support of third parties, and that I used no other sources and aids than those stated.

All parts which are based on the publications or presentations of other authors, either in letter or in spirit, are specified as such in accordance with the citing guidelines. The sections on methodology (in particular, regarding practical work, laboratory regulations, statistical processing) and results (in particular, regarding figures, charts and tables) are exclusively my responsibility.

Furthermore, I declare that I have correctly marked all the data, the analyses, and the conclusions generated from data obtained in collaboration with other persons, and that I have correctly marked my own contribution and the contributions of other persons (cf. declaration of contribution). I have correctly marked all texts or parts of texts that were generated in collaboration with other persons.

My contributions to any publications to this dissertation correspond to those stated in the below joint declaration made together with the supervisor. Partial results of the present work were published in: Xie J, Haeckel A, Hauptmann R, Ray IP, Limberg C, Kulak N, Hamm B, Schellenberger E. Iron(III)-*t*CDTA derivatives as MRI contrast agents: Increased T1 relaxivities at higher magnetic field strength and pH sensing. Magn Reson Med. 2021 Jun;85(6):3370-3382. doi: 10.1002/mrm.28664. Epub 2021 Feb 4. PMID: 33538352. All publications created within the scope of the dissertation comply with the guidelines of the ICMJE (International Committee of Medical Journal Editors; www.icmje.org) on authorship. In addition, I declare that I shall comply with the regulations of Charité – Universitätsmedizin Berlin on ensuring good scientific practice.

I declare that I have not yet submitted this dissertation in identical or similar form to another Faculty.

The significance of this statutory declaration and the consequences of a false statutory declaration under criminal law (Sections 156, 161 of the German Criminal Code) are known to me."

Date Signature

# Declaration of my own contribution to the publications

Jing Xie contributed to the following to the below listed publication:

**Publication:**

**Xie J**, Haeckel A, Hauptmann R, Ray IP, Limberg C, Kulak N, Hamm B, Schellenberger E. **Iron(III)-*t*CDTA derivatives as MRI contrast agents: Increased T1 relaxivities at higher magnetic field strength and pH sensing.** Magn Reson Med. 2021 Jun;85(6):3370-3382. doi: 10.1002/mrm.28664. Epub 2021 Feb 4. PMID: 33538352.

Contribution:

The main focus of this publication was the development of new low molecular weight iron(III) complexes-based contrast agents including iron(III) *trans*-cyclohexane diamine tetraacetic acid [Fe(*t*CDTA)]$^-$ could serve as alternatives to gadolinium-based contrast agents in MRI with enhanced properties. I developed the straightforward two-steps synthetic route to obtain *t*CDTA derivatives, and further iron(III)-based chelators synthesis as well as entire purification of 5 derivatives of [Fe(*t*CDTA)]$^-$ : [Fe(*en*-*t*CDTA)]$^+$, [Fe(*en*-Di-*t*CDTA)], [Fe(*trans*-*t*CDTA)]$^+$, [Fe(*trans*-Di-*t*CDTA)], and [Fe(4-ethoxyaniline-*t*CDTA)]. The molecular modelling of the complexes was done via Marvin software and PyMOL Molecular Graphics System. I performed the analysation of chelators by the high-performance liquid chromatography with certain mobile phases and programs, and infrared spectroscopy for validation. I tested the kinetic stability measurement of the iron complexes.

I conducted the *ex vivo* phantom studies for the relaxivity measurement on a relaxometer as well as on 1.5 T, 3 T, and 7 T MRI scanners. In the next phase, I calculated the post-analysis to the data format of the used preclinical MRI scanner and analysed the performance of [Fe(*t*CDTA)]$^-$ derivatives.

Ex vivo measurements were performed by me. I recorded and evaluated the entire data set of this publication alone and independently. The entire method and result section of the manuscript was written by me. Each figure presented in this publication is the result of my work and was made by me including the measurement and evaluation of the data for the figures and tables except the mentioned ones in the text, which are from the co-authors. I contributed to the explanation of the biological background of the findings. I also contributed to writing, editing and revising the published manuscripts. All the co-authors are involved in the writing of the original draft and make critical revision of the manuscript for the publication.

_____

Signature, date and stamp of first supervising university professor/lecture

_____

Signature of doctoral candidate

# Publications

**Publication :** **Xie J**, Haeckel A, Hauptmann R, Ray IP, Limberg C, Kulak N, Hamm B, Schellenberger E. Iron(III)-tCDTA derivatives as MRI contrast agents: Increased T1 relaxivities at higher magnetic field strength and pH sensing. Magn Reson Med. 2021 Jun;85(6):3370-3382. doi: 10.1002/mrm.28664. Epub 2021 Feb 4. PMID: 33538352. **Impact Factor: 3.635**

Journal Data Filtered By: **Selected JCR Year: 2019** Selected Editions: SCIE,SSCI
Selected Categories: **"RADIOLOGY, NUCLEAR MEDICINE and MEDICAL IMAGING"** Selected Category Scheme: WoS
**Gesamtanzahl: 133 Journale**

| Rank | Full Journal Title | Total Cites | Journal Impact Factor | Eigenfactor Score |
|---|---|---|---|---|
| 1 | JACC-Cardiovascular Imaging | 10,110 | 12.740 | 0.027550 |
| 2 | MEDICAL IMAGE ANALYSIS | 9,028 | 11.148 | 0.017100 |
| 3 | RADIOLOGY | 52,731 | 7.931 | 0.057130 |
| 4 | JOURNAL OF NUCLEAR MEDICINE | 26,844 | 7.887 | 0.032990 |
| 5 | EUROPEAN JOURNAL OF NUCLEAR MEDICINE AND MOLECULAR IMAGING | 15,787 | 7.081 | 0.023630 |
| 6 | IEEE TRANSACTIONS ON MEDICAL IMAGING | 21,657 | 6.685 | 0.030060 |
| 7 | CLINICAL NUCLEAR MEDICINE | 5,042 | 6.587 | 0.006200 |
| 8 | NEUROIMAGE | 102,632 | 5.902 | 0.125360 |
| 9 | Photoacoustics | 715 | 5.870 | 0.001760 |
| 10 | INTERNATIONAL JOURNAL OF RADIATION ONCOLOGY BIOLOGY PHYSICS | 44,197 | 5.859 | 0.042160 |
| 11 | Circulation-Cardiovascular Imaging | 5,574 | 5.691 | 0.016320 |
| 12 | ULTRASOUND IN OBSTETRICS & GYNECOLOGY | 13,078 | 5.571 | 0.018050 |
| 13 | JOURNAL OF CARDIOVASCULAR MAGNETIC RESONANCE | 5,205 | 5.361 | 0.011120 |
| 14 | INVESTIGATIVE RADIOLOGY | 6,136 | 5.156 | 0.008830 |
| 15 | RADIOGRAPHICS | 12,418 | 4.967 | 0.010750 |
| 16 | ULTRASCHALL IN DER MEDIZIN | 2,185 | 4.966 | 0.002530 |
| 17 | RADIOTHERAPY AND ONCOLOGY | 17,774 | 4.856 | 0.026510 |
| 18 | European Heart Journal-Cardiovascular Imaging | 6,359 | 4.841 | 0.023110 |
| 19 | HUMAN BRAIN MAPPING | 23,094 | 4.421 | 0.042760 |
| 20 | Journal of the American College of Radiology | 4,409 | 4.268 | 0.010730 |

| Rank | Full Journal Title | Total Cites | Journal Impact Factor | Eigenfactor Score |
|---|---|---|---|---|
| 21 | EUROPEAN RADIOLOGY | 20,761 | 4.101 | 0.033260 |
| 22 | SEMINARS IN RADIATION ONCOLOGY | 2,531 | 4.076 | 0.003540 |
| 23 | JOURNAL OF MAGNETIC RESONANCE IMAGING | 17,046 | 3.954 | 0.024900 |
| 24 | Biomedical Optics Express | 11,090 | 3.921 | 0.025030 |
| 25 | COMPUTERIZED MEDICAL IMAGING AND GRAPHICS | 2,656 | 3.750 | 0.002940 |
| 26 | JOURNAL OF DIGITAL IMAGING | 2,494 | 3.697 | 0.003790 |
| 27 | MAGNETIC RESONANCE IN MEDICINE | 32,159 | 3.635 | 0.029700 |
| 28 | Insights into Imaging | 1,948 | 3.579 | 0.003260 |
| 29 | INTERNATIONAL JOURNAL OF HYPERTHERMIA | 4,397 | 3.574 | 0.004880 |
| 30 | SEMINARS IN NUCLEAR MEDICINE | 2,194 | 3.544 | 0.002420 |
| 31 | AMERICAN JOURNAL OF NEURORADIOLOGY | 23,135 | 3.381 | 0.027120 |
| 32 | JOURNAL OF NUCLEAR CARDIOLOGY | 3,600 | 3.366 | 0.004570 |
| 33 | MEDICAL PHYSICS | 26,445 | 3.317 | 0.027280 |
| 34 | Quantitative Imaging in Medicine and Surgery | 1,335 | 3.226 | 0.002800 |
| 35 | NMR IN BIOMEDICINE | 7,537 | 3.221 | 0.011610 |
| 36 | Clinical Neuroradiology | 935 | 3.183 | 0.002710 |
| 37 | KOREAN JOURNAL OF RADIOLOGY | 2,967 | 3.179 | 0.004490 |
| 38 | Ultrasonography | 618 | 3.075 | 0.001710 |
| 39 | ULTRASONICS | 7,808 | 3.065 | 0.008930 |
| 40 | JOURNAL OF VASCULAR AND INTERVENTIONAL RADIOLOGY | 9,045 | 3.037 | 0.009790 |
| 41 | AMERICAN JOURNAL OF ROENTGENOLOGY | 32,209 | 3.013 | 0.024770 |
| 42 | Practical Radiation Oncology | 1,879 | 2.948 | 0.005780 |

2

Selected JCR Year: 2019; Selected Categories: "RADIOLOGY, NUCLEAR MEDICINE and MEDICAL IMAGING"

https://onlinelibrary.wiley.com/doi/10.1002/mrm.28664

Received: 16 October 2020 | Revised: 9 December 2020 | Accepted: 9 December 2020

DOI: 10.1002/mrm.28664

FULL PAPER

Magnetic Resonance in Medicine

# Iron(III)-*t*CDTA derivatives as MRI contrast agents: Increased $T_1$ relaxivities at higher magnetic field strength and pH sensing

**Jing Xie**[1] | **Akvile Haeckel**[1] | **Ralf Hauptmann**[1] | **Iweta Pryjomska Ray**[2] | **Christian Limberg**[2] | **Nora Kulak**[3] | **Bernd Hamm**[1] | **Eyk Schellenberger**[1]

[1]Department of Radiology, Charité–Universitätsmedizin Berlin, Berlin, Germany

[2]Department of Chemistry, Humboldt-Universität zu Berlin, Berlin, Germany

[3]Institute of Chemistry, Otto-von-Guericke-Universität Magdeburg, Magdeburg, Germany

**Correspondence**
Eyk Schellenberger, Department of Radiology, Charité–Universitätsmedizin Berlin, Charitéplatz 1, 10117 Berlin, Germany.
Email: eyk.schellenberger@charite.de

**Funding Information**
Supported by the Deutsche Forschungsgemeinschaft (DFG, SCHE 1416/11-1 and sub-project B08 of the SFB-1340)

**Purpose:** Low molecular weight iron(III) complex-based contrast agents (IBCA) including iron(III) *trans*-cyclohexane diamine tetraacetic acid $[Fe(t\text{CDTA})]^-$ could serve as alternatives to gadolinium-based contrast agents in MRI. In search for IBCA with enhanced properties, we synthesized derivatives of $[Fe(t\text{CDTA})]^-$ and compared their contrast effects.

**Methods:** *Trans*-cyclohexane diamine tetraacetic acid (*t*CDTA) was chemically modified in 2 steps: first the monoanhydride of *Trans*-cyclohexane diamine tetraacetic acid was generated, and then it was coupled to amines in the second step. After purification, the chelators were analyzed by high-performance liquid chromatography, mass spectrometry, and NMR spectrometry. The chelators were complexed with iron(III), and the relaxivities of the complexes were measured at 0.94, 1.5, 3, and 7 Tesla. Kinetic stabilities of the complexes were analyzed spectrophotometrically and the redox properties by cyclic voltammetry.

**Results:** Using ethylenediamine (en) and *trans*-1,4-diaminocyclohexane, we generated monomers and dimers of *t*CDTA: en-*t*CDTA, en-*t*CDTA-dimer, *trans*-1,4-diaminocyclohexane-*t*CDTA, and *trans*-1,4-diaminocyclohexane-*t*CDTA-dimer. The iron(III) complexes of these derivatives had similarly high stabilities as $[Fe(t\text{CDTA})]^-$. The iron(III) complexes of the *trans*-1,4-diaminocyclohexane derivatives had higher $T_1$ relaxivities than $[Fe(t\text{CDTA})]^-$ that increased with increasing magnetic field strengths and were highest at 6.8 $L{\cdot}mmol^{-1}{\cdot}s^{-1}$ per molecule for the dimer. Remarkably, the relaxivity of $[Fe(\text{en-}t\text{CDTA})]^+$ had a threefold increase from neutral pH toward pH6.

**Conclusion:** Four iron(III) complexes with similar stability in comparison to $[Fe(t\text{CDTA})]^-$ were synthesized. The relaxivities of *trans*-1,4-diaminocyclohexane-*t*CDTA and *trans*-1,4-diaminocyclohexane-*t*CDTA-dimer complexes were in the same range as gadolinium-based contrast agents at 3 Tesla. The $[Fe(\text{en-}t\text{CDTA})]^+$

complex is a pH sensor at weakly acidic pH levels, which are typical for various cancer types.

**KEYWORDS**

gadolinium, iron chelate, iron oxide nanoparticles, low-molecular-weight iron(III)-based contrast agents, magnetic resonance imaging, nephrogenic systemic fibrosis

## 1 | INTRODUCTION

The occurrence of nephrogenic systemic fibrosis in patients with disturbed kidney function[1] but especially the deposition of gadolinium originating from linear and macrocyclic gadolinium-based contrast agents (GBCA) in several organs, including, skin, bones, and brain,[2-5] in patients with normal kidney function resulted in the suspension of less stable linear GBCA, with the exception of 2 liver-targeted GBCA (gadoxetic acid and gadobenic acid), by the European Medicines Agency in 2017. Furthermore, there is an ongoing controversy about what has been termed *gadolinium deposition disease*.[6] Although apart from the bones the brain appears to accumulate substantial Gd, it appears not to be the most severely affected organ because even a patient who died of nephrogenic systemic fibrosis had no obvious brain tissue alterations.[4] Thus, other organs and cells, especially of the immune system, should be investigated for evidence of potential gadolinium side effects in the future. This situation, along with the low but increasing contamination of rivers and drinking water by gadolinium,[7-10] has motivated us to investigate low molecular weight iron(III) complexes as iron-based contrast agents (IBCA) for use in MRI, although the more stable macrocyclic GBCA are continued to be considered as safe drugs.

Recently, we have demonstrated that IBCA administered at higher doses than GBCA achieved similar results in typical clinical applications such as dynamic contrast-enhanced MRI and magnetic MRA without the need to modify imaging protocols.[11] Especially the iron(III) complex of *trans*-cyclohexane diamine tetraacetic acid ([Fe(*t*CDTA)]$^-$) provided comparable contrast effects at only twice the typical clinical dose of Magnevist (Bayer AG, Pharmaceuticals, Berlin, Germany, gadolinium diethylenetriaminepentaacetic acid). The relatively strong contrast effect in comparison to [Fe(DTPA)]$^{2-}$ might be attributed to the availability of a water coordination site in [Fe(*t*CDTA)]$^-$.[11,12] Since then, an iron(II) complex of PyC3A, which served as a redox sensor through oxidation of low relaxivity $Fe^{2+}$ to high relaxivity $Fe^{3+}$,[13] and a group of macrocyclic iron complexes with good relaxivities and relatively long persistence in liver and kidneys have been reported.[14,15]

The purpose of this work was to produce several *t*CDTA derivatives by coupling amine-containing compounds to 1 carboxyl group of *t*CDTA and to thus obtain compounds with improved or modified contrast agent properties (Figure 1). The amines we tested were ethylenediamine and *trans*-1,4-diaminocyclohexane to generate *t*CDTA monomers that can serve for chemical coupling purposes and to generate *t*CDTA dimers for reduced rotational times and thus potentially increased relaxivities.[14,16]

## 2 | METHODS

### 2.1 | Reagents

If not specified otherwise, all reagents were purchased from Merck KGaA (Darmstadt, Germany).

### 2.2 | Synthesis of *trans-1,2-diaminocyclohexane-N,N,N′,N′-tetraacetic acid* monoanhydride (*t*CDTA-MA)

6.53 g (17.9 mmol) of *trans*-1,2-diaminocyclohexane-N,N,N′,N′-tetraacetic acid (*t*CDTA) (Carl Roth GmbH, Karlsruhe, Germany) was added to a solution of 12.87 mL (136.2 mmol) acetic anhydride and 2.75 mL pyridine (34.0 mmol). After stirring for 24 h at room temperature under an argon atmosphere, the reaction mixture was filtered and washed with acetic anhydride followed by excess ethyl acetate. The solid was collected and dried under vacuum to give 5.30 g (81.2%) of the white powder *t*CDTA-MA.[17]

### 2.3 | Synthesis of chelators

#### 2.3.1 | Synthesis of ethylenediamine-*t*CDTA monomer (en-*t*CDTA)

*t*CDTA-MA (14.4 mmol, 5 g) was added in small portions as solid over a period of 6 h to a solution of 19.31 mL ethylenediamine (289 mmol) and 23.75 mL dimethyl sulfoxide under an argon atmosphere. After addition, the reaction mixture was stirred overnight at room temperature. The mixture was then concentrated under reduced pressure (8 mbar) to a thick orange oil that solidified upon standing. The residue was dissolved in methanol and formed a precipitate at room temperature, which was washed several times with methanol to give 3.98 g (80%) of a white solid. Matrix-assisted laser desorption/ionization

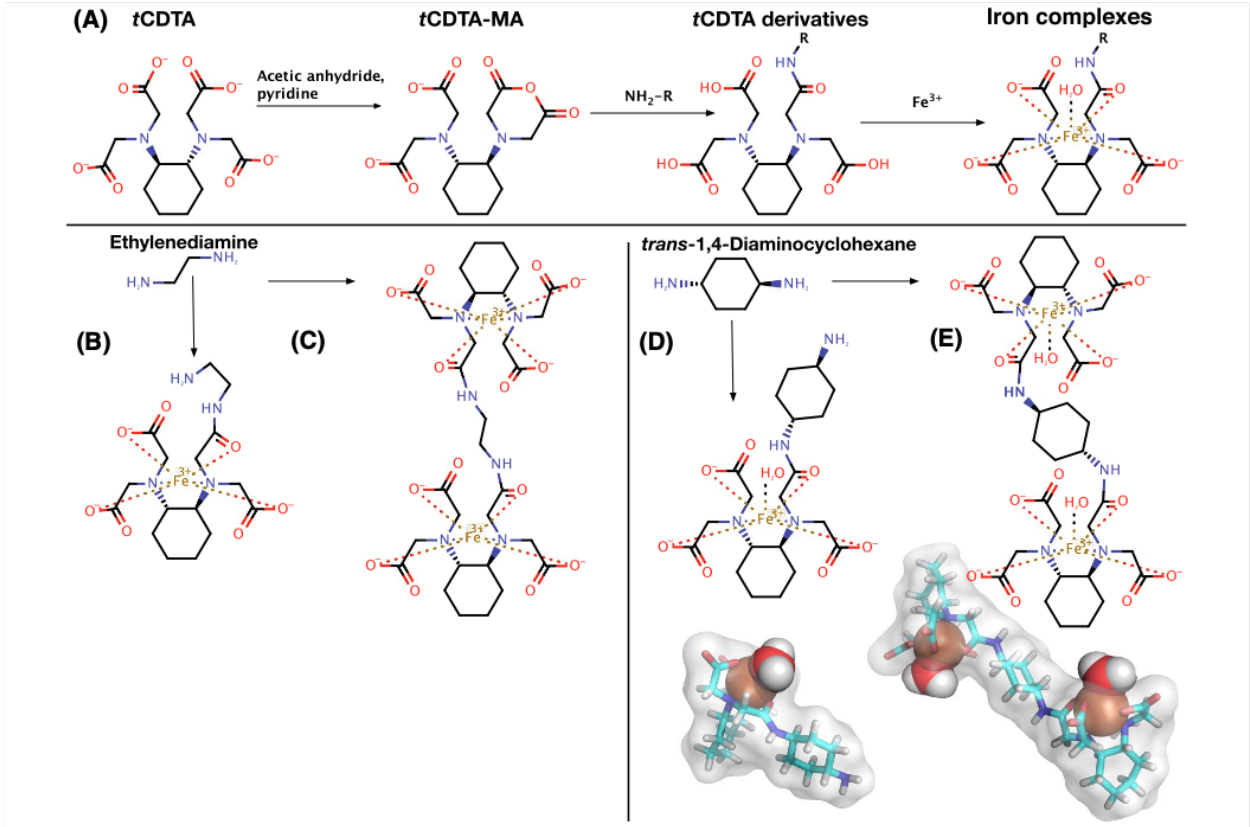


**FIGURE 1** Synthesis of *t*CDTA chelator derivatives. (A) First, *t*CDTA-monoanhydride (*t*CDTA-MA) was generated by reaction of *t*CDTA with acetic anhydride and pyridine followed by purification to remove dianhydrides by filtration with acetic anhydride. In the second step, *t*CDTA-MA reacted with amine-containing compounds to give 4 different carboxamide derivatives of *t*CDTA that are shown as chemical structures and corresponding putative molecular models in (B-E). Following the procedure in (A), the reaction of *t*CDTA-MA with ethylenediamine (flexible) in molar excess resulted in the monomer ethylenediamine-*t*CDTA (B), whereas reaction of ethylenediamine with half-molar (or less) ratio to *t*CDTA-MA gave the dimer ethylenediamine-Di-*t*CDTA (C). The reaction of *trans*-1,4-diaminocyclohexane (rigid) in molar excess to *t*CDTA-MA resulted in the monomer *trans*-1,4-diaminocyclohexane-*t*CDTA (D), whereas reaction of *trans*-1,4-diaminocyclohexane in half-molar ratio to *t*CDTA-MA gave the dimer *trans*-1,4-diaminocyclohexane-Di-*t*CDTA (E). *t*CDTA, trans-cyclohexane diamine tetraacetic acid; *t*CDTA-MA, trans-cyclohexane diamine tetraacetic acid–monoanhydride

(MALDI) mass spectrometry measurements (MALDI-TOF/TOF 4700 Proteomics Analyzer, Applied Biosystems, Foster City, USA) gave an expected/measured mass of 389.42/389.18 [M+H]+ (see Supporting Information Figure S2 and S4)—$^{1}$H-NMR (400 MHz, $D_2O$): 3.57 (s, 3H), 3.53 (s, 3H), 3.48 (s, 1H), 3.44 (s, 1H), 3.03 (t, 2H), 2.92 (m, 4H), 2.16 (m, 2H), 1.82 (m, 2H), 1.26 (m, 4H); $^{13}$C-NMR ($D_2O$): 170.88, 60.26, 50.86, 39.58, 24.17, 23.29; C,H,N-analysis [%]: C 43.94, H 8.12, N 15.07; calculated for $C_{16}H_{27}N_4O_7(NH_4) \times 2\ H_2O$: C 43.98, H 7.84, N 15.23; maximum deviation: 0.28.

### 2.3.2 | Synthesis of ethylenediamine-*t*CDTA dimer (en-Di-*t*CDTA)

*t*CDTA-MA (13.5 mmol, 4.66 g) was added in small portions as solid over a period of 6 h to a solution of 0.45 mL ethylenediamine (6.7 mmol), 22.15 mL dimethyl sulfoxide, and 4.36 mL (53.9 mmol) pyridine under argon atmosphere. After addition, the reaction mixture was stirred overnight at room temperature. This mixture was further washed with excess ethanol and then purified by semipreparative high-performance liquid chromatography (HPLC) (5 mM ammonium bicarbonate buffer with pH 7.78, 2% to 66% acetonitrile gradient over 20 min). The fractions containing en-Di-*t*CDTA were identified by HPLC and lyophilized. MALDI mass spectrometry measurements (MALDI-TOF/TOF 4700 Proteomics Analyzer, Applied Biosystems) gave an expected/measured mass of 717.74/699.11 [M+H]+ −18 (dehydration; see Results section and Supporting Information Figure S2 and S4)—1H-NMR (400 MHz, $D_2O$): 3.65-3.85 (16H), 3.35 (m, 4H), 3.08 (m, 4H), 2.17 (m, 4H), 1.84 (m, 4H), 1.29 (m, 8H)); C,H,N-analysis [%]: C 46.72, H 7.02, N 10.96; calculated for C30H47N6O14Na × 2.15 H2O: C 46.35, H 6.65, N 10.81; maximum deviation: 0.37.

### 2.3.3 | Synthesis of trans-1,4-diaminocyclohexane-*t*CDTA monomer (trans-*t*CDTA)

*t*CDTA-MA (6.93 mmol, 2.4 g) was added in small portions as solid over a period of 6 h to a solution of 3.17 g *trans*-1,4-diaminoclyclohexane (27.7 mmol) dissolved in 18.24 mL dimethyl sulfoxide under argon atmosphere at approximately 90°C and stirred for another 4 h. The reaction mixture was stirred overnight at room temperature. The mixture was then concentrated under reduced pressure (8 mbar) to an ashen solid. After dissolving in methanol, a precipitate formed at room temperature within 2 days. The precipitate was washed several times with methanol to give 1.89 g (79%) of a white solid. MALDI mass spectrometry measurements (MALDI-TOF/TOF 4700 Proteomics Analyzer, Applied Biosystems) gave an expected/measured mass of 443.51/443.26 [M+H]+ (Supporting Information Figure S2 and S4)—$^{1}$H-NMR (400 MHz, $D_2O$): 3.55 (m, 8H), 2.93 (m, 2H), 2.16 (m, 2H), 2.07 (m, 2H), 1.83 (m, 2H), 1.50 (m, 8H), 1.25 (m, 4H); $^{13}$C-NMR ($D_2O$): 172.94, 170.24, 63.16, 60.10, 54.75, 49.08, 48.41, 29.11, 27.98, 24.12, 24.04; C,H,N-analysis [%]: C 51.09, H 8.3, N 13.19; calculated for $C_{20}H_{34}N_4O_7 \times 0.5\ NH_3 \times 1.15\ H_2O$: C 50.92, H 8.08, N 13.36; max. deviation: 0.22).

### 2.3.4 | Synthesis of trans-1,4-diaminocyclohexane-*t*CDTA dimer (trans-Di-*t*CDTA)

*t*CDTA-MA (17.9 mmol, 5.16 g) was added over 6 h as above to a solution of *trans*-1,4-diaminocyclohexane (7.4 mmol, 0.85 g) in 4.82 mL (59.6 mmol) pyridine and 58.80 mL dimethyl sulfoxide. The reaction mixture was stirred overnight under argon atmosphere at room temperature. The mixture was dried in a rotary evaporator to give a whitish solid. The resulting residue was washed and filtrated with ethanol; the filtrate was collected and then lyophilized to provide a white powder. The MALDI mass spectrometry measurements (Mikroflex MALDI mass spectrometer, Bruker Daltonics, Bremen, Germany) gave an expected/measured mass of 771.83/771.18 [M+H]+ (see Supporting Information Figure S2 and S4)—$^{1}$H-NMR (400 MHz, $D_2O$): 3.36 (m, 4H), 3.13 (m, 12H), 2.95 (m, 4H), 2.32 (m, 4H), 1.94 (m, 4H), 1.87 (m, 2H), 1.68 (m, 8H), 1.30 (m, 8H); $^{13}$C-NMR ($D_2O$): 172.68, 60.34, 52.57, 47.73, 38.77, 25.12, 23.47; C,H,N-analysis [%]: C 47.62, H 7.15, N 9.01; calculated for $C_{34}H_{55}N_6O_{14}(HCO_3) \times 3.2\ H_2O$: C 47.21, H 7.06, N 9.44; maximum deviation: 0.43.

## 2.4 | Synthesis of iron(III) complexes

Iron(III) complexes were prepared by reaction of the *t*CDTA chelators (see above) with a stoichiometric equivalent of $FeCl_3$ solution (1 M, adjusted with a commercial iron chloride calibration solution, final concentrations of 20 to 50 mM) to the binding centers (1:1 ratio for monomers and 2:1 ratio for dimers). Next, the solution was adjusted slowly with a saturated meglumine solution to pH 7.4. After 1 day, the iron complex solutions were centrifuged at 13,800 g for 20 min to remove any excess iron in the form of insoluble iron(III) hydroxide (solubility product $2.8 \times 10^{-39}$ at 25°C), and the supernatant was filtered with 0.45 μm syringe filters.

## 2.5 | HPLC analysis

New compounds were assessed after synthesis and purification by reverse-phase HPLC on a Dionex UltiMate 3000 system (Thermo Fisher Scientific, Waltham, USA). The conditions and results are given in the Supplementary Information section Figure S1. Sample detection was performed by absorption measurement at 210 nm using a diode array detector (Dionex UltiMate 3000, Thermo Fisher Scientific, Waltham, USA).

## 2.6 | Mass spectrometry analysis of chelators

After purification and analysis of the purity by HPLC, the *t*CDTA derivatives were analyzed by MALDI-TOF mass spectrometry in the reflector mode on instruments 4700 Proteomics Analyzer (Applied Biosystems, Foster City, USA) and Microflex LRF (Bruker Daltonics, Bremen, Germany). Measurements were performed by the Shared Facility of Mass Spectrometry of the Institute of Biochemistry, Charité—Universitätsmedizin Berlin. Mass spectrometry results are presented in the Supporting Information Figure S2.

## 2.7 | Infrared spectroscopy

Infrared spectroscopy spectra of lyophilized substances were recorded on a Bruker Compact FT- infrared spectroscopy spectrometer ALPHA-P using the OPUS software (OPUS 6.5, Bruker Optik GmbH, Germany). See Supporting Information Figure S3.

## 2.8 | NMR

NMR of the chelators spectra were recorded on a Bruker AV 400 NMR spectrometer ($^{1}$H and $^{13}$C 400 MHz) in $D_2O$ at room temperature. Chemical shifts are reported in ppm relative to residual proton signals of $D_2O$ (4.8 ppm). For NMR spectrometry of trans-Di-*t*CDTA, the sodium salt was used due to the low solubility of the free acid. See also Supporting Information Figure S4.

### 2.9 | Stability measurement

Stability of the iron complexes (1.0 mM Fe) was compared by measuring the changes in absorption spectra between 220 and 500 nm over time during treatment with 100 mM HCl according to Snyder et al.[14] Additionally, we compared the absorption spectra to those of $FeCl_3$ in 100 mM HCl and *t*CDTA in 100 mM HCl, and $[Fe(tCDTA)]^-$ in 1 M HCl.

### 2.10 | Cyclic voltammetry

Electrochemical studies were carried out using a EmStat Blue potentiostat (PalmSens BV, Houten, The Netherlands) in a conventional 1-compartment 3-electrode cell with a glassy carbon electrode (ID 1.6 mm) as the working electrode, a platinum plate (5 × 5 mm) as the counter electrode, and a silver wire in aqueous AgCl solution as the pseudo-reference electrode. All measurements were carried out in deionized and degassed $H_2O$ solutions containing 0.1 M KCl at pH 5.9 under argon atmosphere at ambient temperature. Cyclic voltammograms were collected at a scan rate of 0.1 $Vs^{-1}$. See also Supporting Information Table S1.

### 2.11 | Relaxivity measurement by relaxometry

For relaxivity measurements, all iron complexes were diluted in water or fetal calf serum (FCS) (Gibco, Thermo Fisher Scientific, Rockford, IL) at concentrations of 0.125, 0.25, 0.5, and 1.0 mM at pH 7.4 and loaded into glass NMR tubes (5 mm outside diameter; Wilmad-Lab Glass, Vineland, USA). Measurements at 0.94 Tesla (T) were performed using an NMR relaxometer Minispec mq 40 (Bruker BioSpin, Rheinstetten, Germany) according to the manufacturer's instructions. For measurements of the pH dependence, samples of $[Fe(en\text{-}tCDTA)]^+$ in the concentrations above were dissolved in water or FCS and adjusted to the different pH values.

### 2.12 | Relaxivity measurement by MR imaging

Relaxivities at 1.5 T, 3 T, and 7 T were measured on MRI scanners. Up to 7 samples prepared as above were placed in a circular phantom holder at room temperature. For measurements at 37°C, a phantom holder equipped with water heating was kept at 37°C ± 1°C and monitored by a fiber optic temperature probe. Measurements at 1.5 T were conducted on a Magnetom Sonata (Siemens, Erlangen, Germany) and at 3 T on a Magnetom Lumina (Siemens) clinical MRI scanner using standard 2D spin echo sequences. Different repetition times (TR) of 100, 150, 300, 600, and 1000 ms were used to measure $T_1$ times and calculate $T_1$ relaxivities. Echo time (TE) was 11 ms for 1.5 T and 13 ms for 3 T. Other imaging parameters were matrix of 256 × 256, field of view (FOV) of 75 × 75 $mm^2$, and the slice thickness of 5 mm. The $T_1$ maps were generated from the resulting image datasets using ImageJ with the MRI Analysis Calculator plug-in from Karl Schmidt (v1.0, kfschmidt@bwh.harvard.edu, 2002/06/19).

For measurement at 7 T, the phantoms were imaged on a BioSpec small animal MRI scanner (Bruker, Ettlingen, Germany) using a built-in dedicated multi-TR spin echo sequence with integrated $T_1$ mapping. The TRs were 25, 72, 125, 186, 258, 346, 459, 617, 882, and 2000 ms. TE was 9.0 ms; an imaging matrix of 256 × 256 was used with a FOV 50 × 50 $mm^2$ and slice thickness 1 mm.

$T_1$ times of the samples determined by MRI were measured in circular regions of interest of constant size placed in the center of the cross sections of each tube in the $T_1$ maps.

The $T_1$ and $T_2$ relaxivities were determined by performing linear regression analysis of 1/T versus iron concentration of the complexes using GraphPad Prism version 5.0a (GraphPad Software, Inc., San Diego, CA).

### 2.13 | Molecular modeling

Molecular modeling of the complexes was done based on the X-ray crystal structures of $[Fe(tCDTA)]^{-12}$ using Marvin software followed by Dreiding force field energy minimization (Marvin version 19.17, 2019, ChemAxon, Budapest, Hungary) and the PyMOL Molecular Graphics System (Schrödinger, Inc, New York, USA, Open Source version 1.8.2.1., on Apple XQuartz 2.7.11 X Window System).[18]

## 3 | RESULTS

In this study, we synthesized *t*CDTA derivatives in 2 steps as shown in Figure 1A using a method adapted from Gestin et al.[17] First, a monoanhydride of *t*CDTA (*t*CDTA-MA) was generated using acetic anhydride in the presence of pyridine as proton acceptor. After separation from dianhydrides by filtration, *t*CDTA-MA was reacted either with an excess of the diamine compounds to generate monomers (defined as the 1:1 condensation reaction product) or with less than half-molar amounts of diamines to synthesize dimers (defined as the 2:1 condensation reaction product). In this way, the reaction with ethylenediamine resulted in the monomer ethylenediamine-*t*CDTA (en-*t*CDTA) (Figure 1B, MW 388.42) and the dimer ethylenediamine-Di-*t*CDTA (en-Di-*t*CDTA) (Figure 1C, MW 716.74). Accordingly, reacting *t*CDTA-MA with an excess of *trans*-1,4-diaminocyclohexane gave the monomer *trans*-1,4-diaminocyclohexane-*t*CDTA (*trans*-*t*CDTA) (Figure 1D, MW 442.51), whereas reaction with a half-molar amount of

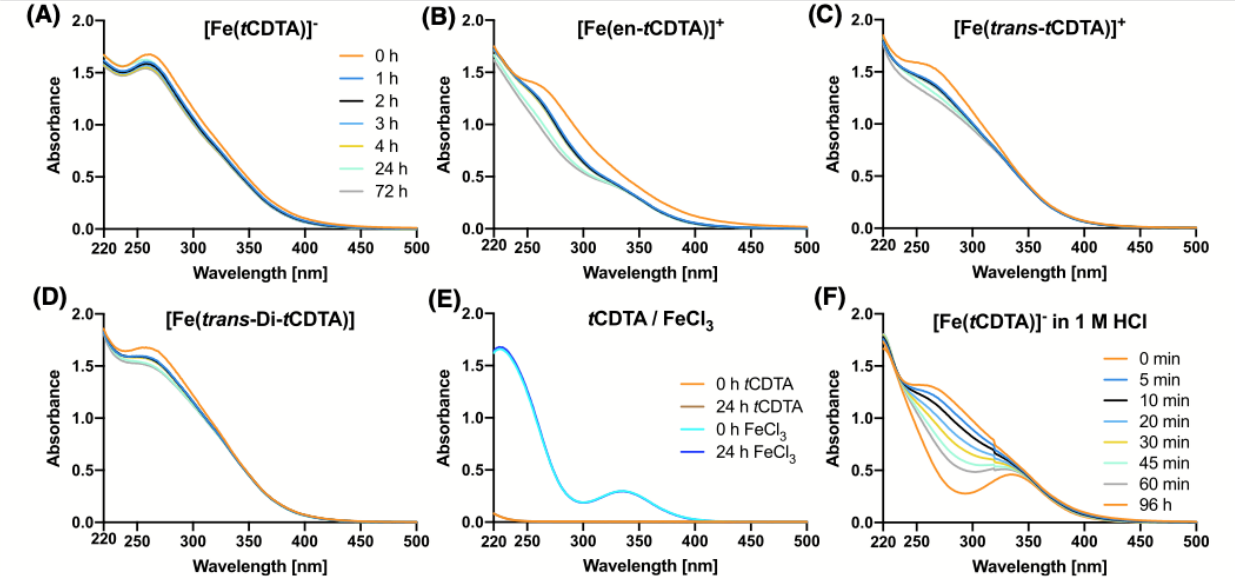


**FIGURE 2** Comparison of stabilities of the iron(III) complexes of *t*CDTA and the new derivatives over time. The dissociation of $[Fe(tCDTA)]^-$ (A), $[Fe(en\text{-}tCDTA)]^+$ (B), $[Fe(trans\text{-}tCDTA)]^+$ (C), and [Fe(*trans*-Di-*t*CDTA)] (D) was monitored by measuring absorption spectra (1.0 mM Fe) over time in 100 mM HCl and observing the reduction of absorbance at 300 nm according to Snyder et al.[14] (E) Free $FeCl_3$ has an absorption minimum at 300 nm, and *t*CDTA has only minimal absorption below 250 nm (both in 100 mM HCl). In comparison to harsh treatment with 1 M HCl, which caused a time-dependent dissociation of $[Fe(tCDTA)]^-$ (F), all $[Fe(tCDTA)]^-$ derivatives were remarkably stable at 100 mM HCl. $[Fe(tCDTA)]^-$, iron(III) complex of *trans*-cyclohexane diamine tetraacetic acid; $[Fe(en\text{-}tCDTA)]^+$, iron(III) complex of ethylenediamine-*t*CDTA; $[Fe(trans\text{-}tCDTA)]^+$, iron(III) complex of *trans*-1,4-diaminocyclohexane-*t*CDTA; [Fe(*trans*-Di-tCDTA)], iron(III) complex of trans-1,4-diaminocyclohexane-Di-tCDTA

*trans*-1,4-diaminocyclohexane resulted in the dimer *trans*-1,4-diaminocyclohexane-Di-*t*CDTA (*trans*-Di-*t*CDTA) (Figure 1E, MW 770.83). HPLC analysis (see Supporting Information Figure S1) of purified amides yielded purities with the following peak area percentages—en-*t*CDTA: 98.1%; en-Di-*t*CDTA: 96.6%; *trans*-*t*CDTA: 99.0%; and *trans*-Di-*t*CDTA: 98.4%. Absence of relevant amounts of *t*CDTA was confirmed by HPLC for all chelators, which is an important precondition for relaxivity measurements excluding contributions from the corresponding iron complexes. Product identities were confirmed by MALDI mass spectrometry, $^1H$ and $^{13}C$ NMR, and elemental analysis (see Supporting Information Figure S4). The main mass peaks of en-Di-*t*CDTA (and to a very small extent, also those of en-*t*CDTA) were reduced by 18 Da, which can be attributed to dehydration during the MALDI mass spectrometry.[19] For confirmation, we compared the infrared spectroscopy spectra of *t*CDTA, *t*CDTA-MA, en-*t*CDTA, and en-Di-*t*CDTA by infrared spectroscopy (see Supporting Information Figure S3). As expected, we found the characteristic bands for anhydrides only for *t*CDTA-MA.

After preparation of the iron(III) complex solutions by letting react the chelators with iron(III) chloride, we compared the stabilities of the new iron complexes with that of $[Fe(tCDTA)]^-$, which was reported to have a rather high complex stability constant, log K, of 27.5[20] or of 29.3.[21] Figure 2 (and Supporting Information Figure S5) shows the absorption spectra of the iron(III) complexes over time during a challenge with 100 mM HCl, as done by Snyder et al.[14] All tested complexes revealed only minimal initial absorbance changes at 100 mM HCl and thus differed from iron(III) chloride at 100 mM HCl and to $[Fe(tCDTA)]^-$ at 1 M HCl.

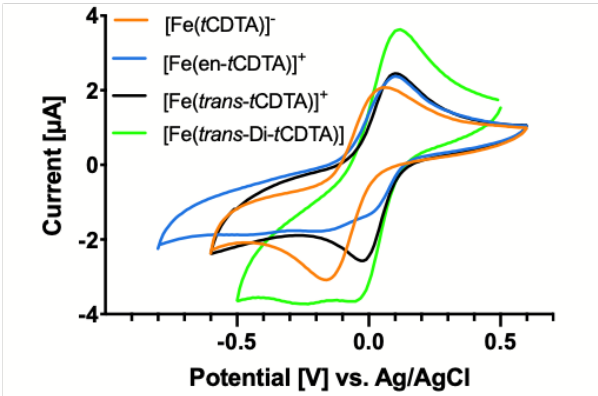


**FIGURE 3** Cyclic voltammetry of iron complexes at neutral pH and a scan rate of 100 mV/s. Solutions contained 1.0 mM of the iron complexes and 100 mM KCl as electrolyte

Redox properties of the iron(III) complexes were examined by cyclic voltammetry using a glassy carbon working electrode and KCl as a supporting electrolyte. The peak potential values obtained for the oxidation/reduction events are compiled (referenced to an Ag/AgCl electrode) in Supporting

**TABLE 1** $T_1$ and $T_2$ relaxivities of iron chelate complexes of *t*CDTA and *t*CDTA derivatives [$mM^{-1}s^{-1}$] per metal ion determined at 0.94, 1.5, 3.0, and 7.0 T (for dimers per molecule in brackets)

| Field Strength (temperature) | Solvent | *t*CDTA | Ethylenediamine-*t*CDTA | Ethylenediamine-Di-*t*CDTA | *Trans*1,4-Diaminocyclohexane-*t*CDTA | *Trans*1,4-Diaminocyclohexane-Di-*t*CDTA-Dimer |
|---|---|---|---|---|---|---|
| 0.94 T 37°C | $r_1$ in water | 1.56 ± 0.03 | 0.78 ± 0.01 | 1.24 ± 0.05 (2.48 ± 0.10) | 1.92 ± 0.10 | 1.99 ± 0.10 (3.98 ± 0.20) |
| | $r_1$ in serum | 1.99 ± 0.13 | 0.72 ± 0.02 | 1.44 ± 0.03 (4.36 ± 0.08) | 2.01 ± 0.04 | 2.18 ± 0.04 (4.36 ± 0.08) |
| | $r_2$ in water | 1.72 ± 0.06 | 0.81 ± 0.02 | 1.50 ± 0.08 (3.00 ± 0.16) | 2.16 ± 0.09 | 2.25 ± 0.29 (4.50 ± 0.58) |
| | $r_2$ in serum | 2.79 ± 0.36 | 0.75 ± 0.03 | 1.68 ± 0.01 (3.36 ± 0.02) | 2.49 ± 0.09 | 2.73 ± 0.03 (5.46 ± 0.06) |
| 1.5 T 23°C | $r_1$ in water | – | – | – | 2.27 ± 0.01 | 2.75 ± 0.21 (5.50 ± 0.42) |
| | $r_1$ in serum | – | – | – | 2.74 ± 0.03 | 3.26 ± 0.41 (6.52 ± 0.82) |
| 3 T 37°C/23°C | $r_1$ in water | 2.07 ± 0.08/2.06 ± 0.13 | – | – | 2.64 ± 0.04/2.64 ± 0.37 | 2.99 ± 0.32/2.80 ± 0.03 (5.98 ± 0.64/5.60 ±0.06) |
| | $r_1$ in serum | 2.35 ± 0.03/2.46 ± 0.17 | – | – | 3.06 ± 0.07/3.08 ± 0.06 | 3.39 ± 0.16/3.53 ± 0.02 (6.78 ± 0.32/7.06 ± 0.04) |
| 7 T 37°C/23°C | $r_1$ in water | 1.87 ± 0.04/1.88 ± 0.07 | – | – | 2.38 ± 0.07/3.40 ± 0.00 | 2.65 ± 0.15/3.80 ± 0.04 (5.30 ± 0.30/7.60 ± 0.08) |
| | $r_1$ in serum | 2.71 ± 0.07/2.79 ± 0.04 | – | – | 2.61 ± 0.26/3.88 ± 0.07 | 3.23 ± 0.35/4.71 ± 0.37 (6.46 ± 0.70/9.42 ± 0.74) |

All measurements were performed in fetal bovine serum or buffer-free water at pH7.4.

$r_1$, $T_1$ relaxivity; $r_2$, $T_2$ relaxivity; T, Tesla; *t*CDTA, trans-cyclohexane diamine tetraacetic acid.

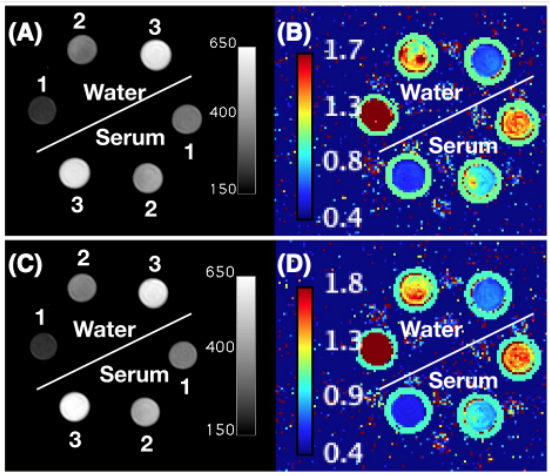


**FIGURE 4** Contrast effects of [Fe(*trans*-*t*CDTA)]$^+$ and [Fe(*trans*-Di-*t*CDTA)] in $T_1$-weighted MR imaging at 3 T. The images show spectrometer tubes containing 3 concentrations (1: 125 μM, 2: 250 μM, and 3: 500 μM Fe) of [Fe(*trans*-*t*CDTA)]$^+$ (A, B) or [Fe(*trans*-Di-*t*CDTA)] (C, D) in water or in 100% fetal bovine serum at neutral pH. (A, C) Signal intensity images acquired with a $T_1$-weighted spin echo sequence at 3 T (TE 13 ms, TR 150 ms). (B, D) Corresponding $T_1$ maps in seconds. Images were acquired at 37°C. T, Tesla

Information Table S1. The cyclic voltammograms of all 3 complexes (Figure 3) exhibited 1 reversible redox wave in the anodic scan ($E_a \approx +0.06$ V for [Fe(*t*CDTA)]$^-$ and around +0.1 V for the other complexes). Whereas reversible cathodic waves were observed for [Fe(*t*CDTA)]$^-$ and [Fe(*trans*-*t*CDTA)]$^+$, the other 2 complexes showed 2 small cathodic peak potentials, indicating the presence of 2 different species. Half-wave potentials $E_{1/2}$ in the range of −0.05 to 0.06 V were calculated (Supporting Information Table S1).

Relaxivity, an important measure for the contrast effect, was analyzed at different field strengths (Table 1). The iron complexes of the chelators en-*t*CDTA (Figure 1B) and en-Di-*t*CDTA (Figure 1C), which were generated with ethylenediamine, had relatively low relaxivities at 0.94 T and neutral pH, whereas *trans*-*t*CDTA (Figure 1D) and *trans*-Di-*t*CDTA (Figure 1E) had relaxivities comparable to *t*CDTA at this field strength. However, at higher field strengths the $T_1$ relaxivities increased substantially and were highest at 7 T for the dimer *trans*-Di-*t*CDTA (Figure 1E), namely 4.71 ± 0.37 $L{\cdot}mmol^{-1}{\cdot}s^{-1}$ per iron and 9.42 ± 0.74 $mM^{-1}s^{-1}$ per dimeric molecule in water and 3.23 ± 0.35 $L{\cdot}mmol^{-1}{\cdot}s^{-1}$/6.46 ± 0.70 $L{\cdot}mmol^{-1}{\cdot}s^{-1}$ in serum (Table 1). Figure 4 demonstrates the contrast effects in MR phantom images of *trans*-*t*CDTA (Figure 4A,B) and *trans*-Di-*t*CDTA (Figure 4C,D) at different concentrations and neutral pH in water and in serum.

The surprisingly low relaxivities of [Fe(en-*t*CDTA)]$^+$ and [Fe(en-Di-*t*CDTA)] compared with [Fe(*trans*-*t*CDTA)]$^+$ and [Fe(*trans*-Di-*t*CDTA)] at neutral pH could be explained by the coordination of the distant amine groups to the chelated iron or alternatively by hydroxide ion coordination (Figure 5). Accordingly, the relaxivities of [Fe(en-*t*CDTA)]$^+$ (Figures 6 and 7) and to a lesser extent of [Fe(en-Di-*t*CDTA)] (Supporting Information Figure S7) determined by relaxometry at 0.94 T increased substantially as the pH was lowered. In water (Figure 6A), en-*t*CDTA had a pH-dependent $T_1/T_2$ relaxivity increase from 0.82/0.85 $L{\cdot}mmol^{-1}{\cdot}s^{-1}$ at pH 7.4 to 1.77/2.02 $L{\cdot}mmol^{-1}{\cdot}s^{-1}$ at pH 5.1. In serum (Figure 6B), the $T_1/T_2$-relaxivity increase was threefold, from 0.72/0.75 $L{\cdot}mmol^{-1}{\cdot}s^{-1}$ at pH 7.4 to 2.24/2.73 $L{\cdot}mmol^{-1}{\cdot}s^{-1}$ at pH 5.0. The sigmoidal dose response plots revealed a 50% pH of 6.79 ± 0.07/6.84 ± 0.07 ($T_1/T_2$) in water and a 50% pH of 6.17 ± 0.11/6.08 ± 0.09 in serum. Figure 6C shows the pH-dependent $T_1$ relaxivity of [Fe(en-*t*CDTA)]$^+$ at 7 T in serum, which was determined by MR imaging with TR variation on a 7 T Bruker small animal scanner.

The high linearity of the relaxivities of [Fe(en-*t*CDTA)]$^+$ over the measured pH range suggests that they are not a function of [Fe(en-*t*CDTA)]$^+$ concentration and thus of the ratio of [Fe(en-*t*CDTA)]$^+$ to hydroxide ions (see Supporting Information Figure S6). A comparable pH dependence below pH7.4 was observed for the [Fe(en-Di-*t*CDTA)] dimer (see Supporting Information Figure S7B). The relaxivities of the iron complexes coupled with the rigid diamine [Fe(*trans*-*t*CDTA)]$^+$ and [Fe(*trans*-Di-*t*CDTA)] (see Supporting Information Figure S7C,D) were also found to have decreasing relaxivities with increasing pH; however, in contrast to the ethylenediamine derivatives, they exhibited this behavior above pH7.4.

## 4 | DISCUSSION

Based on the promising results with IBCA, especially with [Fe(*t*CDTA)]$^-$, as potential alternatives that can replace GBCA in contrast-enhanced $T_1$-weighted MRI,[11] we aimed at modifying *t*CDTA to potentially further improve relaxivities and to generate iron chelates with different molecular properties for various clinical applications.

Using an efficient 2-step synthesis procedure, we created 4 new *t*CDTA derivatives by reaction of 2 different diamine compounds in either an excess or less than half-molar ratio with *t*CDTA-MA, which was generated in the first reaction step. After having confirmed purity of the derivatives and especially the absence of the starting material, *t*CDTA, to rule out a contribution of [Fe(*t*CDTA)]$^-$ to subsequently measured relaxivities and having obtained proof of identity by MALDI mass spectrometry, NMR, and elemental analyses, we made several observations.

The iron complexes of the ethylenediamine derivatives en-*t*CDTA and en-Di-*t*CDTA had surprisingly low $T_1$ and $T_2$ relaxivities in comparison to *t*CDTA at neutral pH. It has been shown previously that the substantially lower relaxivity of the 7-coordinated [Fe(DTPA)]$^{2-}$ complex compared

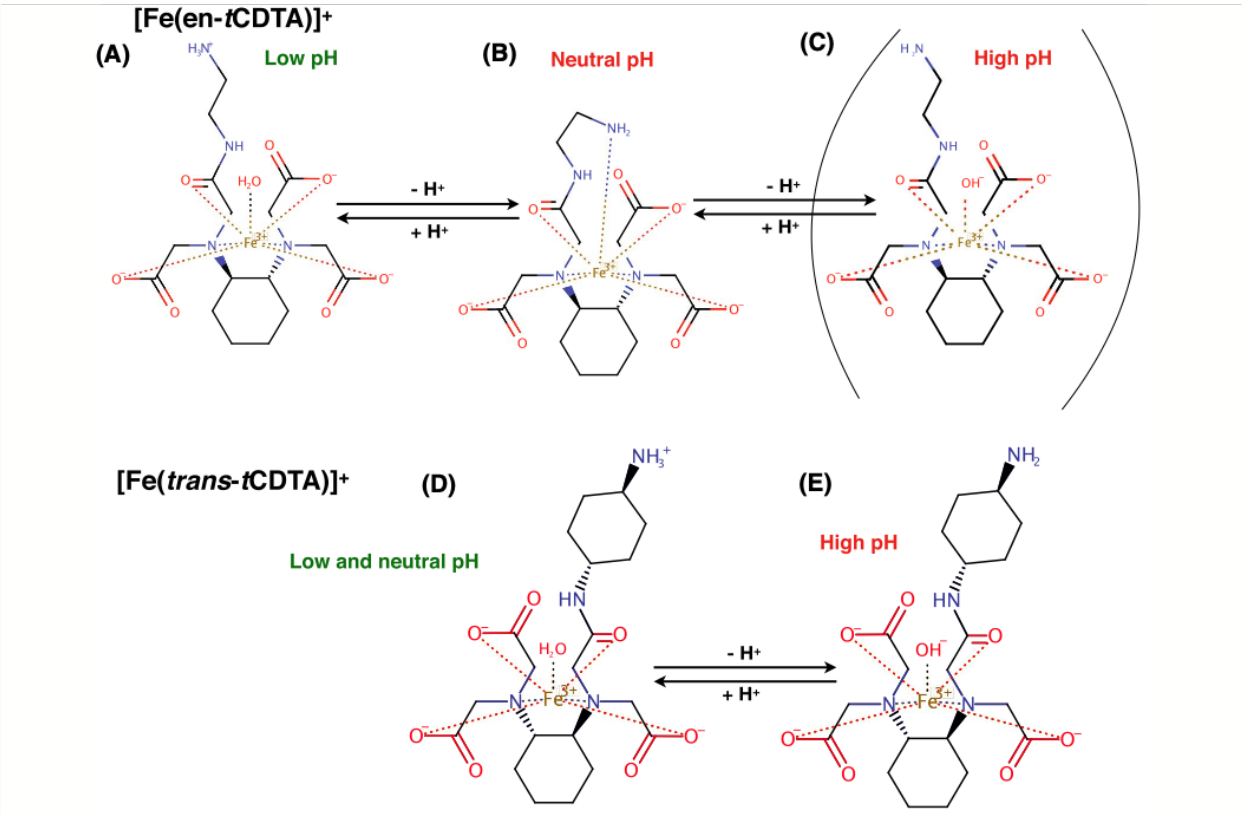


**FIGURE 5** Hypothetical mechanisms of the observed pH-dependent relaxivity changes of $[Fe(en\text{-}tCDTA)]^+$ and $[Fe(trans\text{-}tCDTA)]^+$. (A) At slightly acidic pH, the terminal free amine group could be protonated, which in turn would prevent the iron coordination. Consequently, 1 coordination site would be available for water coordination, allowing efficient inner sphere relaxation. (B) At neutral and high pH, the terminal amine group becomes deprotonated and thus could coordinate to central iron, block water coordination, and prevent efficient inner sphere relaxation. (C) At neutral and higher pH, higher concentrations of hydroxide ions can coordinate the central iron and thus block water coordination and inner sphere relaxation. (B) and (C) could coexist, but (C) seems more likely to occur at higher pHs. (D) The terminal free amine group of the rigid *trans*-1,4-diaminocyclohexane cannot coordinate the iron, which would explain the relatively high relaxivity at neutral and low pH (Supporting Information Figure S7). (E) At higher pH, high concentrations of hydroxide ions can coordinate to iron and thus block water access and reduce relaxivity. The pH-dependent relaxivities of the dimers [Fe(en-Di-*t*CDTA)] and [Fe(*trans*-Di-*t*CDTA)] could be explained accordingly to the correspondent monomers

with the 6-coordinated $[Fe(tCDTA)]^-$ complex is due to the fact that in the latter a coordination site remains open for the coordination of water, which allows inner sphere relaxation.[11,12] Analogously, the low relaxivities of $[Fe(en\text{-}tCDTA)]^+$ and [Fe(en-Di-*t*CDTA)] could be assumed to result from coordination of the terminal amine group in these compounds with the central iron(III), thereby preventing the water coordination and exchange with bulk water, which is required for the important inner-sphere relaxation. This hypothesis (Figure 5) is supported by the strong pH dependence of $[Fe(en\text{-}tCDTA)]^+$ with a substantial relaxivity increase from neutral pH toward pH 5.0. At low pH, the terminal amine should become protonated, which would prevent coordination of the iron and thus leave 1 Fe coordination site available for water coordination (Figure 5A). Interestingly, the pH levels at which half-maximal $T_1$ relaxivity occurred were approximately 6.8 in water and 6.2 in serum, which might be explained by electron density reduction of the distal amine group by the amide group of the coupled ethylenediamine, thereby lowering the pKa of the amine. A similar mechanism might explain the relatively low relaxivity and pH dependence of the [Fe(en-Di-*t*CDTA)] dimer, where the 2 introduced amides of the ethylenediamine bridge possibly coordinate with the 2 Fe(III) ions, thereby blocking inner-sphere water coordination and relaxation. Alternatively, the low relaxivities at neutral and higher pHs might be attributable to blockage of the central iron by coordination of hydroxide ions at higher concentrations, which at the same time would prevent inner sphere relaxation (Figure 5C,E). In fact, $[Fe(trans\text{-}tCDTA)]^+$ and [Fe(*trans*-Di-*t*CDTA)] with rigid diamines were also deactivated at higher pHs (Supporting Information Figure S7C,D) but above pH7.4. This pH dependency may be attributed to increased contribution of

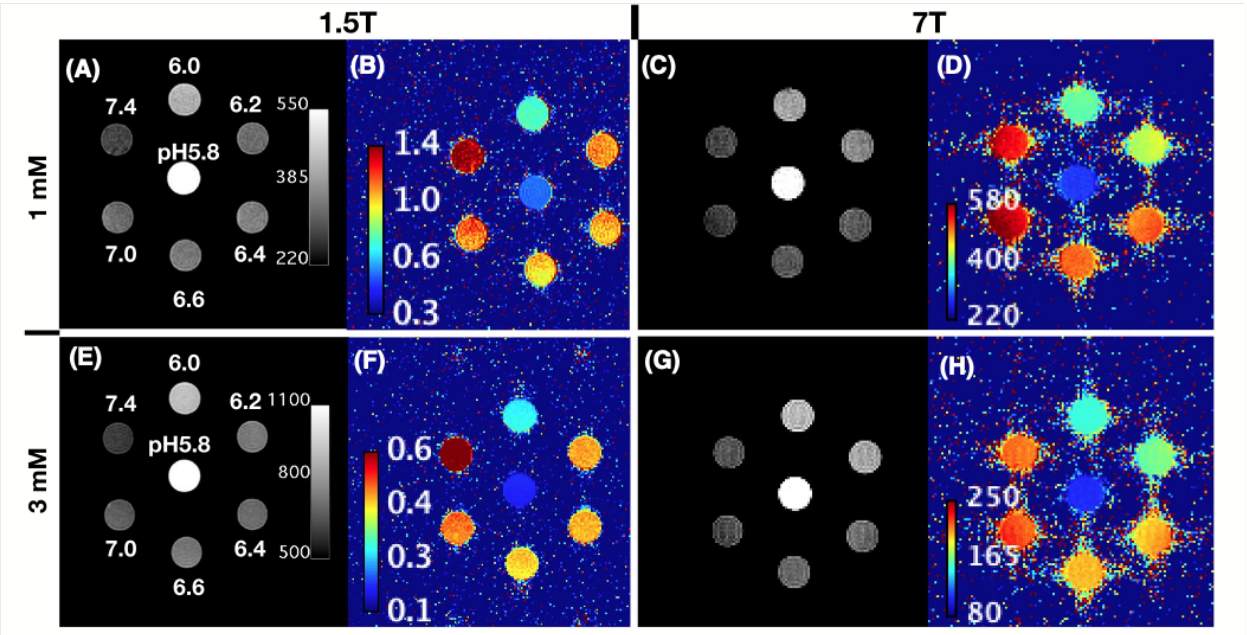


**FIGURE 6** MR imaging of pH-dependent contrast effects of $[Fe(en\text{-}t\text{CDTA})]^+$ at 1.5 T and 7 T. Seven spectrometer tubes containing either 1 mM (A-D) or 3 mM (E-F) of $[Fe(en\text{-}t\text{CDTA})]^+$ in 100% fetal bovine serum with adjusted pHs between 5.8 and 7.4 were imaged with a $T_1$-weighted pulse sequence at magnetic field strengths of 1.5 T and 7 T. (A, E) Signal intensity images (spin echo sequence, TR 150 ms, TE 11 ms) and (B, F) corresponding $T_1$ maps in seconds acquired in a clinical 1.5 T MRI scanner. (C, G) Signal intensity images (spin echo sequence, TR 71.8 ms, TE 9 ms) and corresponding $T_1$ maps in milliseconds (D, H) obtained in a Bruker 7 T small animal MRI scanner. Imaging was performed at room temperature

the iron hydroxide complex as pH increases. Furthermore, $[Fe(en\text{-}t\text{CDTA})]^+$ relaxivities were independent of $[Fe(en\text{-}t\text{CDTA})]^+$ concentration and thus the concentration ratio to hydroxide over the full pH range tested (see Supporting Information Figure S6). Therefore, we hypothesize in Figure 5 that the relaxivity decrease of $[Fe(en\text{-}t\text{CDTA})]^+$ with increasing pHs below pH7.4 is dominated by the coordination of the distal amine, whereas for the 2 *trans*-1,4-diaminocyclohexane derivatives, the relaxivity decrease at higher pH is mainly attributable to hydroxide.

Because slightly lower extracellular pH levels are typical for many cancers,[22,23] the pH-dependent $T_1$ relaxivity increase of $[Fe(en\text{-}t\text{CDTA})]^+$ might be exploited for the detection or characterization of cancer by MRI. Another important example for pH imaging is the identification of salvageable tissue in stroke.[24,25] The low molecular weight complex should be superior to pH nanosensors[26-29] in terms of a faster and broader biodistribution, including a more efficient excretion. The plain activation characteristic and relatively strong $T_1$ relaxivity increase of $[Fe(en\text{-}t\text{CDTA})]^+$ in comparison to previously reported complex-based $T_1$-relaxivity pH sensors[30-33] could be advantageous and simplify MR image analysis in the future. Undeniably, clinical use of such pH sensor probes remains challenging because the $T_1$ contrast effect depends on both relaxivity and local concentration. Nevertheless, probes such as $[Fe(en\text{-}t\text{CDTA})]^+$ can be very useful for preclinical research, for example, when administered by Alzet osmotic pump to achieve constant blood concentrations as demonstrated by Savić et al.[34]

To produce always-on Fe complexes comparable to clinically used GBCA, we chose *trans*-1,4-diaminocyclohexane as a more rigid amine linker molecule that should prevent the potential amine coordination and thus blockage of the important water coordination side. As predicted, the iron complexes of both the monomer *trans*-*t*CDTA and the dimer *trans*-Di-*t*CDTA were shown to have substantially higher relaxivities than their ethylenediamine counterparts at neutral pH (but not at high pH, see above), whereas their relaxivities were not much higher than those of $[Fe(t\text{CDTA})]^-$ at 0.94 T.

Remarkably, $T_1$ relaxivities of the iron complexes increased with higher magnetic field strengths. $[Fe(trans\text{-}t\text{CDTA})]^+$ and [Fe(*trans*-Di-*t*CDTA)] had especially high relaxivities at the typical clinical field strengths of 1.5 T and 3 T and still high relaxivities at 7 T. This is important, especially considering that the $T_1$ relaxivities of 2 of the 3 macrocyclic GBCA products currently available clinically in Europe decrease with increasing field strengths.[35] At 3 T, [Fe(*trans*-Di-*t*CDTA)] in blood serum has slightly higher $T_1$ relaxivity per metal ion than gadoteridol (ProHance, Bracco Diagnostic S.p.S, Milan, Italy) and gadoterate (Dotarem, Guerbet LLC, Paris, France) and slightly lower $T_1$ relaxivity compared with gadobutrol (Gadovist, Bayer AG, Pharmaceuticals, Berlin, Germany) in blood plasma, whereas

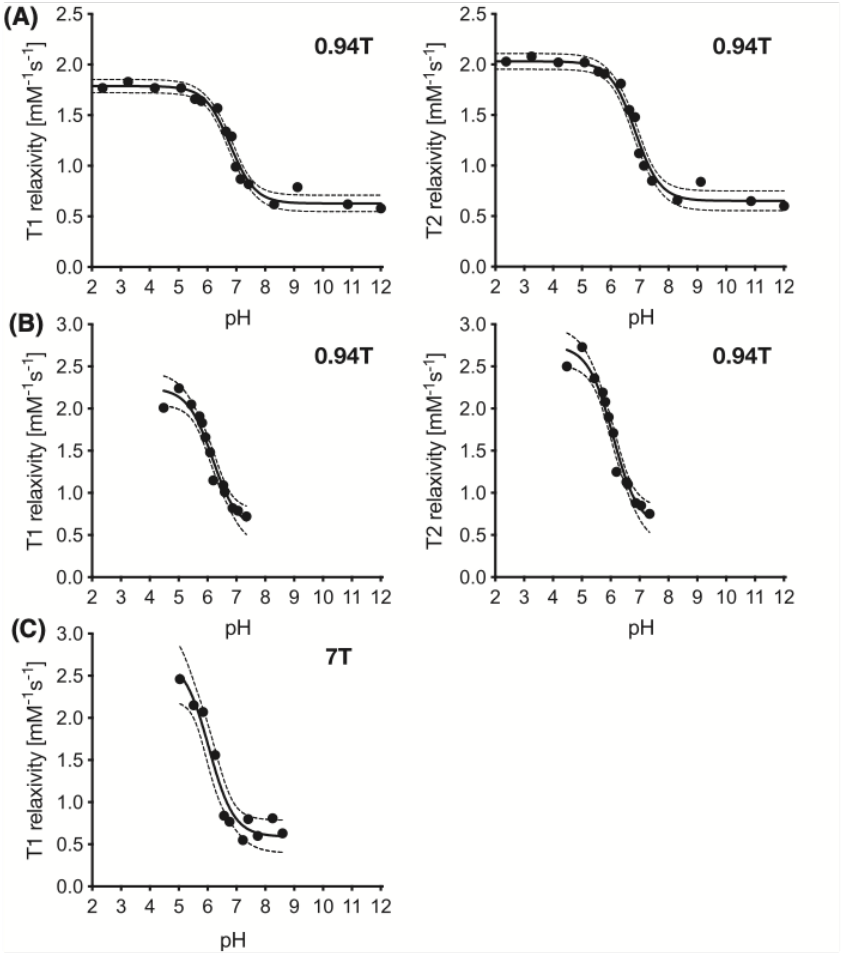


**FIGURE 7** [Fe(en-*t*CDTA)]$^+$ is a pH sensor. (A) pH dependence of $T_1$ and $T_2$ relaxivity of [Fe(en-*t*CDTA)]$^+$ in water at 0.94 T. (B) pH dependence of $T_1$ and $T_2$ relaxivity of [Fe(en-*t*CDTA)]$^+$ in serum at 0.94 T. (B) pH dependence of $T_1$ and $T_2$ relaxivities of [Fe(en-*t*CDTA)]$^+$ in serum at 7 T. Curves represent the sigmoidal dose-response fits with 95% confidence bands (dotted lines). (A, B) Relaxivities determined with a relaxometer, (C) $T_1$ values calculated from MR imaging performed in a 7 T Bruker scanner with built-in RARE $T_1$-mapping sequence

its $T_1$ relaxivity per molecule is higher than that of all 3 of these products. Field strength-dependent $T_1$ relaxivity peaked at 7 T for [Fe(*t*CDTA)]$^-$, whereas it was highest at 3 T for [Fe(*trans*-*t*CDTA)]$^+$ and [Fe(*trans*-Di-*t*CDTA)]. The relaxivity increases in serum in comparison to water were slightly lower than for the mentioned macrocyclic GBCA in plasma, indicating a similar low plasma protein adsorption.[36] Therefore, [Fe(*trans*-*t*CDTA)]$^+$ and [Fe(*trans*-Di-*t*CDTA)] might be potential alternatives to GBCA. Additionally, using the terminal amino group as linker, [Fe(*trans*-*t*CDTA)]$^+$ could serve as an MRI-detectable label, for example, when coupled to specific imaging probes. Because specific probes principally bind to tissue structures, delayed excretion and gadolinium depositions would become even more likely when GBCA would be used for such imaging probes.

Importantly, the very high stability of [Fe(*t*CDTA)]$^{-20}$ was not substantially reduced by our modifications of *t*CDTA. In fact, like *t*CDTA, all new *t*CDTA derivatives resisted the challenge with 100 mM HCl for 72 h, which was not the case for the macrocyclic iron complexes presented by Snyder et al.[14] We observed a small change in absorption during the first hour, which we attribute to protonation of the chelating amines of *t*CDTA and thus cleavage of the respective coordinative bonds. The rapid time course of this small absorption change for [Fe(*trans*-Di-*t*CDTA)] is shown in Supporting Information Figure S5. However, the iron complexes appeared to retain their stability with the 4 remaining coordinating oxygens. This might also explain, based on the hard and soft acids and bases-principle—hard acid Fe(III) and hard base O—the lower stability of the macrocyclic chelators of Snyder et al., which coordinate with 3 or 4 amines but only with 2 oxygens.[14]

Electrochemical data suggest that the [Fe(*t*CDTA)]$^-$ complex is not prone to iron redox cycling and thus ROS-induced toxicity under physiological conditions. Merkofer et al. had reported an ascorbyl/monohydroascorbate physiological electrode potential of approx. +0.1 V versus NHE (corresponding to −0.1 V vs. Ag/AgCl,[37] which means that "unproblematic" Fe(III) complexes should show electrode potentials lower than −0.1 V. [Fe(*t*CDTA)]$^-$ ($E_c$= −0.16 V vs. Ag/AgCl), which is well below this value, whereas the other complexes are at least close with $E_c \approx 0$ V. However, it should be noted that, for the presented cyclic voltammetry measurements, conditions are not completely matching physiological conditions such as micromolar concentrations of the complexes

and pH 7.[37] It is to be expected that even more negative electrode potentials would result[12] at higher pH values than the value applied here (pH 5.9). The fact that we observed 2 cathodic peak potentials for the [Fe(*trans*-Di-*t*CDTA)] complex and $[Fe(en\text{-}tCDTA)]^+$ might originate from 2 different reasons: the presence of different metal-bound species like $Fe\text{-}OH_2$ and Fe-OH (the aqua form is reduced more readily than the hydroxide form[12]) and/or, in the case of [Fe(*trans*-Di-*t*CDTA)], slightly different potentials for the 2 Fe(III) centers. Future studies will be necessary to thoroughly investigate redox activities under physiological conditions.

Although thermodynamically possible, it is unclear to what degree this redox cycling will occur in blood and other fluids comprising the extracellular spaces. These complexes likely distribute through the extracellular spaces and should be very rapidly and efficiently excreted, suggesting that, even if redox cycling does occur, it is unclear whether transient exposure will lead to any toxic effect.

## 5 | CONCLUSION

Straightforward 2-step synthesis allowed the generation of 2 derivatives of $[Fe(tCDTA)]^-$, $[Fe(trans\text{-}tCDTA)]^+$ and [Fe(*trans*-Di-*t*CDTA)] with improved relaxivities while preserving high stability compared with $[Fe(tCDTA)]^-$. These new IBCA have favorable relaxivities at 1.5, 3, and 7 T that are in the range of clinically available GBCA. A third derivative, $[Fe(en\text{-}tCDTA)]^+$, provides pH sensing capability and is activated at weakly acidic pH, making it a potential candidate for better MRI-based characterization of cancer tissues or tissue at risk in stroke by MRI.

## ACKNOWLEDGMENT

We thank Monika Ebert and Harald Kratz for their practical assistance. We thank Bettina Herwig for language editing. We thank Susanne Müller from the Charité Core Facility 7 T Experimental MRIs for her support. We thank Petra Henklein and Katharina Janek of the Shared Facility of Mass Spectrometry of the Institute of Biochemistry, Charité–Universitätsmedizin Berlin, for performing the MALDI analyses.

## ORCID

*Eyk Schellenberger* https://orcid.org/0000-0003-4096-6865

## REFERENCES

1. Grobner T. Gadolinium—a specific trigger for the development of nephrogenic fibrosing dermopathy and nephrogenic systemic fibrosis. *Nephrol Dial Transplant*. 2006;21:1104-1108.
2. Murata N, Gonzalez-Cuyar LF, Murata K, et al. Macrocyclic and other non-group 1 gadolinium contrast agents deposit low levels of gadolinium in brain and bone tissue: preliminary results from 9 patients with normal renal function. *Invest Radiol*. 2016;51:447-453.
3. Gulani V, Calamante F, Shellock FG, et al. Gadolinium deposition in the brain: summary of evidence and recommendations. *Lancet Neurol*. 2017;16:564-570.
4. Fingerhut S, Sperling M, Holling M, et al. Gadolinium-based contrast agents induce gadolinium deposits in cerebral vessel walls, while the neuropil is not affected: an autopsy study. *Acta Neuropathol*. 2018;136:127-138.
5. El-Khatib AH, Radbruch H, Trog S, et al. Gadolinium in human brain sections and colocalization with other elements. *Neurol Neuroimmunol Neuroinflamm*. 2019;6:e515.
6. Layne KA, Wood DM, Dargan PI. Gadolinium-based contrast agents—what is the evidence for 'gadolinium deposition disease' and the use of chelation therapy. *Clin Toxicol (Phila)*. 2020;58:151-160.
7. Lindner U, Lingott J, Richter S, et al. Speciation of gadolinium in surface water samples and plants by hydrophilic interaction chromatography hyphenated with inductively coupled plasma mass spectrometry. *Anal Bioanal Chem*. 2013;405:1865-1873.
8. Birka M, Wehe CA, Hachmöller O, et al. Tracing gadolinium-based contrast agents from surface water to drinking water by means of speciation analysis. *J Chromatogr A*. 2016;1440:105-111.
9. Parant M, Perrat E, Wagner P, et al. Variations of anthropogenic gadolinium in rivers close to waste water treatment plant discharges. *Environ Sci Pollut Res Int*. 2018;25:36207-36222.
10. González V, Vignati DAL, Pons M-N, et al. Lanthanide ecotoxicity: first attempt to measure environmental risk for aquatic organisms. *Environ Pollut*. 2015;199:139-147.
11. Boehm-Sturm P, Haeckel A, Hauptmann R, et al. Low-molecular-weight iron chelates may be an alternative to gadolinium-based contrast agents for T1-weighted contrast-enhanced MR imaging. *Radiology*. 2018;286:537-546.
12. Seibig S, van Eldik R. Structural information on trans-1, 2-diaminocyclohexane-N, N -tetraacetateferrate (III) in the solid and aqueous phase. *Inorg Chim Acta*. 1998;279:37-43.
13. Wang H, Jordan VC, Ramsay IA, et al. Molecular magnetic resonance imaging using a redox-active iron complex. *J Am Chem Soc*. 2019;141:5916-5925.
14. Snyder EM, Asik D, Abozeid SM, et al. A new class of Fe(III) macrocyclic complexes with alcohol donor groups as effective T1 MRI contrast agents. *Angew Chem Int Ed*. 2020;59:2414-2419.
15. Asik D, Smolinski R, Abozeid SM, et al. Modulating the properties of Fe(III) macrocyclic MRI contrast agents by appending sulfonate or hydroxyl groups. *Molecules*. 2020;25:2291.
16. Caravan P, Farrar CT, Frullano L, et al. Influence of molecular parameters and increasing magnetic field strength on relaxivity of gadolinium- and manganese-based T1 contrast agents. *Contrast Media Mol Imaging*. 2009;4:89-100.
17. Gestin JF, Faivre-chauvet A, Mease RC, et al. Introduction of five potentially metabolizable linking groups between 111In-cyclohexyl EDTA derivatives and F(ab')2 fragments of anti-carcinoembryonic antigen antibody–I. A new reproducible synthetic method. *Nucl Med Biol*. 1993;20:755-762.
18. DeLano WL. *The PyMOL Molecular Graphics System*. San Carlos, CA: DeLano Scientific; 2002.
19. Giordanengo R, Viel S, Allard-Breton B, et al. Tandem mass spectrometry of poly(methacrylic acid) oligomers produced by negative mode electrospray ionization. *J Am Soc Mass Spectrom*. 2009;20:25-33.

20. Fornasiero D, Bellen JC, Baker RJ, et al. Paramagnetic complexes of manganese(II), iron(III), and gadolinium(III) as contrast agents for magnetic resonance imaging. The influence of stability constants on the biodistribution of radioactive aminopolycarboxylate complexes. *Invest Radiol*. 1987;22:322-327.
21. Bond J, Jones TI. Iron chelates of polyaminocarboxylic acids. *Trans Faraday Soc*. 1959;55:1310-1318.
22. Webb BA, Chimenti M, Jacobson MP, et al. Dysregulated pH: a perfect storm for cancer progression. *Nat Rev Cancer*. 2011;11:671-677.
23. Thews O, Riemann A. Tumor pH and metastasis: a malignant process beyond hypoxia. *Cancer Metastasis Rev*. 2019;38:113-129.
24. Wu L, Jiang L, Sun PZ. Investigating the origin of pH-sensitive magnetization transfer ratio asymmetry MRI contrast during the acute stroke: correction of $T_1$ change reveals the dominant amide proton transfer MRI signal. *Magn Reson Med*. 2020;84:2702-2712.
25. Harston GWJ, Tee YK, Blockley N, et al. Identifying the ischaemic penumbra using pH-weighted magnetic resonance imaging. *Brain*. 2015;138:36-42.
26. Lu J, Sun J, Li F, et al. Highly sensitive diagnosis of small hepatocellular carcinoma using pH-responsive iron oxide nanocluster assemblies. *J Am Chem Soc*. 2018;140:10071-10074.
27. Caro C, García-Martín ML, Pernia Leal M. Manganese-based nanogels as pH switches for magnetic resonance imaging. *Biomacromol*. 2017;18:1617-1623.
28. Li B, Gu Z, Kurniawan N, et al. Manganese-based layered double hydroxide nanoparticles as a $T_1$ -MRI contrast agent with ultrasensitive pH response and high relaxivity. *Adv Mater*. 2017;29.
29. Yang L-M, Zheng H, Ratnakar JS, et al. Engineering a pH-sensitive liposomal MRI agent by modification of a bacterial channel. *Small*. 2018;14:e1704256.
30. Zhang S, Wu K, Sherry AD. A novel pH-sensitive MRI contrast agent. *Angew Chem Int Ed Engl*. 1999;38:3192-3194.
31. Moriggi L, Yaseen MA, Helm L, et al. Serum albumin targeted, pH-dependent magnetic resonance relaxation agents. *Chemistry*. 2012;18:3675-3686.
32. Raghunand N, Howison C, Sherry AD, et al. Renal and systemic pH imaging by contrast-enhanced MRI. *Magn Reson Med*. 2003;49:249-257.
33. Garcia-Martin ML, Martinez GV, Raghunand N, et al. High resolution pH(e) imaging of rat glioma using pH-dependent relaxivity. *Magn Reson Med*. 2006;55:309-315.
34. Savić T, Gambino G, Bokharaie VS, et al. Early detection and monitoring of cerebral ischemia using calcium-responsive MRI probes. *Proc Natl Acad Sci USA*. 2019;116:20666-20671.
35. Szomolanyi P, Rohrer M, Frenzel T, et al. Comparison of the relaxivities of macrocyclic gadolinium-based contrast agents in human plasma at 1.5, 3, and 7 T, and blood at 3 T. *Invest Radiol*. 2019;54:559-564.
36. Rohrer M, Bauer H, Mintorovitch J, et al. Comparison of magnetic properties of MRI contrast media solutions at different magnetic field strengths. *Invest Radiol*. 2005;40:715-724.
37. Merkofer M, Kissner R, Hider RC, et al. Fenton chemistry and iron chelation under physiologically relevant conditions: electrochemistry and kinetics. *Chem Res Toxicol*. 2006;19:1263-1269.

## SUPPORTING INFORMATION

Additional Supporting Information may be found online in the Supporting Information section.

**FIGURE S1** HPLC
**FIGURE S2** MALDI Mass spectrometry
**FIGURE S3** Infrared spectroscopy
**FIGURE S4** Nuclear magnetic resonance analysis
**FIGURE S5** Absorbance change of [Fe(trans-Di-*t*CDTA)] in 100 mM HCl during first hour. (A) Corresponding to figure 2, a small change of the absorption spectrum of [Fe(trans-Di-*t*CDTA)] was recorded during first hour (interval 2 min) after diluting in 100 mM HCl. (B) Time-course of absorption at 300 nm. The rapid change (exponential decay, K = 0.130 ± 0.007) during the first minutes might be explained by protonation of the chelating amines and thus cleavage of the respective coordinative bonds (but maintaining stability through coordinative oxygen bonds, Figure 2)
**FIGURE S6** Relaxivity determination of Fe[en-*t*CDTA]$^+$ calculated from relaxometer measurements at 0.94T. x-axis: Fe[en-*t*CDTA]$^+$ concentrations [mM] iron; y-axis: 1/T1 in [1/s]
**FIGURE S7** Comparison of the pH-dependent relaxivities of the iron(III)-*t*CDTA derivates coupled with flexible ethylenediamine (*en*) versus rigid trans-1,4-diaminoclyclohexane (*trans*). (A) [Fe(en-*t*CDTA)]$^+$ monomer, (B) [Fe(en-Di-*t*CDTA)] dimer, (C) [Fe(*trans*-*t*CDTA)]$^+$ monomer, and (D) [Fe(*trans*-Di-*t*CDTA)] dimer. The relaxivity decrease occurred for the en derivates below pH7.4 and for the trans derivatives above pH 7.4. Relaxivities were measured on a relaxometer at 0.94T and 37°C in water
**TABLE S1** Cyclic voltammetry. Cathodic, anodic and half-wave potentials of iron-complexes

**How to cite this article:** Xie J, Haeckel A, Hauptmann R, et al. Iron(III)-*t*CDTA derivatives as MRI contrast agents: Increased $T_1$ relaxivities at higher magnetic field strength and pH sensing. *Magn Reson Med*. 2021;85:3370–3382. https://doi.org/10.1002/mrm.28664

# Curriculum Vitae

## Personal Data

My curriculum vitae does not appear in the electronic version of my paper for reasons of data protection.

# Acknowledgments

My thanks and appreciation to all the number of wonderful individuals for being part of my Ph.D. process journey and making this dissertation possible. First and foremost, I owe my deepest gratitude to my supervisor Prof. Dr. Eyk Schellenberger for his dedicated involvement in every step throughout my Ph.D. study and research, for his patience, guidance, and immense knowledge. The door to Eyk's office was always open whenever I ran into a trouble spot or had a question about my research or writing.

Besides my advisor, I would like to thank the experts who were involved in the validation survey for this research project: Dr. Akvile Häckel, Dr. Ralf Hauptmann, Prof. Dr. Bernd Hamm for their passionate participation, insightful comments and encouragement, which inspired me to widen my research from various perspectives.

Also, this thesis could not have been successfully conducted without the help of my cooperation partners from the Department of Chemistry, Humboldt - Universität zu Berlin and Institute of Chemistry, Otto von Guericke Universität Magdeburg. Therefore, I would like to thank Dr. Jörg Schnorr, Prof. Dr. Christian Limberg, Dr. Ray, Iweta Pryjomska, Prof. Dr. Nora Kulak, Dr. Philipp Boehm-Strum, Susanne Müller for the incredible cooperation and fruitful discussions regarding the experimental samples, details, and data analysis.

I take this opportunity to place my sincere thanks to all the Institute of Radiology members. Angela Schellenberger, Azadeh Mohtashamdolatshahi, Fei Ni, Franziska Rausch, Jing Guo, Ledia Lilaj for their friendship, for creating a cordial working environment, as well as for the stimulating discussions we had in the past years. I would also like to thank Dr. Beatrix Schnorr, Dr. Tobias Dietrich Haase for providing valuable help and support.

Last but not the least, I would like to express my deep and sincere gratitude to my family for their unceasing and unparalleled love, help and endless support. I am forever indebted to my mom for rendering me the opportunities and experience that have made me who I am. I am grateful to my sister for always being there for me a friend. It is a pleasure to thank my intimates Huang Wang and Jing Shi for their constant motivation and companion. I had a bad accident in the challenging year of 2021. However, their selfless encouragement inspires me to explore new directions for the future and to seek my own destiny. This journey would be the delighted sunlight in my life and embraces me to be a better myself that could fulfil my value to the community.

Jing Xie